IMPLEMENTATION OF AUTOMATICALLY SIMPLIFIED CHEMICAL KINETICS THROUGH INTRINSIC LOW-DIMENSIONAL MANIFOLDS FOR GASEOUS HMX

by

John D. Hedengren

A thesis submitted to the faculty of
Brigham Young University
in partial fulfillment of the requirements for the degree of

Master of Science

Department of Chemical Engineering
Brigham Young University
December 2002

BRIGHAM YOUNG UNIVERSITY

GRADUATE COMMITTEE APPROVAL

of a thesis submitted by

John D. Hedengren

This thesis has been read by each member of the following graduate committee and by a majority vote has been found satisfactory.

Date	Merrill W. Beckstead, Chair
Date	Jennifer P. Spinti
Date	Larry L. Baxter

BRIGHAM YOUNG UNIVERSITY

As chair of the candidate's graduate committee, I have read the dissertation of John D. Hedengren in its final form and have found that (1) its format, citations, and bibliographical style are consistent and acceptable and fulfill university requirements; (2) its illustrative materials including figures, tables, and charts are in place; and (3) the final manuscript is satisfactory to the graduate committee and is ready for submission to the university library.

Date	Merrill W. Beckstead Chair, Graduate Committee

Accepted for the Department

Thomas H. Fletcher
Graduate Coordinator

Accepted for the College

Douglas M. Chabries
Dean, College of Engineering and Technology

ABSTRACT

IMPLEMENTATION OF AUTOMATICALLY SIMPLIFIED CHEMICAL KINETICS THROUGH INTRINSIC LOW-DIMENSIONAL MANIFOLDS FOR GASEOUS HMX

John D. Hedengren
Department of Chemical Engineering
Master of Science

An automated method to generate, validate, and implement an Intrinsic Low-Dimensional Manifold (ILDM) has been developed. This method has been applied to a detailed gaseous HMX (Octahydro-1,3,5,7-Tetranitro-1,3,5,7-Tetrazocine) mechanism that contains 44 species and 232 reactions. A three-dimensional manifold tracked detailed chemistry based on enthalpy, pressure, and mass fraction of N_2. A four-dimensional manifold adds the mass fraction of NO. A one-dimensional (in space) BYU combustion program has been used to compare the three- and four-dimensional manifolds with a full kinetic mechanism. Simulations show that the three-dimensional manifold is an adequate representation of the full kinetic mechanism away from the reacting surface (> 60 μm at 20 atm). The four-dimensional manifold is an adequate representation of the full kinetic mechanism closer to the reacting surface (>19 μm at 20 atm). An advantage of the ILDM method is that computational time is reduced by an order of magnitude. However, this advantage can be offset by the development time required to create and implement the ILDM method. Another portion of this project is two-dimensional (in space) simulations that model high explosives in a container. Even though this portion of the project does not implement an ILDM, it gives insight to meaningful simulations that can be performed with an ILDM. The simulations explore heat feedback of equilibrium gases in a heated container filled with solid HMX. Heat feedback is calculated to investigate flame propagation and burning characteristics of the solid HMX. Further work is necessary to implement the ILDM approach in similar container simulations. The methodology used to implement the four-dimensional ILDM into the one-dimensional (in space) combustion code is available to be used in other applications. One application of interest is the University of Utah's three-dimensional (in space) CFD code, ARCHES.

ACKNOWLEDGEMENTS

I would like to thank all the people who have helped me with this project, especially my thesis advisor, Dr. Merrill W. Beckstead. Dr. Beckstead provided helpful comments and guidance from the start. I have thoroughly enjoyed the autonomy that he has given me while working on this project. In addition, I appreciate opportunities he has given me to present my work at a conference and poster session.

Ephraim Washburn and Karl Meredith have both contributed by helping me understand the computer codes available to our research group. Also, Ephraim's suggestions were invaluable during the project's development.

Ryan Stevens, Ben Hardy, and Matt Gross have each helped at various points in the development of this project by generating plots, exploring tangent ideas, and by supplying stress relief for the research group.

I would especially like to thank the people at the University of Utah's C-SAFE program for funding through this project. Dr. Phillip J. Smith contributed seminal ideas and helpful comments throughout this project. In addition, I would like to thank Dr. Jennifer P. Spinti for the practical suggestions in developing the manifold code.

My wife, Sarah, has been supportive when deadlines approached. The occasional evening or Saturday spent without me is a tribute to her support.

Table of Contents

CHAPTER 1 INTRODUCTION 1

CHAPTER 2 LITERATURE REVIEW 5

2.1 Reduced Mechanism Methods 5
  2.1.1 Sensitivity Analysis..6
  2.1.2 Species Lumping Procedures 6
  2.1.3 Computational Singular Perturbation (CSP) Technique 7

2.2 Intrinsic Low-Dimensional Manifold (ILDM)..7
  2.2.1 The Equations 9
  2.2.2 Chemical and Physical Process Time Scales 9
  2.2.3 Decoupling Fast Chemical Time Scales..10
  2.2.4 Manifold Dimension 11
  2.2.5 One-Dimensional Manifolds..12
  2.2.6 Two-Dimensional Manifolds 13
  2.2.7 Higher-Dimensional Manifolds 14
  2.2.8 Examples of Manifold Implementation..15
  2.2.9 Recent Improvements to the Manifold Method 16

CHAPTER 3 MANIFOLD GENERATION FOR GASEOUS HMX....................19

3.1 Manifold Generation 20
  3.1.1 Dimension of the Manifold..20
  3.1.2 Starting Points in the Composition Space 21
  3.1.3 Reaction Progression..22
  3.1.4 Manifold Identification 25
    3.1.4.1 Graphical Method..25
    3.1.4.2 Eigenvector Analysis..26
  3.1.5 Choice of Parameterization..26

3.2 Manifold Storage and Retrieval 27

CHAPTER 4 3-D MANIFOLD VALIDATION WITH 1-D SIMULATION 29

4.1 3-D Manifold Direct Substitution..31

4.2 3-D Manifold Implementation in 1-D Laminar Simulation 33
  4.2.1 The Equations 34
  4.2.2 Discretization of the Equations 34
  4.2.3 Iterative Solving Routine 35
  4.2.4 Grid Independent Study 37

4.2.5 Results 39

CHAPTER 5 4-D MANIFOLD VALIDATION WITH 1-D SIMULATION 43

5.1 4-D Manifold Direct Substitution 43

5.2 4-D Manifold Implementation in 1-D Laminar Simulation 44
5.2.1 The Equations 44
5.2.2 Discretization of the Equations 45
5.2.3 Iterative Solving Routine 45
5.2.4 Grid Refinement for Enthalpy Profile 46
5.2.5 Grid Independent Study 48
5.2.6 A Model for Near-Surface Kinetics 49
5.2.7 Results 53

CHAPTER 6 CONTAINER SIMULATION 57

6.1 C-SAFE Container Simulation 57

6.2 A Post-Ignition Model with Gas Products at Equilibrium 58
6.2.1 Heat Transfer Analysis 60
6.2.2 Open System Simulation 62
6.2.2.1 The Model 63
6.2.2.2 Ignition Model 63
6.2.2.3 Grid Independent Study 65
6.2.2.4 Simulation Results 66
6.2.2.5 Gap Thickness Parametric Study 69
6.2.2.6 Conclusions for the Open System Simulation 70
6.2.3 Closed System Simulation 71
6.2.3.1 The Model 71
6.2.3.2 Ignition Model 73
6.2.3.3 Simulation Results 73
6.2.3.4 Conclusions for the Closed System Simulation 77

CHAPTER 7 CONCLUSIONS 79

CHAPTER 8 FUTURE WORK 81

CHAPTER 9 REFERENCES 83

APPENDIX A 87

List of Figures

Figure 1 - Time Scales Important to Reacting Flow 10
Figure 2 - One-Dimensional Manifold 12
Figure 3 - Two-Dimensional Manifold 14
Figure 4 - Multi-Dimensional Manifold 15
Figure 5 - Reaction Path for Manifold Generation 22
Figure 6 – Generating a Gas Phase Chemkin Link File 23
Figure 7 – Manifold Generation 23
Figure 8 - Batch Reactor Results 24
Figure 9 - Portion of HMX Manifold 25
Figure 10 - ILDM Implementation into 1-D, Steady-State Laminar Simulation 29
Figure 11 – Generating a Condensed Phase Chemkin Link File 30
Figure 12 – Generating a Transport Properties Chemkin Link File 30
Figure 13 – 1-D, Steady-State Laminar Simulation 31
Figure 14 – Direct Substitution of 3-D Manifold 32
Figure 15 - Flow Time Scale 33
Figure 16 - Control Volume Layout 34
Figure 17 - Iterative Solving Procedure 36
Figure 18 - Oscillations in the Final Solution 37
Figure 19 - Grid Independent Study 38
Figure 20 - Grid Independent Study 39
Figure 21 - Results of One-Dimensional, Steady-State Simulation 40
Figure 22 - Results of One-Dimensional, Steady-State Simulation 40
Figure 23 - Results of One-Dimensional, Steady-State Simulation 41
Figure 24 - Results of One-Dimensional, Steady-State Simulation 41
Figure 25 – Full Kinetic Mechanism Compared to Manifold Results 44
Figure 26 - Iterative Solving Procedure 46
Figure 27 - Data Flow with Enthalpy Grid Refinement 47
Figure 28 - Grid Independence Study (0-50 μm) 48
Figure 29 - Grid Independence Study (>25 μm) 49
Figure 30 - NO Profile for Various Starting Points at 20 atm 50
Figure 31 - NO Profile for Various Starting Points at 5 atm 51
Figure 32 - NO Profile for Various Starting Points at 60 atm 51
Figure 33 - Enthalpy Profile at 60 atm 52
Figure 34 - Results of One-Dimensional, Steady-State Simulation 53
Figure 35 - Results of One-Dimensional, Steady-State Simulation 54
Figure 36 - Results of One-Dimensional, Steady-State Simulation 54
Figure 37 - Results of One-Dimensional, Steady-State Simulation 55
Figure 38 - Pressurization of Container 58
Figure 39 - Model of Container 59

Figure 40 - Heat Transfer Simulation 61
Figure 41 - Heat Transfer at the Solid-Gas Interface 62
Figure 42 - Open System Model 63
Figure 43 - Ignition Data from Heating Tests 64
Figure 44 - Grid Layout 65
Figure 45 - Temperature Contours 67
Figure 46 - Comparison of Heat Fluxes 68
Figure 47 - Distance to Ignition for a 5 mm Gap 69
Figure 48 - Ignition Prediction for Various Gap Widths 70
Figure 49 - Closed System Model 72
Figure 50 - Initial Velocity Profile 74
Figure 51 - Temperature Profile in the Closed System Simulation 75
Figure 52 - Heat Flux Analysis for Flame Propagation 76

List of Tables

Table 1 - Eigenvalue Analysis 10

Chapter 1 Introduction

Modeling of reacting flows is a computational challenge even for the world's largest supercomputers (Tomlin, Turanyi, and Pilling 1997). This challenge is being explored by DOE's ASCI (Accelerated Strategic Computing Initiative) program. Part of the program is delegated to the University of Utah through C-SAFE (Center for the Simulation of Accidental Fires and Explosions). In 1996, the University of Utah received funding from the DOE ASCI (Accelerated Strategic Computational Initiative) program to develop new tools for the simulation of accidental fires and explosions. To carry out this program, the University of Utah created C-SAFE. This initiative seeks to simulate the rapid heating of a container filled with a plastic bonded explosive, PBX-9501, in a large jet-fuel pool fire. PBX-9501 is composed of 95% HMX (Octahydro-1,3,5,7-Tetranitro-1,3,5,7-Tetrazocine) as the explosive and 5% binder. To simplify the chemical kinetics, the high explosive is modeled as pure HMX. In the simulation, heat from the jet-fuel fire ignites the high explosive. As the high explosive combusts, the container pressurizes, swells, and finally bursts. C-SAFE's goal is to simulate this scenario from just after the ignition of the pool fire up to the rupture of the container.

The challenge of such a simulation lies in calculating detailed transport and complex chemical kinetics simultaneously. Currently, it is very computationally expensive to calculate both. Therefore, the options are to make simplified transport calculations (i.e. Reynolds Averaged Navier-Stokes methods), reduce the chemical kinetics, or both.

Efforts to reduce chemical kinetics include systematically reduced mechanisms, the constrained equilibrium approach, repro-modeling, computational singular perturbation, the method of Intrinsic Low-Dimensional Manifolds (ILDM), and dynamic dimension reduction (Blasenbrey, Schmidt, and Maas 1998). All of these methods fall under one of two general categories: (1) reduced mechanism methods or (2) ILDM methods. The appeal of the ILDM method over reduced mechanism methods is that much of the detailed chemistry is maintained while still showing a dramatic computational speedup for chemistry calculations (Yang and Pope 1998b). Instead of simplifying a reaction mechanism by eliminating reactions or species, the manifold method explores time scales for chemical reactions. For reacting flow calculations, the progression of reactions with fast time scales (compared to flow time scales) can be ignored. The manifold method ignores reactions with fast time scales yet is still based on detailed kinetics.

To assist in the C-SAFE effort of providing a full-physics simulation at a reasonable computational cost, the ILDM method for reducing chemical kinetics has been applied to a detailed, gaseous HMX mechanism. The objectives of this project were to:

- Automate a system for generating an ILDM for gaseous HMX.
- Implement the ILDM in a 1-D (in space), steady-state laminar simulation.
- Evaluate the performance of the HMX ILDM by comparison with full kinetics in the 1-D (in space), steady-state laminar simulation.
- Lay a foundation for higher-dimensional (in space) simulations that apply ILDM-simplified chemistry by investigating 2-D (in space) simulations with equilibrium gas properties.

This thesis describes the achievement of these objectives. Specifically, Chapter 2 reviews two methods for simplifying chemical kinetics: reduced mechanism methods and ILDM methods. The ILDM method is described mathematically, and successful applications of this method are reviewed. Chapter 3 describes original work of this project in generating a 3-D (in pressure, enthalpy, and mass fraction of N_2) ILDM for HMX. The application of the 3-D HMX ILDM in a 1-D (in space), steady-state laminar simulation is described in Chapter 4. Because of shortcomings of the 3-D ILDM, a 4-D (in pressure, enthalpy, and mass fractions of N_2 and NO) ILDM was created. Chapter 5 describes the application of the 4-D ILDM in the 1-D (in space), steady-state laminar simulation. Because of the 4-D ILDM inadequacy in the fast reaction zone, a model for near-surface kinetics is proposed. Chapter 6 describes 2-D (in space) simulations with equilibrium HMX products. These simulations lay a foundation for higher-dimensional (in space) simulations that apply ILDM-simplified chemistry. Conclusions and general observations about the ILDM method are given in Chapter 7. Chapter 8 describes future work that can be done by other researchers to meet C-SAFE's objective of implementing more accurate HMX chemistry into container simulations.

Chapter 2 Literature Review

This chapter discusses efforts to reduce chemical kinetics that fall into two general categories: reduced mechanism methods and ILDM methods (Yang and Pope 1998b). The ILDM method, in particular, is described in theoretical detail. The final two sections of the chapter show applications of ILDM techniques to practical combustion simulations and recent improvements to the method.

2.1 Reduced Mechanism Methods

Traditionally, when chemical kinetic mechanisms were constructed manually, it required the technical expertise of someone familiar with the reaction mechanism (Tomlin, et. al. 1997). This person selected chemical species and reactions that would be important under given conditions. In the pre-computer era, the chemical expert would apply either the steady-state or partial-equilibrium approximation to various elementary reactions in the mechanism to come up with an analytical solution. Because analytical solutions were necessary, the size of the kinetic mechanisms was limited.

With the development of faster computers, it became possible, though still very expensive, to model complex chemical reactions with detailed kinetics. To reduce the cost of computing, the chemical expert would systematically reduce the complex mechanisms into skeletal mechanisms. The advantage of using skeletal mechanisms over analytical solutions is that less development time is required. The drawbacks to this method are that it requires substantial knowledge of a detailed mechanism to generate a reduced mechanism. In addition, the resultant reduced mechanism only works for a limited range of temperature, pressure, and composition. The range of the reduced mechanism is limited because reactions can depend greatly on physical conditions. For example, there is a change in reaction pathway as the combustion moves from fuel-rich to fuel-lean conditions.

Other techniques have also been developed to assist in reduced mechanism development. Three of these techniques are described below.

2.1.1 Sensitivity Analysis

A sensitivity analysis or principal component analysis is one of the tools to reduce complex chemical kinetics (Tomlin, et. al. 1997). The sensitivity analysis identifies reactions that have little effect on the overall reaction by measuring a normalized local sensitivity. The normalized local sensitivity represents the amount that a species concentration changes after a small perturbation in one of the system parameters (e.g. temperature, pressure, etc.). Reactions that contain species with low sensitivities can be eliminated from the detailed mechanism. In this way, reactions that involve principal components remain in the new, reduced mechanism.

2.1.2 Species Lumping Procedures

Even after a reduced mechanism is achieved, the number of reactions can still be too great to implement the mechanism into a practical combustion code. Lumping procedures can be used to reduce the reaction system to a lower-dimensional system of equations (Tomlin, et. al. 1997). This technique is founded on the assumption that chemically similar species have similar rate parameters and can therefore be treated as a single compound. Accordingly, the dimension of the lumped mechanism is equal to the number of unique classifications of chemical species. The weakness of this method is that it is a compromise between a detailed mechanism and a global mechanism. By lumping species together, much of the detailed reaction information is lost.

2.1.3 Computational Singular Perturbation (CSP) Technique

The CSP technique is a formal way to apply partial-equilibrium approximations on an *a priori* basis (Lam and Goussis 1988). The procedure begins by evaluating time scales of reactions and ordering them from fastest to slowest. The entire chemistry calculation proceeds with the time scale of the fastest reaction. As the reaction proceeds, the fastest reaction becomes exhausted and its reaction rate approaches zero. Once the fastest reaction is exhausted, it is labeled as a dead mode and is discarded from the calculation. The chemistry calculation is then allowed to proceed at the time scale of the next fastest reaction. As the fastest reactions are eliminated, the system of equations becomes less stiff and therefore less computationally expensive to solve. CSP has been used to investigate mechanisms and to reduce them rather than to provide a computationally efficient technique for combustion modeling (Tomlin, et. al. 1997).

2.2 Intrinsic Low-Dimensional Manifold (ILDM)

Many of the previously mentioned methods for creating reduced mechanisms rely on steady-state or partial-equilibrium approximations. However, the reduced mechanisms are generally limited to a range of temperature, pressure, and/or species' concentrations (i.e. state space). Outside of this defined state space, large errors can occur.

To overcome this deficiency, Mass and Pope proposed a new method for reducing chemical kinetics based on Intrinsic Low-Dimensional Manifolds (ILDM) (Maas and

Pope 1992a, Maas and Pope 1992b). Mathematically, a manifold is a topological space or surface. An ILDM is a topological space or surface defined by independent thermochemical parameters. Maas and Pope's original work proposed a method to automatically apply the steady-state and partial-equilibrium approximations over all possible thermochemical states of the system (state space). A thermochemical system can be characterized by fast and slow reactions. It is assumed that the fastest reactions can be decoupled from the slow ones. Then, the decoupled fast reactions (those that are faster than the flow time scales) can be ignored while those with slow time scales are tracked using progress variables. For example, for a particular mechanism, three variables (e.g. enthalpy, pressure, and mass fraction of N_2) could be selected as the progress variables. By this means, a limited number of progress variables can be used to characterize the entire thermochemical system. Once these variables are calculated, all state-space variables, including mass fractions of chemical species, temperature, entropy, and reaction rates, are known. Since the progress variables completely describe the system, only these variables must be calculated. This leads to a dramatic reduction of CPU time for solving the chemistry in a reacting flow calculation.

The ILDM method is especially suited for non-premixed reacting flow calculations where mixing controls much of the chemical reaction. In premixed reacting flow calculations, fewer of the fast time scales can be decoupled. This can lead to higher-dimensional manifolds that are more difficult to implement in realistic combustion simulations.

2.2.1 The Equations

The composition vector (ϕ) is composed of all intensive variables that define the thermochemical state of a system. It includes enthalpy (H) and all species mass fractions (Y_i, i=1,2,…,n_s), and is written as $\phi = (H, Y_1, Y_2,\ldots,Y_{ns})$. The equations for the composition ϕ can be written as (Tomlin, et. al. 1997)

$$\frac{d\phi(x,t)}{dt} = S[\phi(x,t)] + \Gamma(x,t) \tag{1}$$

where S is the rate of change due to reactions (for enthalpy, S = 0) and Γ is the rate of change due to transport effects (convection, diffusion, etc).

2.2.2 Chemical and Physical Process Time Scales

Chemical mechanisms typically have a much larger range of time scales than necessary for the accurate calculation of a reacting flow system. Typically, reaction time scales are on the order of 10^{-9} seconds (e.g. some radical reactions) to 10^{2} seconds (e.g. NO formation in coal combustion) in reactions important to chemical combustion. On the other hand, the time scales necessary to model physical processes are on the order of 10^{-4} to 10^{-2} seconds. Figure 1 illustrates these ranges (Maas and Pope 1992b).

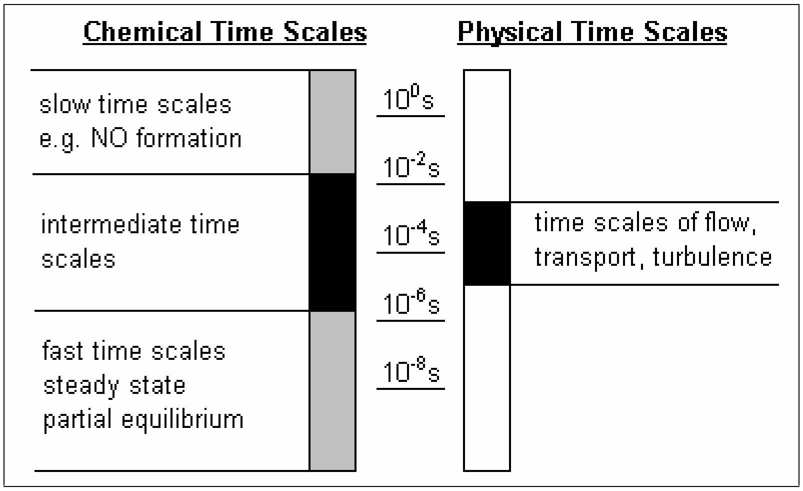
Chemical Time Scales
Physical Time Scales
slow time scales
e.g. NO formation
intermediate time
scales
fast time scales
steady state
partial equilibrium
10^0s
10^{-2}s
10^{-4}s
10^{-6}s
10^{-8}s
time scales of flow,
transport, turbulence

Figure 1 - Time Scales Important to Reacting Flow

Species involved in reactions that happen much faster than the physical processes can be decoupled and eliminated (Blasenbrey, et. al. 1998).

2.2.3 Decoupling Fast Chemical Time Scales

Mass and Pope used an eigenvalue analysis to determine if a system is on a lower-dimensional manifold and is governed by slow chemistry. The eigenvalues are those of the Jacobian ($dS_i/d\phi_j$). A large negative eigenvalue associated with an elementary reaction means that the reaction is governed by fast chemistry and is in local equilibrium. Conserved variables (e.g. pressure in an isobaric system) create eigenvectors that have eigenvalues of zero (see Table 1).

Table 1 - Eigenvalue Analysis

Eigenvalue (real part)	**Response to Physical Perturbations**
Positive	Perturbation will increase (instability)
Zero	Perturbation will not change with time (change of a conserved variable)
Negative	Perturbation will relax to zero

For every reacting flow calculation, there is a time scale for the flow (τ_{flow}) based on the resolution of the transport calculations. If the real part of an eigenvalue is greater than $-1/\tau_{flow}$, then the corresponding eigenvector is in the slow subspace (Yang and Pope 1998a). However, if the eigenvalue is less than $-1/\tau_{flow}$, then the corresponding eigenvector is in the fast subspace and can be decoupled from the reaction system. The number of progress variables that cannot be decoupled form a reduced set. The progress variables in the reduced set are the only ones that must calculated for a laminar or turbulent combustion calculation.

2.2.4 Manifold Dimension

The number of variables in the reduced set determines the dimension of the manifold. Since it is difficult to implement an adaptive-dimensional manifold into a CFD (Computational Fluid Dynamics) code, the dimension of the manifold should be fixed over the entire state space of the manifold (Blasenbrey, et. al. 1998). This makes the implementation much less time consuming but also has some drawbacks. These drawbacks include:

- Calculation of an ILDM is attempted over the whole state space even though some domains of the state space are never accessed in practical applications.
- Fixed parameterization does not guarantee the uniqueness or existence of solutions and can yield ill-conditioned equation systems for the manifold.
- Higher-dimensional manifolds may be required in some regions of the state space. This means that too few progress variables are tracked and could lead to errors typical of an invalid steady-state approximation.

Despite these drawbacks, a manifold of constant dimension is the only practical way to implement the ILDM method for combustion calculations at this time.

2.2.5 One-Dimensional Manifolds

Up to this point, the manifold approach has been described mathematically. Manifolds can also be observed through graphical techniques (Maas and Pope 1994). The simplest case is a manifold plotted against one progress variable. Figure 2 shows the specific mole number of H_2O (mol of H_2O/gm of mixture) plotted against the specific mole number of CO_2 for CO-H_2-air as reactants (Maas and Pope 1992b). The beginning of each trajectory represents an initial composition for the reaction. All initial compositions have the same elemental fractions but different species fractions. The trajectories represent the reaction progression and the square is the final equilibrium condition.

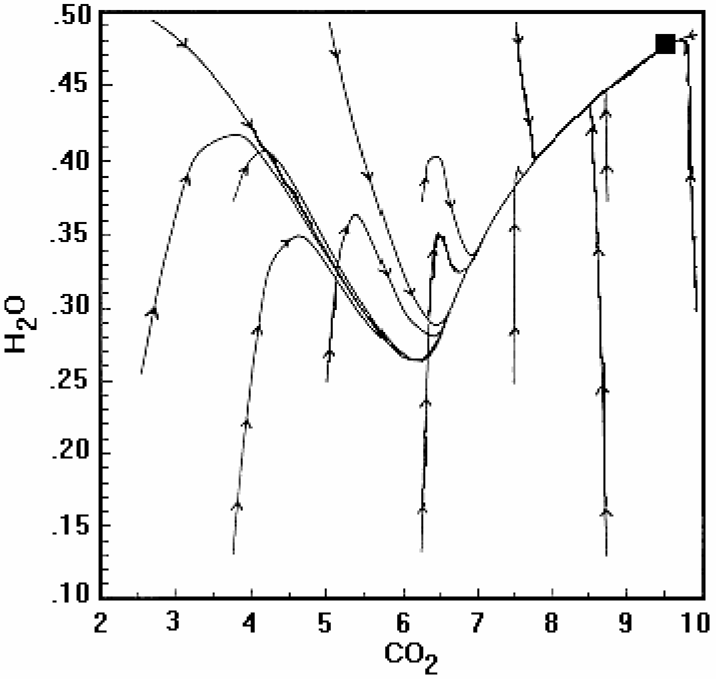

Figure 2 - One-Dimensional Manifold

In this case, the specific mole number of CO_2 is the manifold coordinate. The trajectories have the following properties (Maas and Pope 1992b):

- All approach one common point (equilibrium)
- All approach one common trajectory (manifold)
- On the manifold, only slow time scales govern the chemical reaction
- Once a thermochemical system is on the manifold, it will always remain on the manifold if there are no perturbations ($\Gamma = 0$).

A thermochemical system is drawn to a unique manifold and progresses along it until the system is perturbed through physical processes (e.g. molecular diffusion, mixing, heat convection). If it is perturbed at a time scale slower than the fastest time scale of the manifold, the manifold is an accurate representation of the chemical dynamics. However, if the perturbations happen at a time scale that is faster than the existing manifold, a higher-dimensional manifold should be employed (Blasenbrey, et. al. 1998). A higher-dimensional manifold simply means that more progress variables must be added to the manifold to capture a larger number of time scales. This can dramatically increase the storage requirements for the manifold.

2.2.6 Two-Dimensional Manifolds

A two-dimensional manifold has the same general characteristics as the one-dimensional manifold. The only difference is that two progress variables must be used to describe the state of the system. Figure 3 is an example of a two-dimensional manifold (Blasenbrey, et. al. 1998).

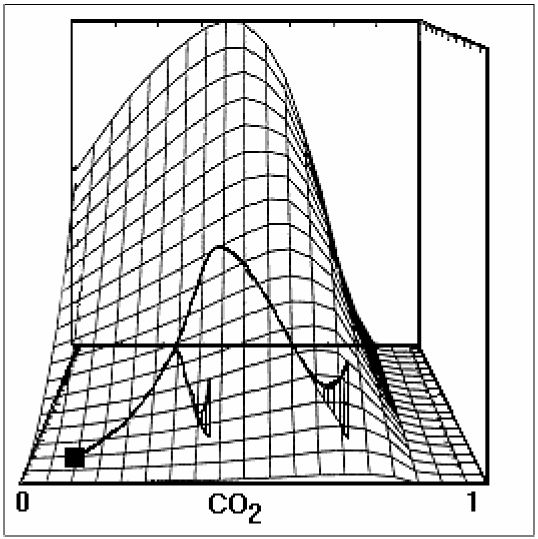

Figure 3 - Two-Dimensional Manifold

The manifold is the grid surface. Each trajectory represents a starting point in the state space. Each trajectory relaxes to the grid surface quickly and stays on that surface until the thermochemical system reaches equilibrium (square point on the plot).

2.2.7 Higher-Dimensional Manifolds

At equilibrium, a 0-D manifold (no progress variables) represents the thermochemical system because there is no change. Near equilibrium (i.e. a final rate determining step before equilibrium), a 1-D (one progress variable) manifold adequately characterizes the reaction system. The dimension of a manifold increases further from equilibrium to account for faster reaction time scales. Figure 4 shows a multi-dimensional manifold (Bongers 2002).

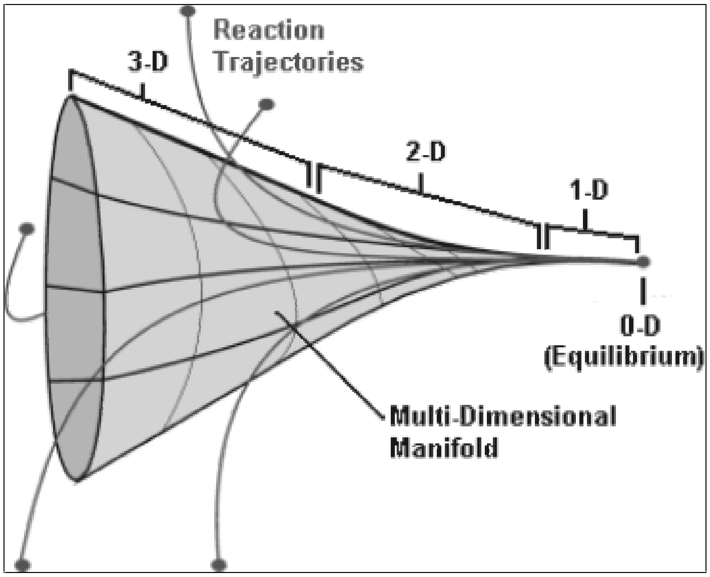

Figure 4 - Multi-Dimensional Manifold

Higher-dimensional manifolds can be visualized through lower-dimensional plots by taking slices of the full manifold. For example, a three-dimensional manifold of the CH_4-air system can be characterized by enthalpy, pressure, and mass fraction of CO_2. If the enthalpy is held constant, the manifold can be plotted as a two-dimensional manifold. Then the enthalpy can be held constant at another value and another two-dimensional manifold plot can be generated. In this way, a higher-dimensional manifold can be visualized and selected graphically.

2.2.8 Examples of Manifold Implementation

The ILDM method has been implemented successfully for laminar premixed CO-H_2-O_2-N_2 flames (Maas and Pope 1994). The CO-H_2-O_2-N_2 ILDM tracks all species, including radicals, within 3% error. In addition, there is a speedup in the calculation of the chemistry by a factor of 10.

The ILDM method has also been implemented successfully in turbulent flame calculations. Three examples include:

- A numerical simulation of a turbulent non-premixed CH_4-H_2-air flame shows that the ILDM method models flames near extinction and near equilibrium (Xiao, Schmidt, and Maas 1998).
- A piloted CO-H_2-N_2-air diffusion flame simulation shows that extinction can be predicted within 5% of the experimental value (Norris and Pope 1995).
- A CH_4-air combustion system shows that the ILDM method is 1,500 times faster in computing chemistry than a skeletal mechanism (Yang and Pope 1998b).

2.2.9 Recent Improvements to the Manifold Method

New strategies have been developed to overcome some of the shortcomings of the original ILDM method. The drawbacks to the original ILDM method are (Yang and Pope 1998b):

- The entire state space must be calculated for a fixed dimensional manifold.
- The storage space required to record the manifold can be very large and increases dramatically for higher-dimensional manifolds.
- For higher-dimensional manifolds, the work to retrieve information is not trivial.

To overcome these shortcomings, the method of *In Situ* Adaptive Tabulation in Principal Directions (ISAT) was created (Yang and Pope 1998b). The ISAT method operates under the same principles as the ILDM method, but it calculates and stores a full-dimensional manifold during the reacting flow calculation. Thus, only areas of the state space that are accessed are included in the manifold. Unlike the ILDM approach, the dimension of the manifold is not reduced. All dimensions are stored (up to 20 species). Even with the increased dimensions, a reduction by a factor of 1000 in computational effort can still be observed (Pope 1997).

Another technique to overcome the drawbacks of the standard tabulation method is to store the manifold as a piecewise polynomial. As a polynomial, only the coefficients to the polynomial need to be stored. For a test case, this method reduces the storage requirements of the manifold by a factor of 100 compared with the storage requirements for individual points (Niemann, Schmidt, and Maas 1997).

Chapter 3 Manifold Generation for Gaseous HMX

One of the major challenges for the ILDM method has proved to be the application of the theory to actual systems. The developers of the method have shown success of the method for laminar and turbulent flame calculations (Maas and Pope 1992a, Maas and Pope 1994, Yang and Pope 1998a, Yang and Pope 1998b, Norris and Pope 1995, Maas and Pope 1992b). The University of Utah C-SAFE developers have also used the ILDM approach in a CFD simulation of a heptane pool fire (C-SAFE Program 2001).

As stated previously, the goal of C-SAFE is the simulation of the heat-up and pressurization of a container engulfed in a pool fire. Currently, the pool fire simulation and the container simulation are performed independently. Within the container, a global mechanism is used to model the gas-phase reactions of HMX combustion.

A major development towards tighter coupling between the container dynamics and the pool fire codes would be to include a more detailed model of the gas-phase HMX chemistry inside the container. This would provide a more fundamental representation of the gas-phase chemistry with respect to pressurization.

The ILDM method is an attractive alternative to detailed kinetics in the container calculations. A three-dimensional (based on mixture fraction, enthalpy, and the mass fraction of CO2 +CO) manifold is already used to characterize the gas-phase reactions and soot chemistry in a turbulent heptane pool fire (C-SAFE Program 2001). Based on the success of the ILDM approach for hydrocarbon chemistry, it was proposed to simplify the high explosive chemistry with the same approach. The following section describes the generation of the HMX manifold that will be used in the simulation of the gas phase of the container.

3.1 Manifold Generation

There are six steps to the generation of a fixed-dimensional manifold: selecting the dimension, generating starting points in the composition space, tracking each starting point to equilibrium, identifying the manifold, choosing the parameterization, and storing the manifold.

3.1.1 Dimension of the Manifold

The dimension of the manifold has been investigated through an eigenvalue analysis of the Jacobian (a matrix formed during the iterative Newton's method). The number of eigenvalues that have a real portion greater than $-1/\tau_{\text{flow}}$ determines the dimension of the manifold. For gaseous HMX, an eigenvalue analysis could not be performed because of numerical errors in calculating the eigenvalues. An analysis of the Jacobian revealed that many of the array values approach zero while others are very large. These numerical errors lead to extraneous eigenvalues. Because the eigenvalue analysis did not reveal adequate information about the system, the dimension of the manifold was initially fixed to three (enthalpy, pressure, and mass fraction of N_2). Later, a four-dimensional manifold was developed (mass fraction of NO added) to increase the accuracy.

3.1.2 Starting Points in the Composition Space

To generate starting points in the composition space, all but one of the parameters must be held constant. For the adiabatic batch reactor combustion code, enthalpy and pressure were held constant. The other parameters (Y_{N2} and Y_{NO}) were recorded as the simulated reactions proceeded. In the simulation, radicals were introduced to initiate the reaction. The generation of radicals was simulated in an adiabatic Perfectly Stirred Reactor (PSR).

A PSR code was developed by Glarborg et. al. (Glarborg, Kee, Grcar, and Miller 1992). Differing residence times for the PSR were attempted. However, because the HMX reaction time scales are extremely fast, only fully reacted HMX or totally unreacted HMX resulted. To generate sufficient radicals, fully reacted HMX were used. These simulated reacted gases from the PSR were then mathematically mixed (in a subroutine separate from the PSR code) in proportions of 5%, 20%, 35%, 50%, and 65% with unreacted HMX on a mass basis according to the following equation:

$$Y_j = Y_{PSR_j}(1 - f_{\text{Reactants}}) + Y_{\text{Reactants}_j} f_{\text{Reactants}} \tag{2}$$

where j is an index number for each species, Y is the mass fraction, Y_{PSR} is the mass fraction of PSR products, $Y_{\text{Reactants}}$ is the species mass fraction in the unreacted feed, and $f_{\text{Reactants}}$ is the fraction of unreacted feed that is mixed with the PSR products.

After the mass fractions were evaluated, the temperature of the new mixture was computed in a subroutine separate from the PSR code. Since the PSR is specified as an adiabatic reactor, the products of the PSR had the same enthalpy as unreacted HMX. Therefore, the mixture of PSR products and unreacted HMX had a known enthalpy. By this means, the temperature of the mixture was solved iteratively. The secant method

(Burden and Faires 1997) was used to find the temperature with the initial guess midway between the high temperature of the PSR products and the low temperature of the reactants. Generally, the temperature met a 10^{-11}K convergence criteria in fewer than 10 iterations.

3.1.3 Reaction Progression

The calculated mixture of PSR products and unreacted HMX is the simulated input stream to an adiabatic batch reactor program. Figure 5 illustrates the flow of a trajectory calculation from the simulated initial reactants, through the simulated PSR, and finally to the simulated batch reactor.

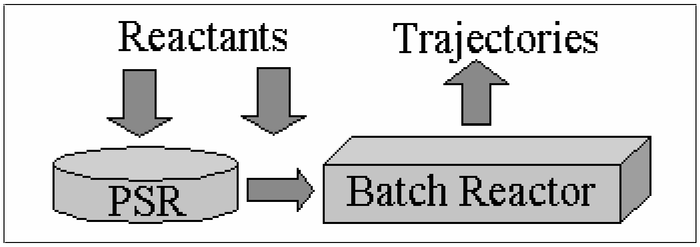

Figure 5 - Reaction Path for Manifold Generation

The simulations use the Chemkin-II subroutines developed at Sandia National Laboratories (Kee, et. al. 1989) to calculate thermodynamic and kinetic properties. In order to use the Chemkin Subroutine Library, a Chemkin link file must be created (see Figure 6).

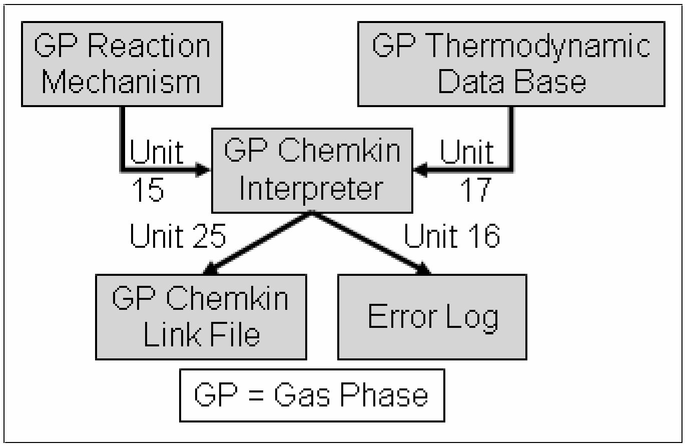
GP Reaction Mechanism
GP Thermodynamic Data Base
Unit 15
GP Chemkin Interpreter
Unit 17
Unit 25
Unit 16
GP Chemkin Link File
Error Log
GP = Gas Phase

Figure 6 – Generating a Gas Phase Chemkin Link File

After the Chemkin link file is created, the manifold can be automatically generated (see Figure 7).

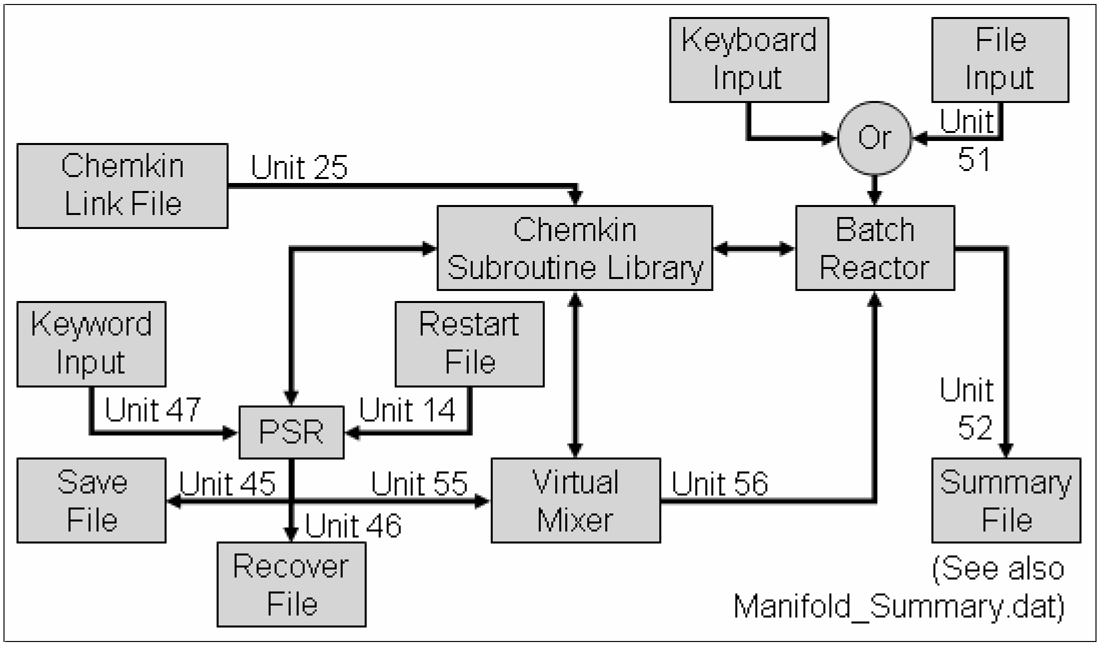
Keyboard Input
File Input
Or
Unit 51
Chemkin Link File
Unit 25
Chemkin Subroutine Library
Batch Reactor
Keyword Input
Restart File
Unit 47
PSR
Unit 14
Unit 52
Save File
Unit 45
Unit 55
Virtual Mixer
Unit 56
Summary File
Unit 46
Recover File
(See also Manifold_Summary.dat)

Figure 7 – Manifold Generation

In the simulated batch reactor, mass fractions of the species, temperature, reaction rate of the species, entropy, and enthalpy were computed starting at the initial time and stepping forward until equilibrium is reached. The progression towards equilibrium forms a trajectory when plotted against time. Figure 8 shows an example of the mass fraction of CO_2 plotted against time for three different initial compositions at the same enthalpy, pressure, and elemental composition.

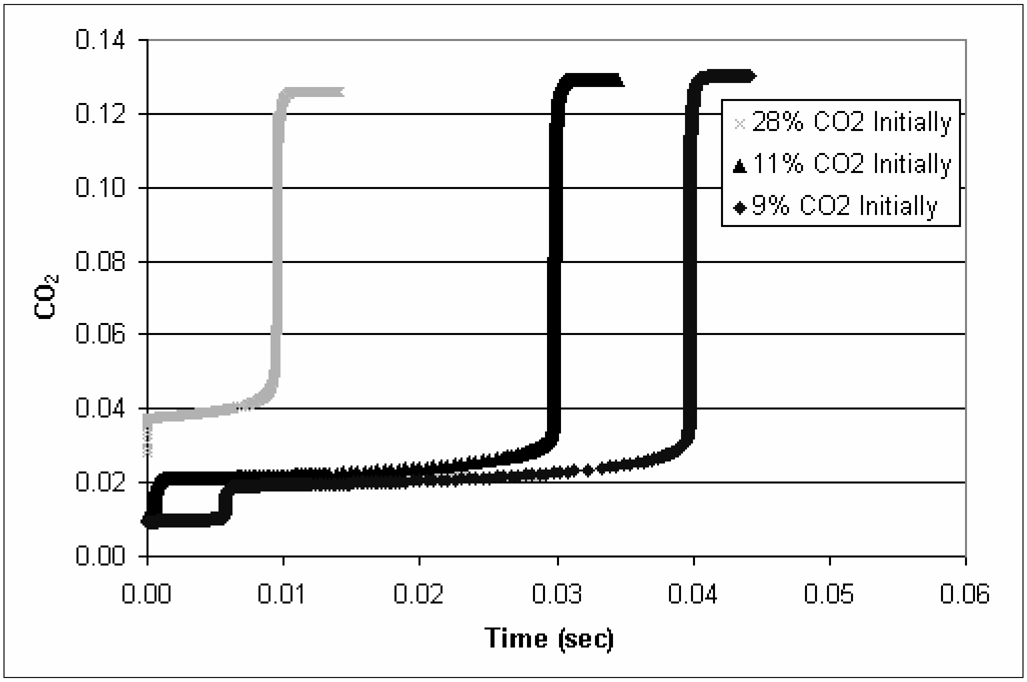

Figure 8 - Batch Reactor Results

Each point on the graph represents a time instance where all of the state space is computed and recorded. Initially, the time step must be set by the user to be small to account for fast reactions and to avoid errors in the numerical integrator. The original batch reactor program only allowed for a constant time step equal to the smallest time step during the entire calculation. Therefore, the batch reactor program was modified to allow for changing time steps. The original program stopped when the numerical integrator (DVODE) returned an error. Instead of stopping the execution of the program, the modified program retries the numerical integration with a lower time step. If a certain number of numerical integrations have passed since an error, then the time step is increased. This modification speeds up the calculation by many orders of magnitude without affecting the accuracy of the calculation.

3.1.4 Manifold Identification

During the course of a batch reactor simulation, the calculated species, temperature, and reaction rates are stored in data files. These data files are analyzed to identify the ILDM.

3.1.4.1 Graphical Method

Figure 9 shows an example of the graphical method for identifying the lower-dimensional manifold. Each trajectory represents a separate simulation performed in an adiabatic batch reactor. Each starting point represents a different percentage of unreacted HMX mixed with products of HMX combustion from a simulated PSR. The values in the legend refer to the percent of unreacted HMX (see Equation 2). In this case, entropy is plotted against the calculated mass fraction of N_2. The initial temperature of the unreacted HMX gas is 127 °C and the pressure is 20 atm. All the trajectories are attracted towards the manifold and end at the point that represents equilibrium.

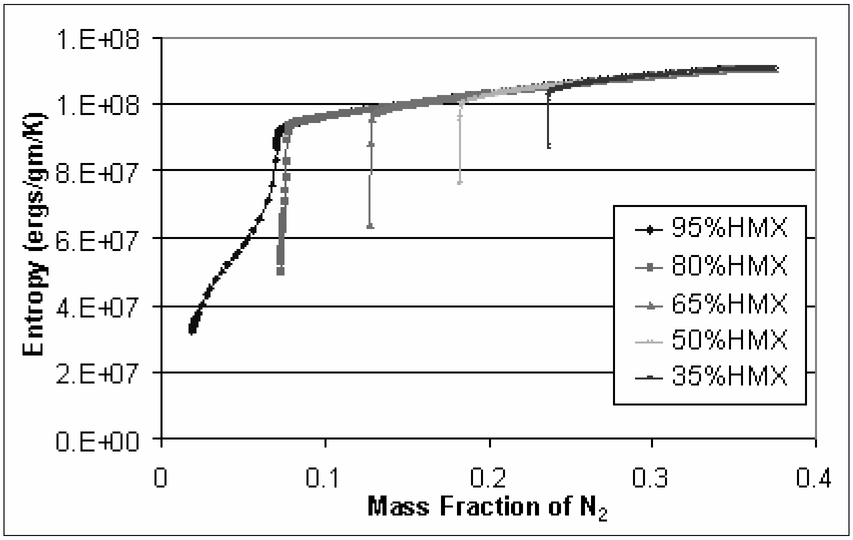

Figure 9 - Portion of HMX Manifold

To generate a complete manifold, the pressure and enthalpy must be varied over a range necessitated by the state space of the combustion system that will employ the manifold. With each change in pressure or enthalpy, a separate graph is generated, analogous to Figure 9. Additional graphs can be made for all the species and temperature as a function of N_2 mass fraction. These graphs can aid in identifying the ILDM.

3.1.4.2 Eigenvector Analysis

An eigenvector analysis requires more development time but results in a more automated system for selecting a manifold. The eigenvector analysis allows for the calculation of only one trajectory and identifies when that trajectory reaches the manifold. For this project, the graphical method for selecting the manifold was employed, so an eigenvector analysis was not developed.

3.1.5 Choice of Parameterization

Three (enthalpy, pressure, and mass fraction of N_2) or four (enthalpy, pressure, and mass fraction of N_2 and NO) parameters were chosen as dependent variables of the manifold. Therefore, if these three or four parameters are known, all other species concentrations are also known.

A special requirement of one of the species progress variables is that it must be monotonically increasing or decreasing in the area of the manifold. Additional species progress variables must also meet this specification if aliasing occurs. Major products (i.e. N_2, CO_2, H_2O) are often considered as the first species progress variable instead of intermediates (i.e. NO, CO, HCN).

3.2 Manifold Storage and Retrieval

Once the manifold is identified, it is stored in a data file for future use in a combustion code. Because the project uses computers with varying operating systems, the files are stored in ASCII format instead of binary.

At runtime, the data files are loaded into arrays within the combustion application. A multivariable linear interpolator looks up values in the tables based on enthalpy, pressure, and mass fractions of N_2 and NO. One of the challenges to the retrieval process is accounting for values that are outside of the manifold state space. For example, at a pressure of 20 atm and an enthalpy of 10^{10} erg/gm, the lowest accessible value for mass fraction of N_2 may be 0.10. What values are returned when the code attempts to access 0.05 for a mass fraction of N_2? Blasenbrey, et. al. suggest a linear extrapolation between the lowest available value and the initial concentration (Blasenbrey, et. al. 1998). Another option is to include reaction trajectories that have not reached the manifold. The latter option was implemented in this project because it represents more realistic conditions for the simulated reactions.

Chapter 4 3-D Manifold Validation with 1-D Simulation

In order to validate the effectiveness of the HMX manifold, results from a full kinetic mechanism and a manifold approach are compared in a one-dimensional (in space) combustion code. The code that is used to test the manifold includes a condensed (solid and liquid) phase and a gas phase (Davidson 1996). The one-dimensional combustion model is simplified further with a steady-state assumption by specifying that the liquid-gas interface as stationary. In such a Lagrangian reference, the simulated combustion products move through advection. With high advection, diffusion is assumed to be negligible. Figure 10 shows how the ILDM replaces the full kinetics calculation in the 1-D, steady-state laminar simulation.

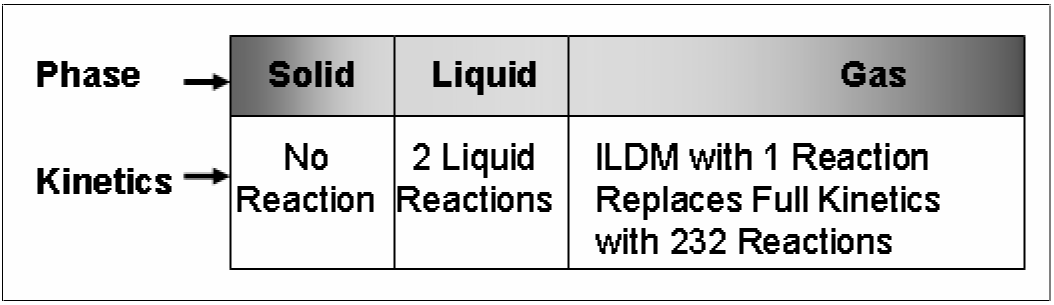

Phase →	Solid	Liquid	Gas
Kinetics →	No Reaction	2 Liquid Reactions	ILDM with 1 Reaction Replaces Full Kinetics with 232 Reactions

Figure 10 - ILDM Implementation into 1-D, Steady-State Laminar Simulation

In addition to the gas phase Chemkin link file (see Figure 6), a condensed phase Chemkin link file (see Figure 11), and a transport properties Chemkin link file (see Figure 12) must be created.

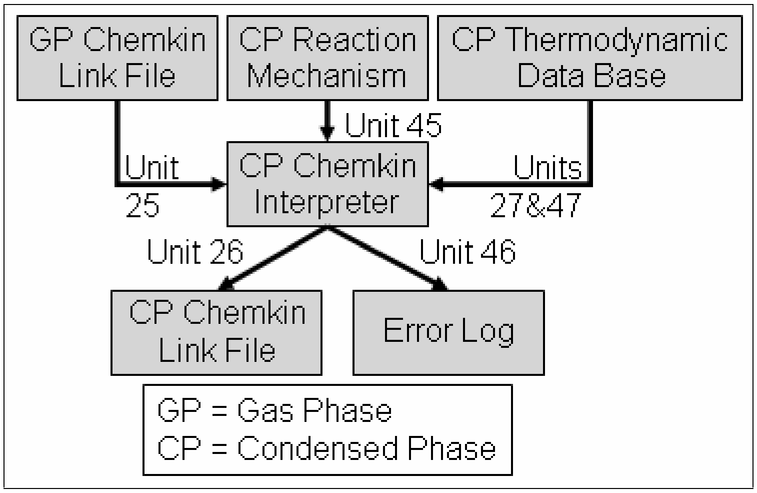
GP Chemkin Link File
CP Reaction Mechanism
CP Thermodynamic Data Base
Unit 45
Unit 25
CP Chemkin Interpreter
Units 27&47
Unit 26
Unit 46
CP Chemkin Link File
Error Log
GP = Gas Phase
CP = Condensed Phase

Figure 11 – Generating a Condensed Phase Chemkin Link File

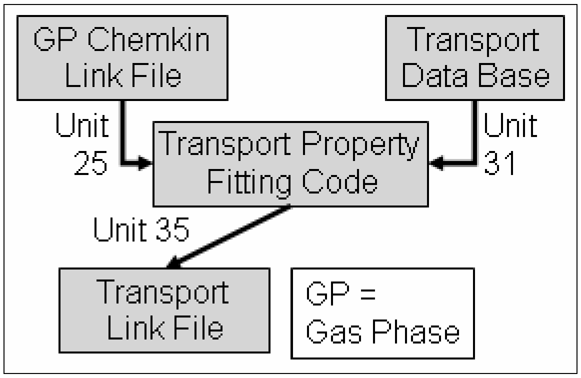
GP Chemkin Link File
Transport Data Base
Unit 25
Transport Property Fitting Code
Unit 31
Unit 35
Transport Link File
GP = Gas Phase

Figure 12 – Generating a Transport Properties Chemkin Link File

Once the required link files are created, the 1-D, steady-state laminar simulation can be run (see Figure 13).

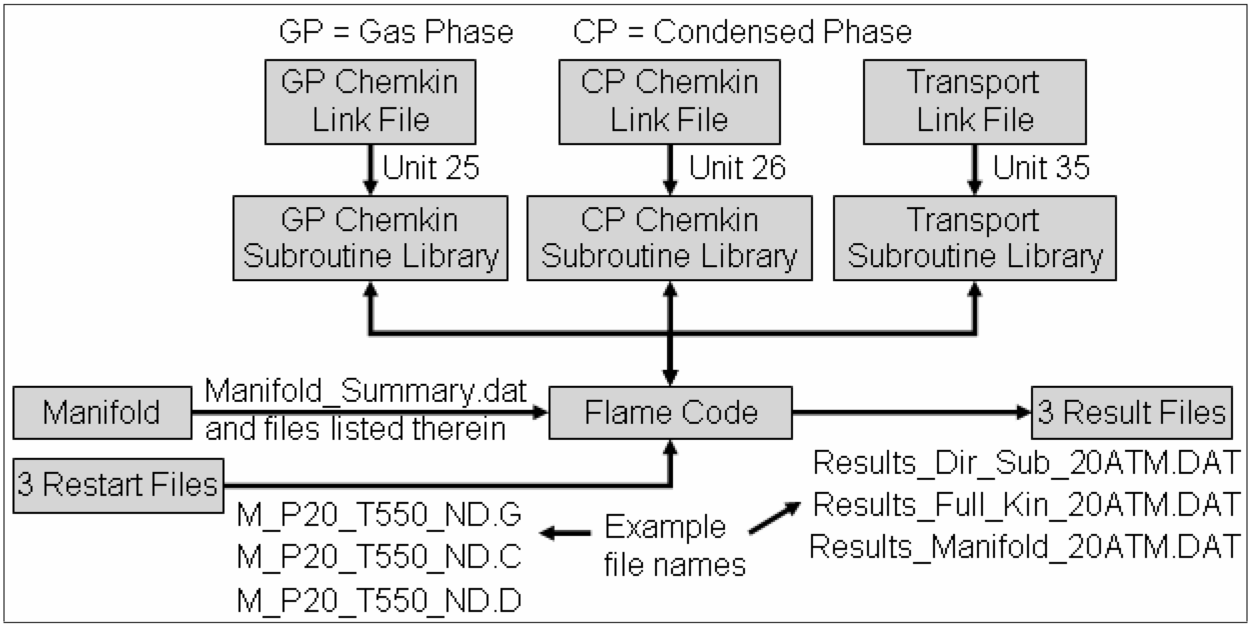
GP = Gas Phase
CP = Condensed Phase
GP Chemkin Link File
CP Chemkin Link File
Transport Link File
Unit 25
Unit 26
Unit 35
GP Chemkin Subroutine Library
CP Chemkin Subroutine Library
Transport Subroutine Library
Manifold
Manifold_Summary.dat and files listed therein
Flame Code
3 Result Files
3 Restart Files
Results_Dir_Sub_20ATM.DAT
Results_Full_Kin_20ATM.DAT
Results_Manifold_20ATM.DAT
M_P20_T550_ND.G
M_P20_T550_ND.C
M_P20_T550_ND.D
Example file names

Figure 13 – 1-D, Steady-State Laminar Simulation

Since the calculation of the gas phase kinetics typically requires more than 99% of the CPU time, the manifold is only used to simplify the calculation of the gas-phase reactions. The three result files are the solutions to direct substitution of the manifold (using the full kinetics solution of enthalpy and mass fraction of N_2), full kinetics, and iterative solution of the manifold.

4.1 3-D Manifold Direct Substitution

A quick check to see how well the manifold follows the detailed kinetics is to substitute manifold values for detailed kinetics values. The final solution of enthalpy and mass fraction of N_2 from the detailed kinetics calculation is used to look up manifold values. Figure 14 shows the concentration of CO_2 versus distance from the surface.

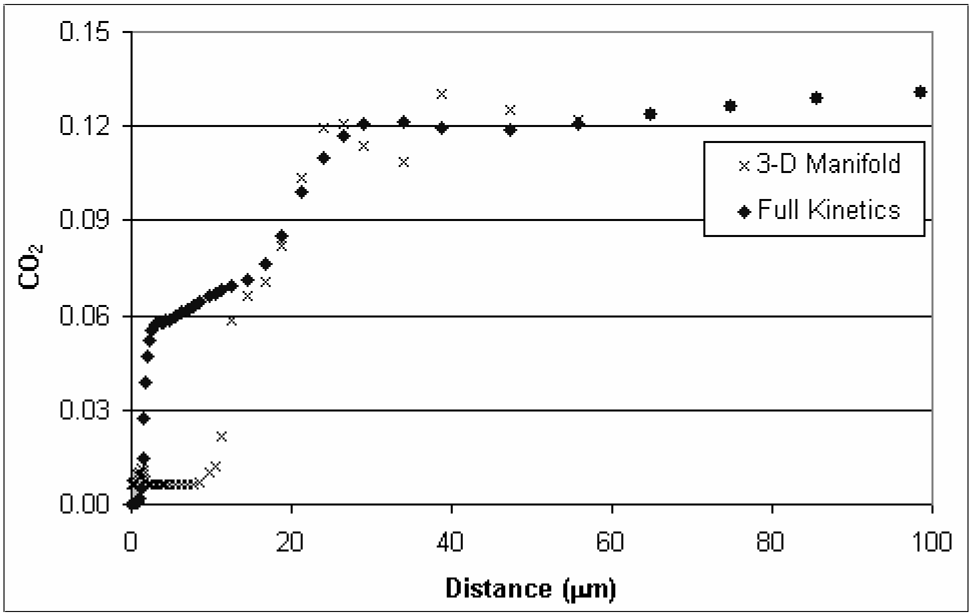

Figure 14 – Direct Substitution of 3-D Manifold

Near the surface (0 to 60 μm) the manifold does not agree with the detailed kinetics while away from the surface (60 μm to infinity) the two are exactly equal. This is due to the varying time scales along the flame. The time scale of the one-dimensional flow is computed by the following equation:

$$\tau_{flow} = \frac{\Delta \text{distance}}{\text{velocity}} \qquad (3)$$

Figure 15 shows the time scale versus distance.

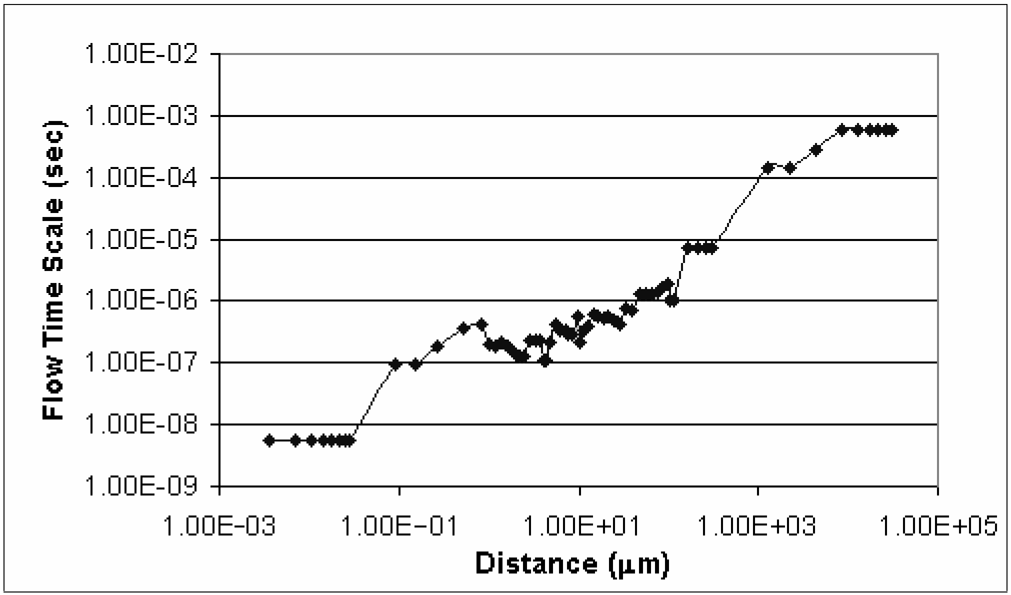

Figure 15 - Flow Time Scale

Because the time scale is so small near the surface, a higher-dimensional manifold should be used to get accurate results. As long as a sufficiently high dimension of the manifold is used, the manifold should accurately represent the detailed kinetics everywhere.

4.2 3-D Manifold Implementation in 1-D Laminar Simulation

Using detailed kinetics requires the solution to the energy equation and to the continuity equations. For HMX, this means that 45 ordinary differential equations must be solved. Using a low-dimensional manifold reduces the number of dependent variables. The number of differential equations that must be solved is equal to the dimension of the manifold. For example, using a 4-D manifold means that only 4 ordinary differential equations must be solved.

4.2.1 The Equations

In an isobaric simulation, the HMX manifold is only a function of enthalpy and mass fraction of N_2. Therefore, the equations that best describe the chemistry are the energy equation in the enthalpy form and the continuity equation for N_2. The energy equation in the enthalpy form is:

$$n_{mass} \frac{dH}{dx} = \frac{d}{dx} k \frac{d}{dx} T \tag{4}$$

(where H is enthalpy, n_{mass} is the mass flux, k is the thermal conductivity, and T is the temperature). The N_2 continuity equation is:

$$n_{mass} \frac{d}{dx} Y_{N_2} = \omega_{N_2} W_{N_2} \tag{5}$$

(where Y_{N2} is the mass fraction of N_2, ω_{N2} is the reaction rate of N_2, and W_{N2} is the molecular weight of N_2).

4.2.2 Discretization of the Equations

The enthalpy equation and N_2 continuity equation are discretized using the control volume layout as shown in Figure 16.

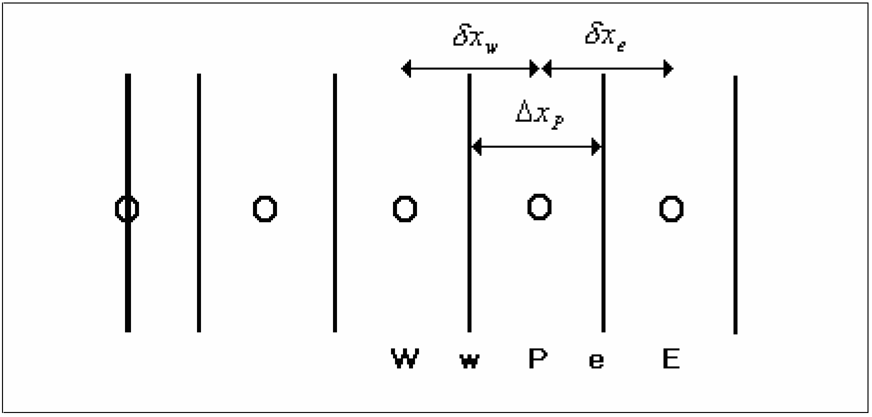

Figure 16 - Control Volume Layout

The control volume approach integrates the equations over a distance from e (east) to w (west). Using the control volume approach and integrating between the control surfaces for P, the energy equation becomes

$$n_{mass}(H_e - H_w) = k_e\left(\frac{dT}{dx}\right)_e - k_w\left(\frac{dT}{dx}\right)_w \tag{6}$$

and the N_2 conservation equation becomes

$$n_{mass}(Y_{N2_e} - Y_{N2_w}) = \varpi_P \cdot W_P \cdot \Delta x_P \tag{7}$$

where Δx_P is the distance across the control volume for P from e to w.

Assuming a linear temperature profile between nodes, using an under-relaxation parameter ($\alpha < 1$) to ensure the stability of the solver, and using an upwind scheme (valid for high Peclet numbers) the enthalpy equation becomes

$$H_{P,i} = H_{P,i-1} + \alpha\left[\frac{\left(n_{mass} \cdot H_{W,i} + \left(k_e \cdot \frac{T_E - T_P}{\delta x_e} - k_w \cdot \frac{T_P - T_W}{\delta x_w}\right)\right)}{\frac{n_{mass}}{\alpha}} - H_{P,i-1}\right] \tag{8}$$

and the N_2 conservation equation becomes

$$Y_{N2_{P,i}} = Y_{N2_{P,i-1}} + \alpha\left[\frac{\left(n_{mass} \cdot Y_{N2_{W,i}} + (\omega_P \cdot W_P \cdot \Delta x_P)_{i-1}\right)}{\frac{n_{mass}}{\alpha}} - Y_{N2_{P,i-1}}\right] \tag{9}$$

where the subscript (i) denotes the current iteration value and the subscript (i-1) denotes the value from the previous iteration.

4.2.3 Iterative Solving Routine

Both of the discretized equations are explicit in time and distance yet the overall solving routine is implicit. The overall solving routine is iterative because the manifold is a function of both enthalpy and the mass fraction of N_2. Once the enthalpy profile is calculated, the mass fraction profile of N_2 is calculated. This iterative process repeats until the solution converges (see Figure 17).

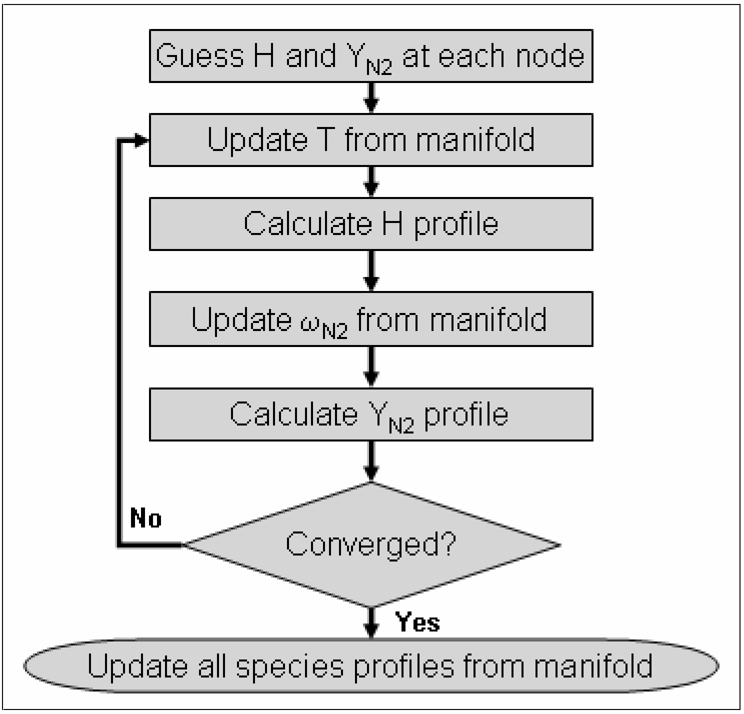
Guess H and Y_{N2} at each node
Update T from manifold
Calculate H profile
Update ω_{N2} from manifold
Calculate Y_{N2} profile
No
Converged?
Yes
Update all species profiles from manifold

Figure 17 - Iterative Solving Procedure

An interesting characteristic of the manifold solution is that the mass fraction of N_2 and enthalpy continue to oscillate slightly around a solution but never stabilize to a fixed solution. This is due to the discontinuities in the reaction trajectories when they have not reached the manifold. Figure 18 shows the last iteration of 1000 total iterations versus the temperature averaged over the last 100 iterations for grid spacing at 6 μm.

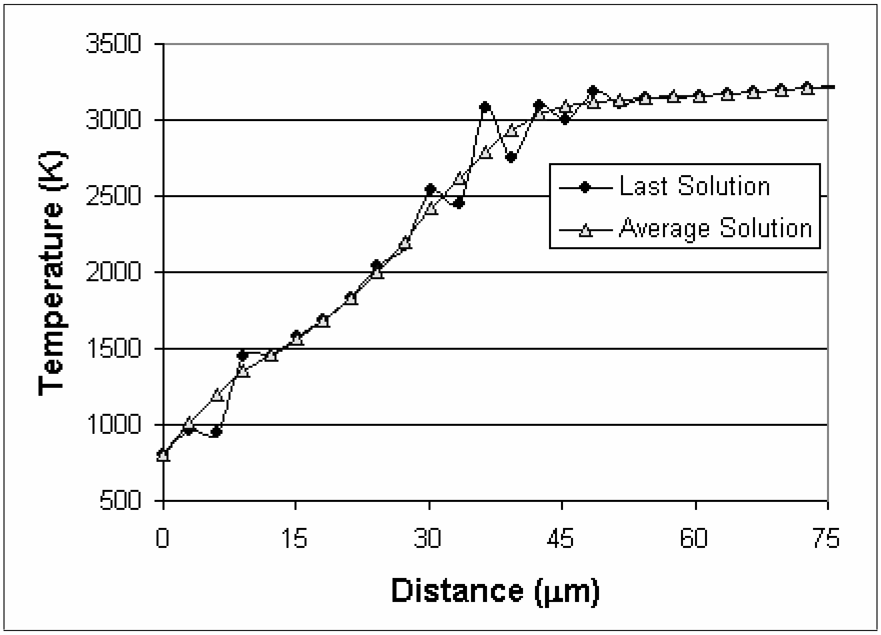

Figure 18 - Oscillations in the Final Solution

The averaged solution over the last 100 iterations will be used to ensure physically realistic results and to smooth out the oscillations.

4.2.4 Grid Independent Study

An important aspect of numerical analysis is a grid independent study. Generally, a numerical solution becomes more accurate as more nodes are used. However, using additional nodes also increases the required computer memory and computational time. The appropriate number of nodes can be determined by increasing the number of nodes until the numerical solution changes by less than a specified tolerance. Figure 19 shows the calculated temperature versus distance for the grid independent study. The numbers in the legend refer to the grid spacing.

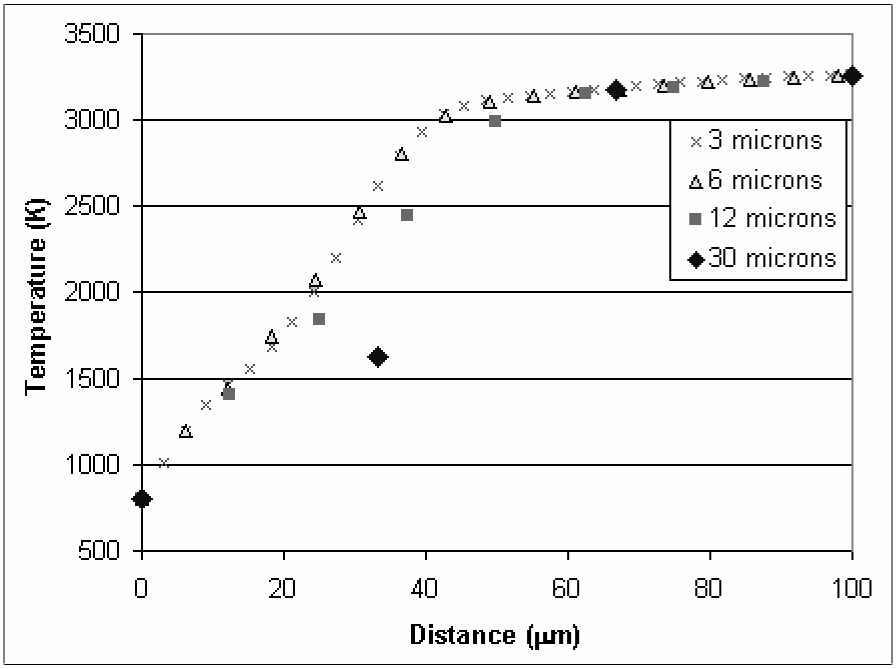

Figure 19 - Grid Independent Study

Grid spacing less than 6 µm gives a grid independent solution. However, decreasing the grid spacing gives increased oscillations during the implicit solving routine. The oscillations are likely the result of using reaction trajectories that have not yet reached the lower-dimensional manifold. Small jumps in the temperature lead to large values of the second derivative for temperature in the enthalpy equation. Large values for the second derivative of temperature leads to large jumps in enthalpy. These big jumps in enthalpy are handled by decreasing the under-relaxation parameter (α) and attempting to solve the equation again. With large jumps the under-relaxation parameter decreases to the point that reaching a converged solution is very computationally expensive. Figure 20 shows the enthalpy profiles for a grid spacing of 3 µm and 0.6 µm.

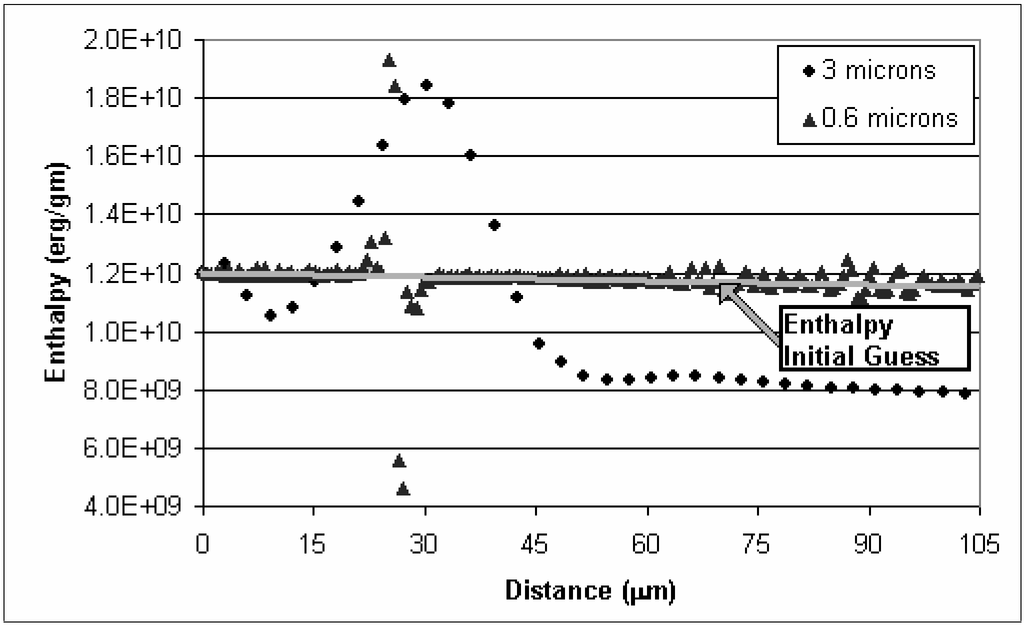

Figure 20 - Grid Independent Study

After 1000 iterations, the final value of the under-relaxation parameter for the enthalpy equation is 0.125 for a grid spacing of 3.0 μm. For a grid spacing of 0.6 μm, the under-relaxation parameter is 6.94 x 10^{-18} for the energy equation in the enthalpy form. With an under-relaxation so low, a converged solution is not reached.

For the purposes of the grid independent study, any grid spacing less than 6 μm will yield a grid independent solution. Any grid spacing less than 0.6 μm requires excessive computational time to get a converged solution. A grid spacing of 3 μm is recommended for the HMX manifold one-dimensional calculations.

4.2.5 Results

One of the advantages of using the ILDM approach over reduced mechanism approaches is that all of the species profiles, even the minor radicals, are calculated. Graphs of all the species profiles are included in Appendix A. To illustrate the capabilities of the ILDM approach, the species profiles of NO, CO_2, H_2O, and the temperature profile for the manifold and full kinetic mechanism are shown in Figures 21 - 24. Reasonable agreement between the 3-D manifold and full kinetics is found beyond 60 µm. Even though it is not shown in the plots, excellent agreement is found beyond 100 µm, as equilibrium is approached.

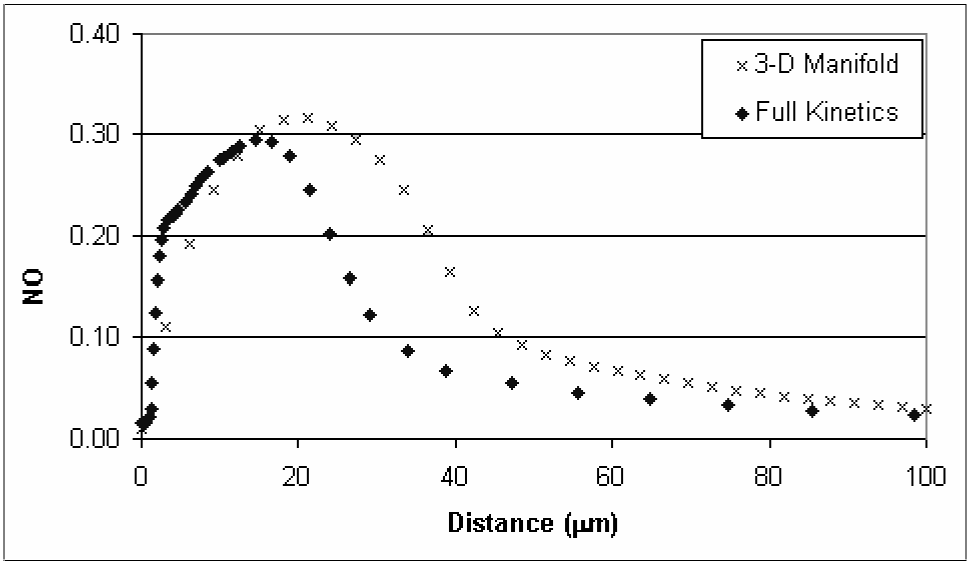

Figure 21 - Results of One-Dimensional, Steady-State Simulation

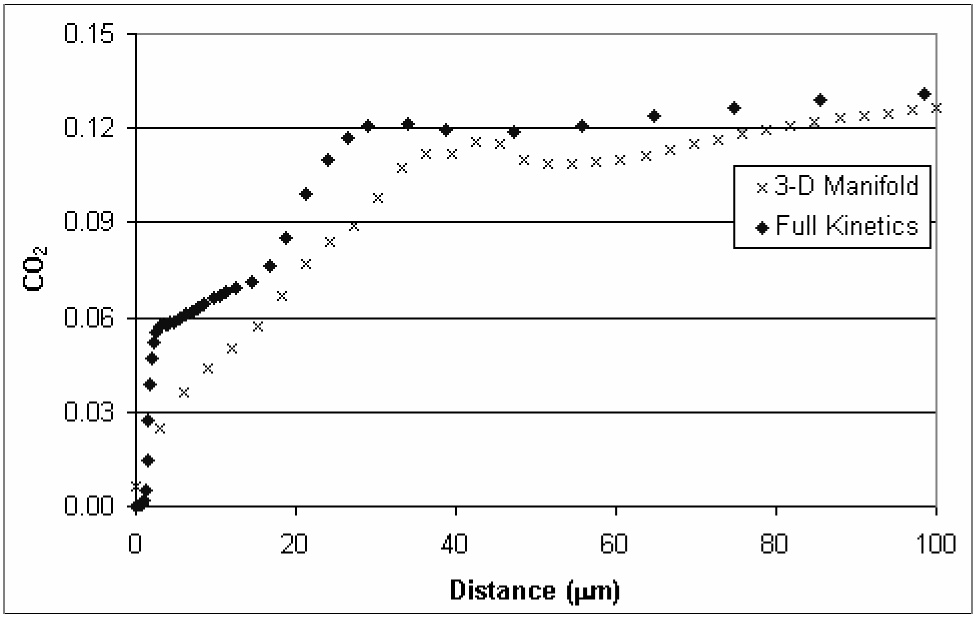

Figure 22 - Results of One-Dimensional, Steady-State Simulation

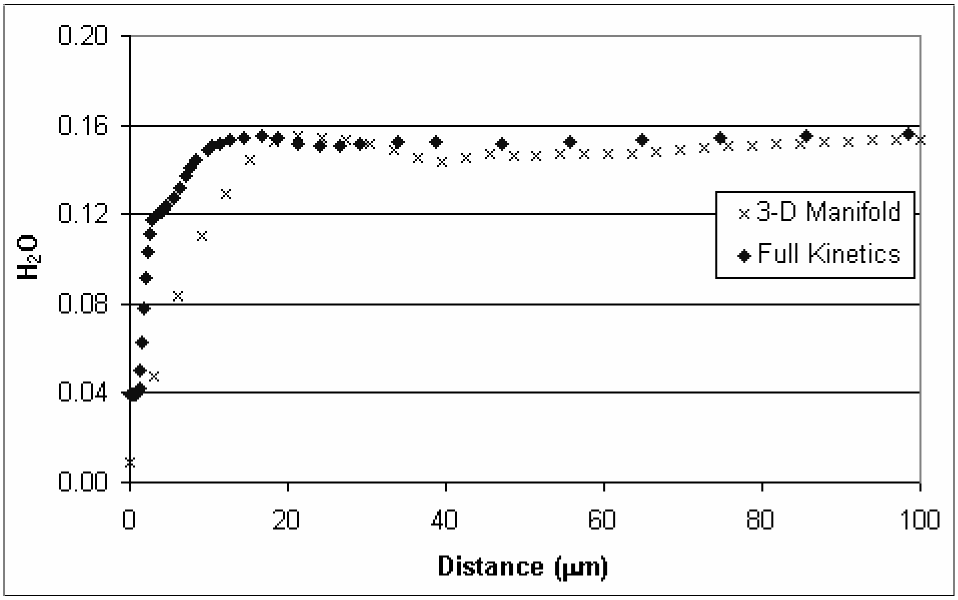

Figure 23 - Results of One-Dimensional, Steady-State Simulation

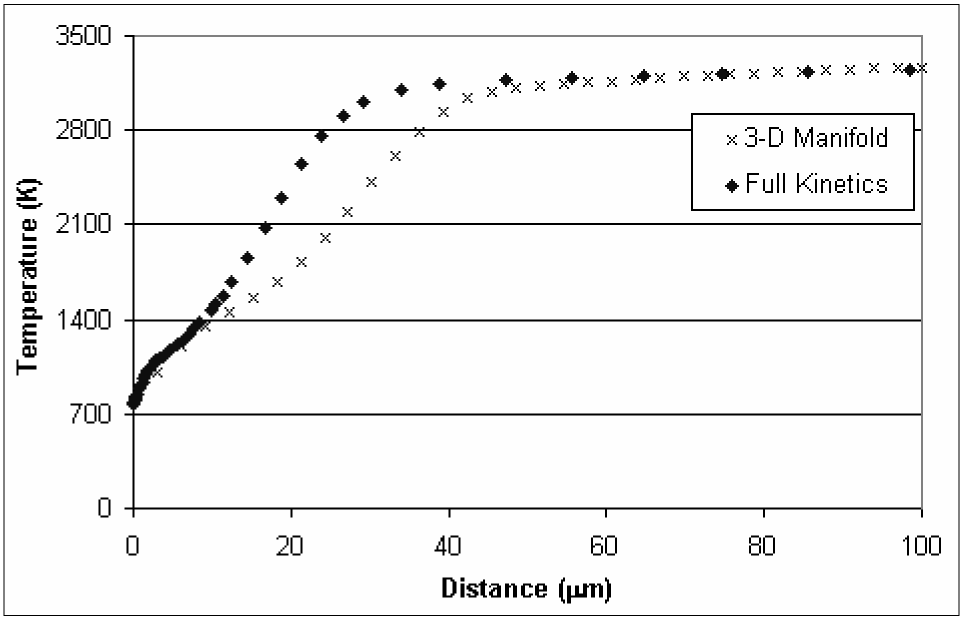

Figure 24 - Results of One-Dimensional, Steady-State Simulation

The manifold lags the detailed mechanism in the formation of the major product species. This is due to a dark zone where NO is the limiting reactant and dominant species near the surface. One method to overcome this lag is to include another species in the manifold, such as the mass fraction of NO. Increasing the dimension of the manifold poses new challenges in the creation and implementation of the manifold. A 4-D manifold is discussed in the next chapter.

Chapter 5   4-D Manifold Validation with 1-D Simulation

An additional reaction parameter can be added to increase the accuracy of the ILDM approximation to the one-dimensional laminar simulation. The addition of another reaction parameter raises the complexity of the ILDM generation, and implementation into a CFD code. Rather than review the complete procedure for the generation and implementation of the 4-D ILDM, only the major additions to the 3-D ILDM approach are discussed.

5.1 4-D Manifold Direct Substitution

An indication of how well the higher-dimensional manifold follows the detailed kinetics is to substitute manifold values at every node using the solution of enthalpy, mass fraction of N_2, and mass fraction of NO from the detailed kinetics calculation. Since the correct solution is already known, there is no reason to approximate the solution. Direct substitution is not used to predict chemical kinetics, only to predict the accuracy of the manifold. The power of direct substitution is that it can give a quick indication of the accuracy of the manifold. Figure 25 shows the concentration of NO versus distance from the surface using the detailed mechanism, 3-D manifold, and 4-D manifold.

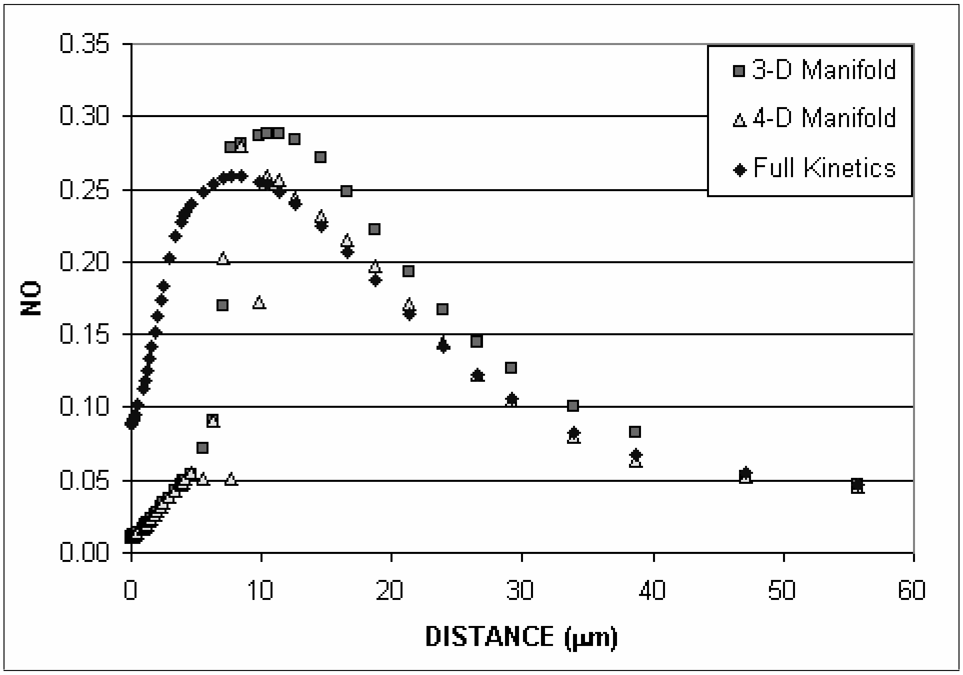

Figure 25 – Full Kinetic Mechanism Compared to Manifold Results

The 3-D manifold agrees with the detailed kinetics above ~60 μm away from the surface (see Figure 21-19). The advantage of the 4-D manifold over the 3-D manifold is that the 4-D manifold is closer to the exact solution from 12 μm and larger. Overall, as the dimension of the manifold is increased, the manifold more accurately represents the detailed kinetics. The 4-D manifold is expected to be more accurate than the 3-D manifold.

5.2 4-D Manifold Implementation in 1-D Laminar Simulation

5.2.1 The Equations

An additional equation (continuity equation of NO) must be solved to implement the 4-D manifold. The 4-D HMX manifold is a function of enthalpy, pressure, mass fraction of N_2, and mass fraction of NO. The equations for enthalpy and mass fraction of

N_2 are the same as those in the 3-D manifold implementation. The additional NO species conservation equation is

$$n_{mass} \frac{d}{dx} Y_{NO} = \omega_{NO} W_{NO} \tag{10}$$

where Y_{NO} is the mass fraction of NO, ω_{NO} is the reaction rate of NO, and W_{NO} is the molecular weight of NO.

5.2.2 Discretization of the Equations

The control volume approach is also used to discretize the NO species equation. The resulting equation is equivalent to the discretized equation for N_2 (see Equation 7) when NO is substituted for N_2.

5.2.3 Iterative Solving Routine

As with the 3-D manifold, the 4-D manifold solving routine is implicit. The 4-D solving routine adds the solution to the NO profile directly after the solution to the N_2 profile. The iterative routine repeats until the solution converges (see Figure 17 and Figure 26).

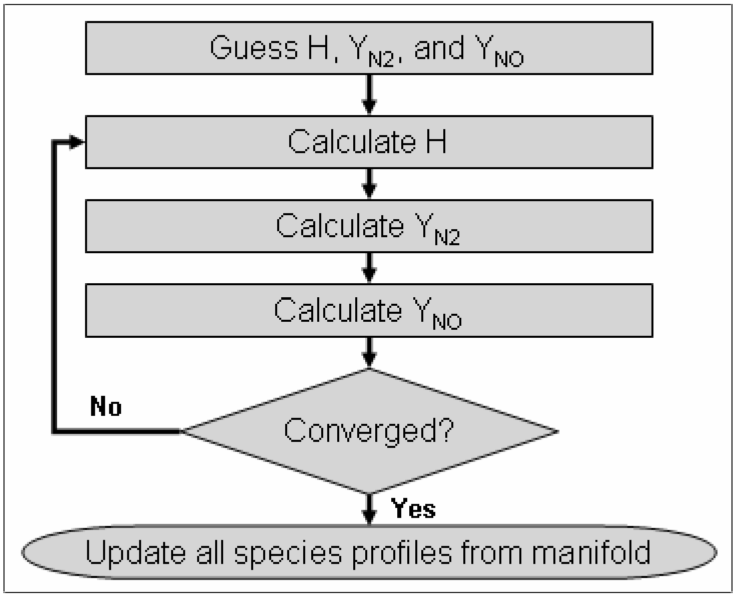
Guess H, Y_{N2}, and Y_{NO}
Calculate H
Calculate Y_{N2}
Calculate Y_{NO}
Converged?
No
Yes
Update all species profiles from manifold

Figure 26 - Iterative Solving Procedure

For the 3-D manifold, an average value was taken to average out an oscillating solution. However, for the 4-D manifold the solution is more stable and therefore, an average value is not necessary.

5.2.4 Grid Refinement for Enthalpy Profile

One of the causes of instability using a 3-D manifold is the enthalpy solution. In the region near the surface where the 3-D manifold does not track the fast kinetics, temperature oscillations result in unrealistic enthalpy values. When unrealistic enthalpy values are computed, the enthalpy equation under-relaxation factor is automatically decreased, and the variables are reinitialized. Without grid refinement, the under-relaxation factor can become so small that a grid independent solution is computationally prohibitive (see Section 4.2.4). To overcome this problem, the iterative solving routine includes a grid-refinement for the enthalpy profile. When an enthalpy profile is outside of the manifold state space, the iterative solving routine is reinitialized with a coarser enthalpy grid. A coarser enthalpy grid reduces the temperature oscillations and decreases the computational cost. The solution procedure with enthalpy refinement is shown Figure 27.

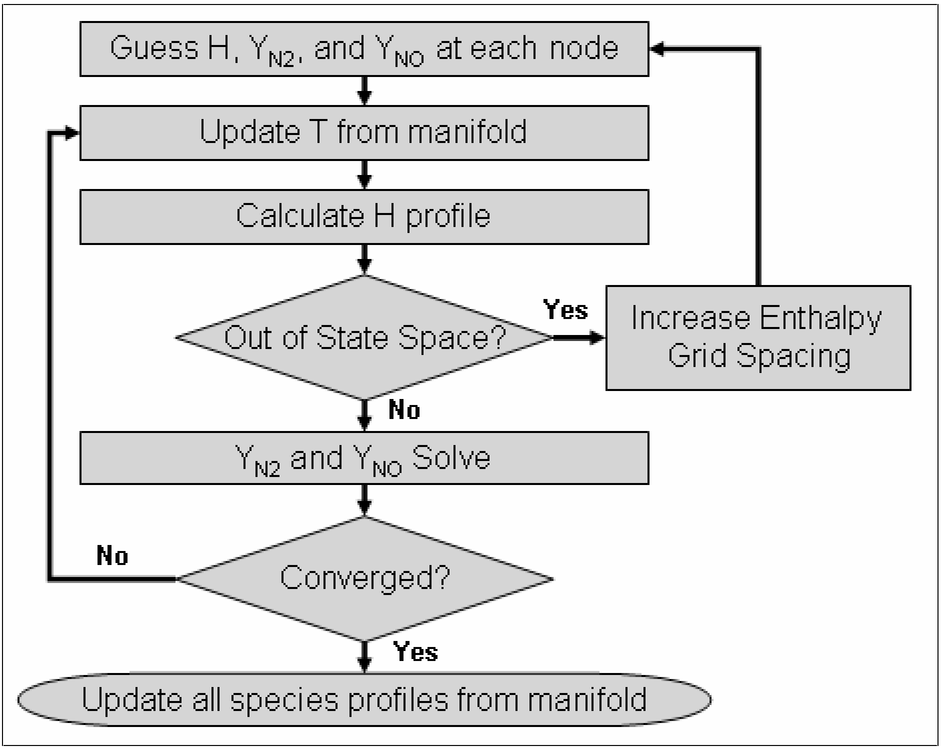
Guess H, Y_{N2}, and Y_{NO} at each node
Update T from manifold
Calculate H profile
Out of State Space?
Yes
Increase Enthalpy Grid Spacing
No
Y_{N2} and Y_{NO} Solve
No
Converged?
Yes
Update all species profiles from manifold

Figure 27 - Data Flow with Enthalpy Grid Refinement

To prevent grid dependent results, a restriction is imposed on the maximum grid spacing of the enthalpy profile. When the enthalpy grid spacing becomes greater than a specified value, the enthalpy grid layout is restored to the original configuration and the under-relaxation factor is decreased. Through a grid independent study, the maximum allowable enthalpy grid spacing at 20 atm was found to be 30 μm.

5.2.5 Grid Independent Study

Figure 28 shows the calculated mass fraction of NO plotted versus distance (up to 20 μm) for the grid independent study. The values in the legend refer to the distance between nodes.

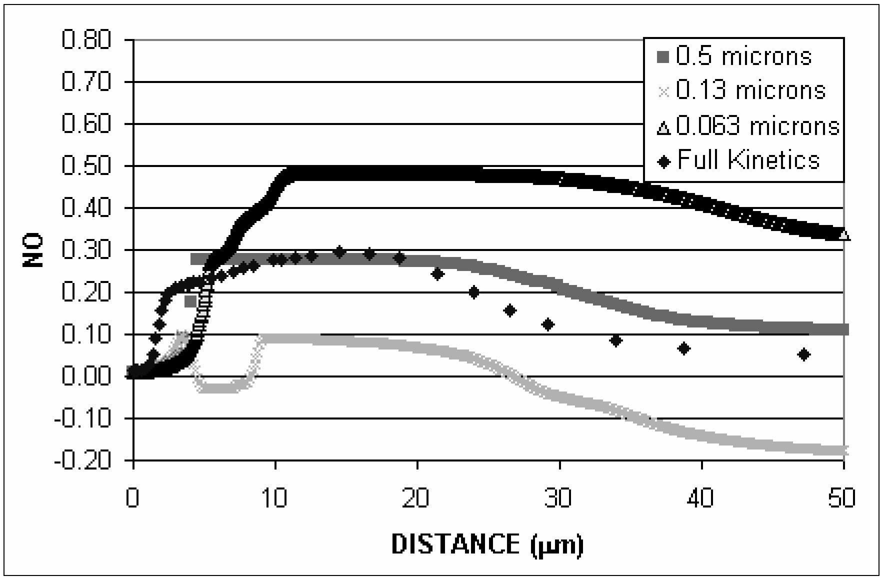

Figure 28 - Grid Independence Study (0-50 μm)

Even with significant grid refinement, the calculated NO profiles of the 4-D manifold solution and full kinetics solution do not produce grid-independent results in the 20 μm nearest the burning surface. This is most likely due to the issue that the 4-D manifold does not describe detailed kinetics in that region. As shown with direct substitution (see Figure 25), the 4-D manifold does not represent the fast reaction kinetics in the near-surface region.

A similar grid refinement study was performed on the region greater than 25 μm (see Figure 29). The idea is to completely skip the region where the NO profile diverges. This is accomplished by using the full kinetics solution at 25 μm as the initial point for the 4-D manifold solution.

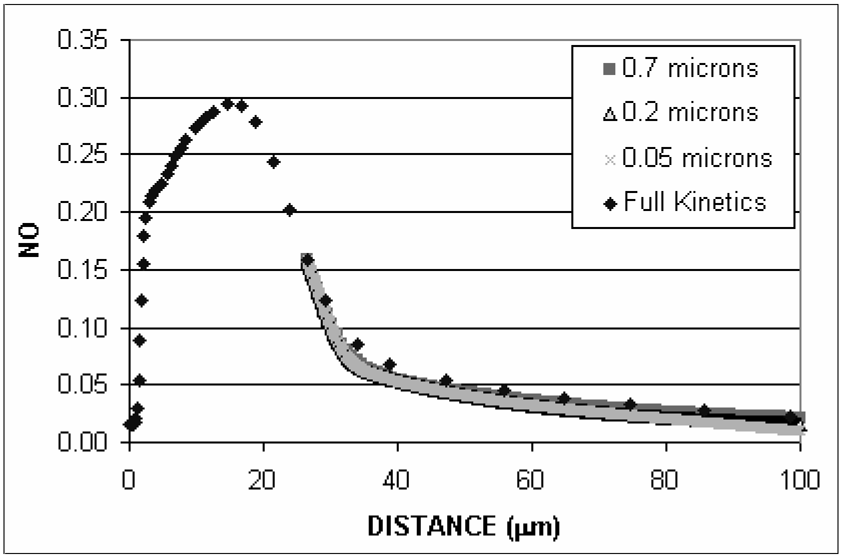

Figure 29 - Grid Independence Study (>25 μm)

When starting the solution at 25 μm, a grid spacing smaller than 0.7 μm appears to be adequate.

5.2.6 A Model for Near-Surface Kinetics

Because the 4-D manifold does not accurately represent fast kinetics near the burning surface, a model based on the full kinetics solution is used, and the 4-D manifold is employed where it accurately represents the full kinetic solution. Figure 30 shows the calculated mass fraction of NO plotted as a function of distance for various starting points using the combined approach. The values in the legend are the distance from the burning surface where the 4-D manifold is used. Based on the grid independent study, the grid spacing is fixed at 0.25 μm.

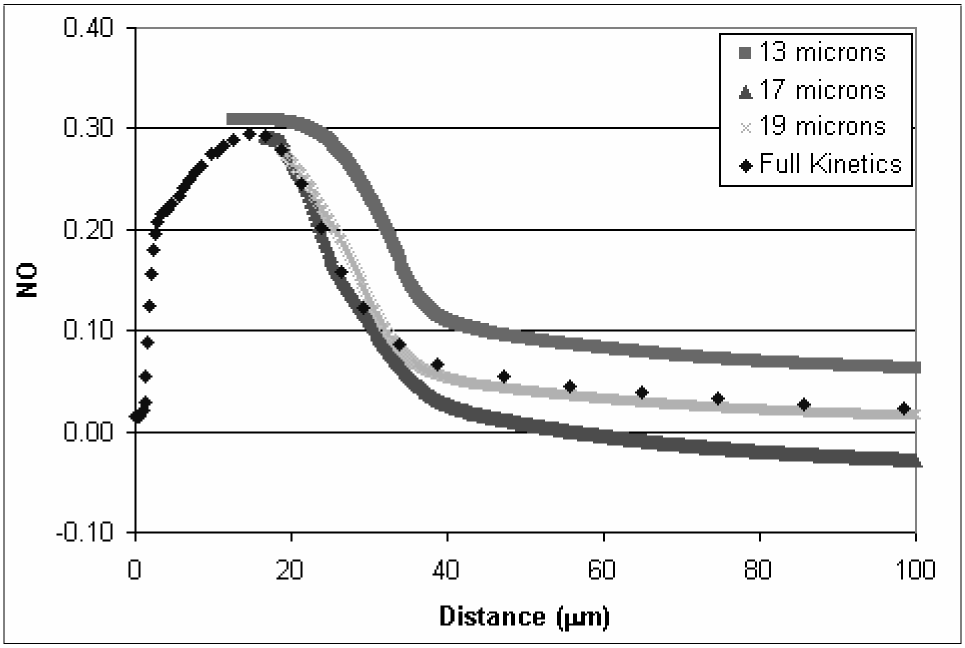

Figure 30 - NO Profile for Various Starting Points at 20 atm

The 4-D manifold accurately represents detailed kinetics beyond 19 μm. Previous results (see Figure 25) suggest good agreement beyond 12 μm. The cause of this 7 μm discrepancy is unknown. Previous results, such as direct substitution, can only suggest an approximate range where the manifold will produce good results. The real test of the 4-D manifold's performance is through an iterative solution as shown in Figure 30.

A challenge for implementing the near-surface model is recognizing the correct point to begin solving with the 4-D manifold. While at 20 atm, a starting point of 19 μm appears to be adequate. However, as pressure changes the starting distance from the surface should change. To evaluate this trend, 4-D manifolds were generated at 5 and 60 atm. Figures 31 and 32 show the results of using these 4-D manifolds in the 1-D, steady-state laminar combustion code. The different curves represent different starting points for the 4-D manifold. Grid spacing of 0.6 μm was used at 5 atm, and 0.1 μm was used at 60 atm for the 4-D manifold solutions.

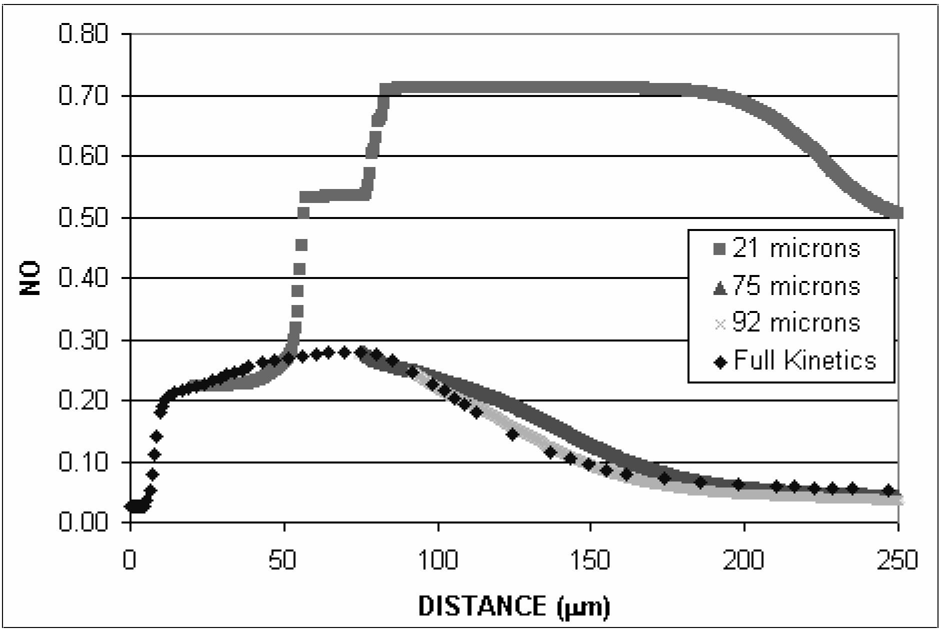

Figure 31 - NO Profile for Various Starting Points at 5 atm

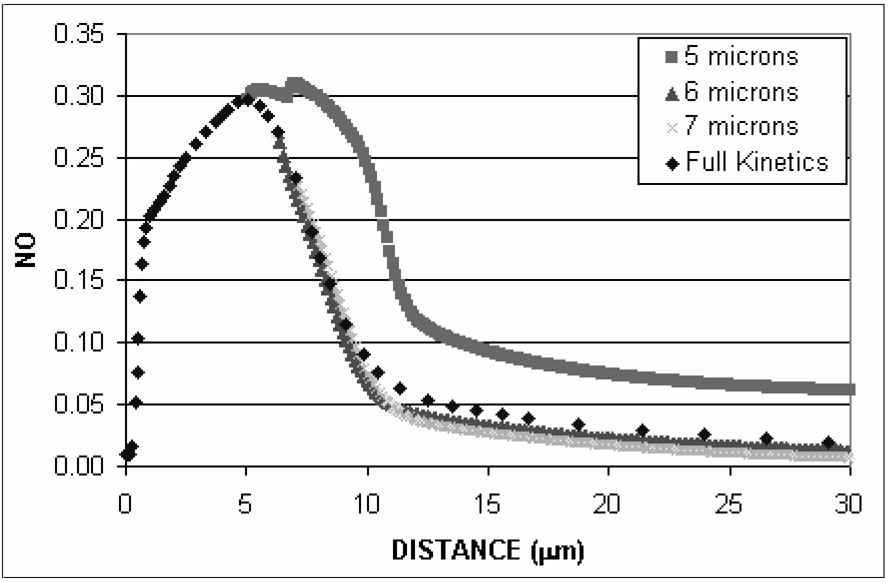

Figure 32 - NO Profile for Various Starting Points at 60 atm

At 5 atm, the 4-D manifold accurately starts at ~92 μm. At 60 atm, the 4-D manifold accuracy is sufficient at ~6 μm. In the region before the 4-D manifold is sufficiently accurate, the NO solution diverges. With an upwind approximation, the "downwind" solution is strongly influenced by deviations "upwind". "Downwind" errors caused "upwind" deviations are apparent in the curve with a starting point at 21 μm (Figure 31) and the curve with a starting point at 5 μm (Figure 32).

One method to approximate the beginning point of the 4-D manifold solution is obtained by observing the enthalpy profile. Figure 33 shows the enthalpy profile at 60 atm. A grid spacing of 0.1 μm was used.

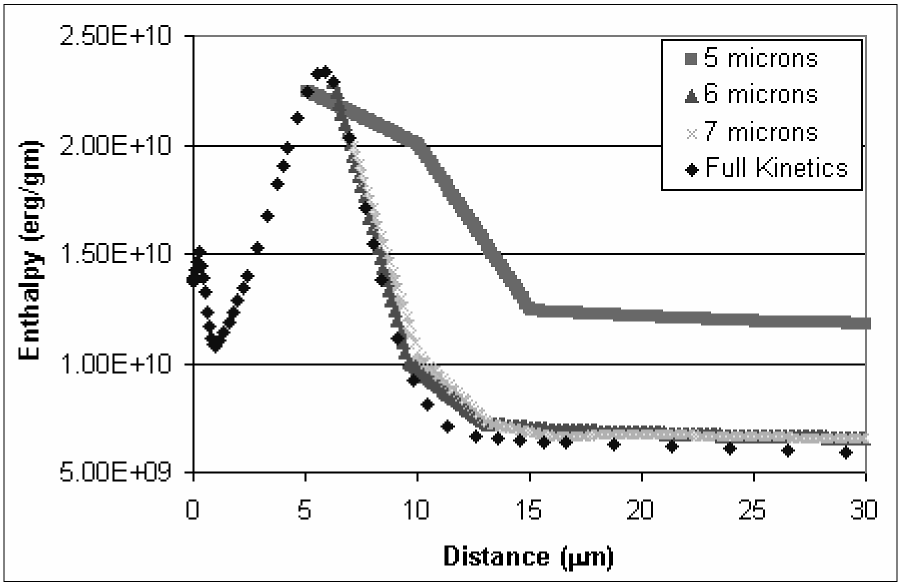

Figure 33 - Enthalpy Profile at 60 atm

At 60 atm the 4-D manifold represents the detailed kinetics after the maximum enthalpy is reached. The curve starting at 5 μm shows major deviations while the curves starting at 6 and 7 μm represent the enthalpy profile reasonably well. The difference is that the latter curves begin after the maximum enthalpy. This same trend holds for 20 atm and 5 atm profiles. Therefore, the near-surface model should extend to the maximum enthalpy and the 4-D manifold should be used thereafter.

5.2.7 Results

To illustrate the capabilities of the 4-D manifold approach with a near-surface model, the species profiles of N_2, CO_2, H_2O, and the temperature profile for the manifold and full kinetic mechanism are shown in Figures 34 - 37. For comparison, the 3-D manifold results are also shown. For the 4-D manifold, the calculations were performed with a grid spacing of 0.25 μm and a starting location of 19 μm. For the 3-D manifold the grid spacing is 3 μm (see Section 4.2.4) and the starting location is 0 μm. All calculations were performed at 20 atm.

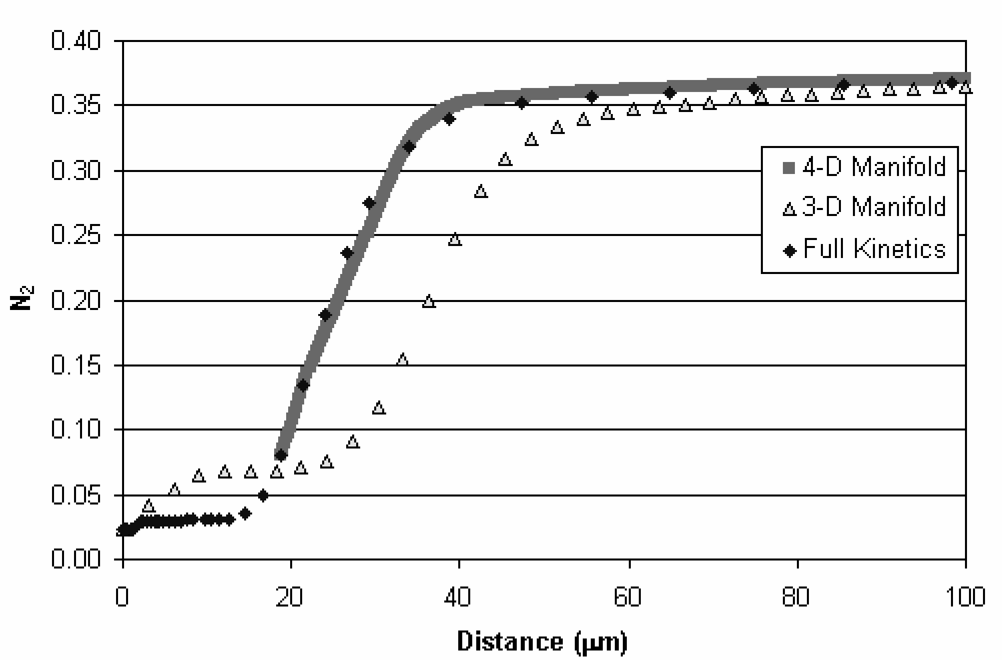

Figure 34 - Results of One-Dimensional, Steady-State Simulation

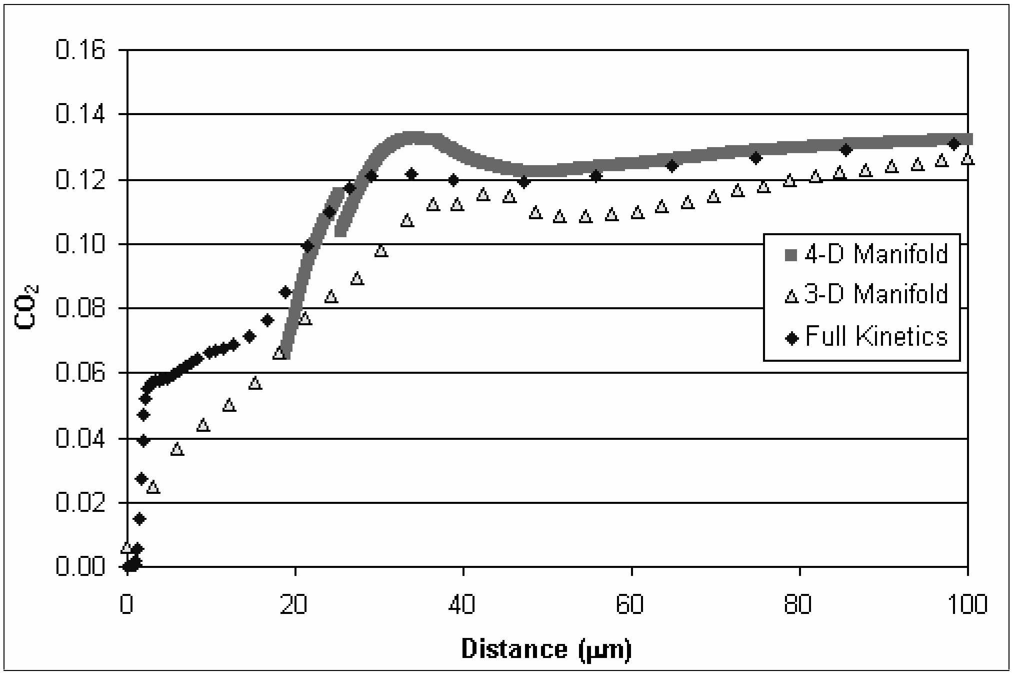

Figure 35 - Results of One-Dimensional, Steady-State Simulation

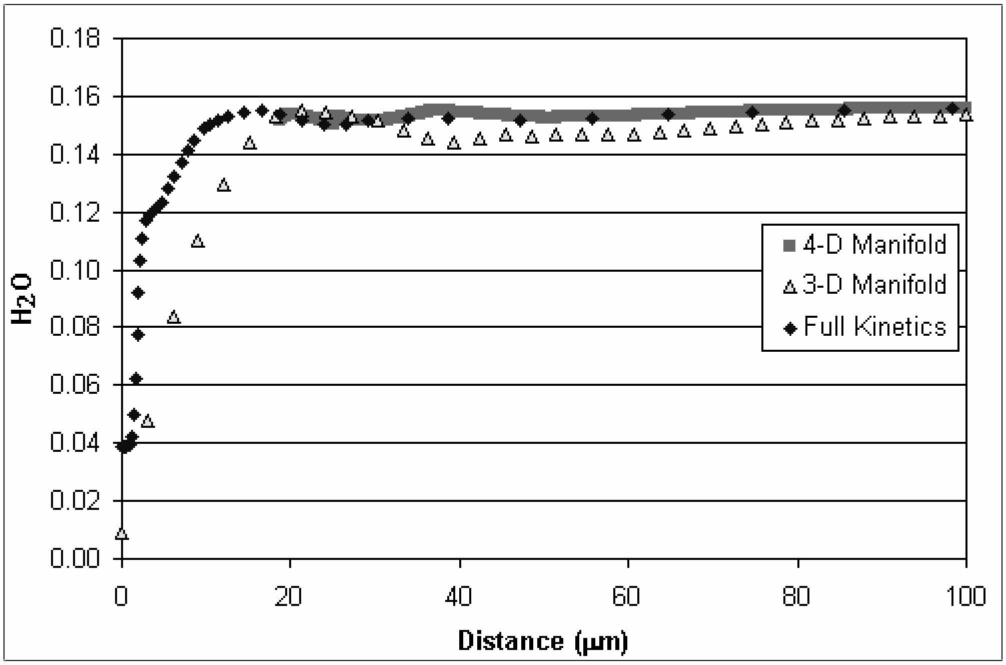

Figure 36 - Results of One-Dimensional, Steady-State Simulation

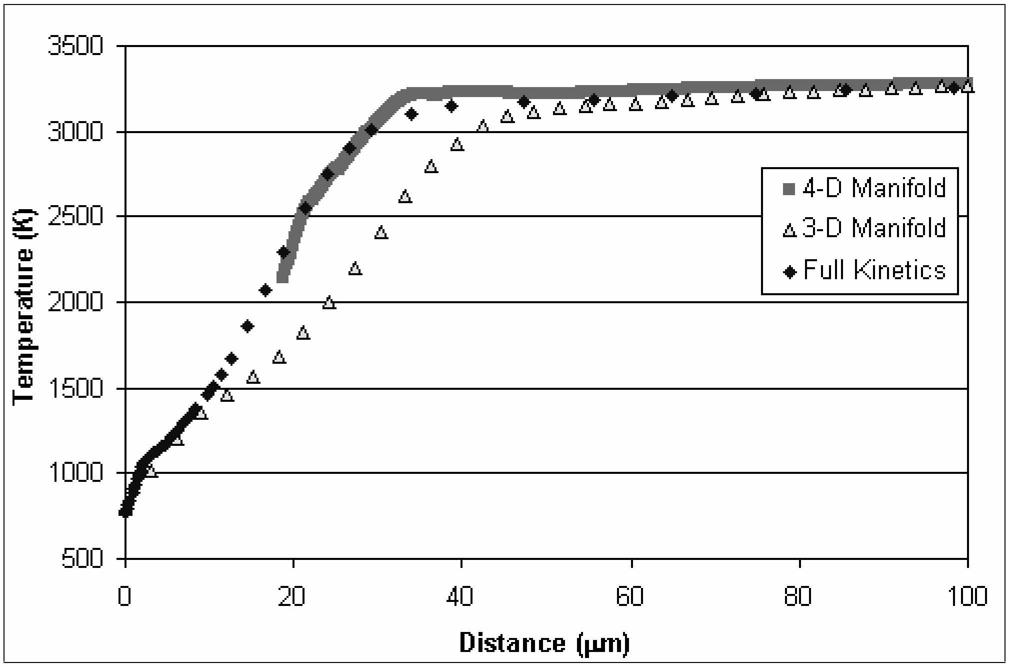

Figure 37 - Results of One-Dimensional, Steady-State Simulation

Graphs of all the species profiles for steady-state combustion at 20 atm are included in Appendix A. Generally, there is good agreement between the 4-D manifold and the full kinetics, even with the minor species. A few of the curves (i.e. CO_2) have discontinuities at ~25 μm (see Figure 35). This is due to discontinuities within the 4-D manifold at that point. The problem can be minimized by generating and using a manifold with greater resolution.

Chapter 6 Container Simulation

The overall goal of the HMX manifold generation and testing is to incorporate the ILDM approach in the gas-phase of the C-SAFE container simulation. Simulations have been performed by C-SAFE to investigate deformation of the container, cracking of the solid high explosive, and heating of the solid high explosive. In addition, cookoff tests (heating a container of high explosive until explosion) have been performed to validate the models. A few of these studies are reported and referenced in this report.

It was suggested that one way to increase the accuracy of the container simulations would be to include a simulation of the gas phase chemistry inside the container through the ILDM approach. Further work is necessary to fulfill this objective. This section discusses results from three simplified simulations of the gas phase with the gas at equilibrium. Although the simulations do not implement an ILDM, they are insightful with respect to heat transfer at the solid-gas interfaces. Also, these simplified simulations reveal information about gas flow and flame propagation within the container. The intention of this work is to provide a foundation for future work in implementing the HMX manifold.

6.1 C-SAFE Container Simulation

As noted previously, the C-SAFE project includes simulation of a container filled with PBX-9501. PBX-9501 is an explosive with 95% energetic material (HMX) and 5% binder (2.5% Estane and 2.5% BDNPF/A). Experimental tests have been performed to determine the time to explosion of a heated container filled with PBX-9501. A cylindrical container (4-inch diameter x 12-inch length) filled with the explosive was subjected to a high heat flux (~10^4W/m^2). Ignition times ranged from 1.6-2.4 minutes (Eddings, Sarofim, Ciro, and Beckstead 2000).

A simulation by the University of Utah models the pressurization of the container after ignition (C-SAFE Program 2001). Figure 38 shows a stress simulation performed on the container and high explosive.

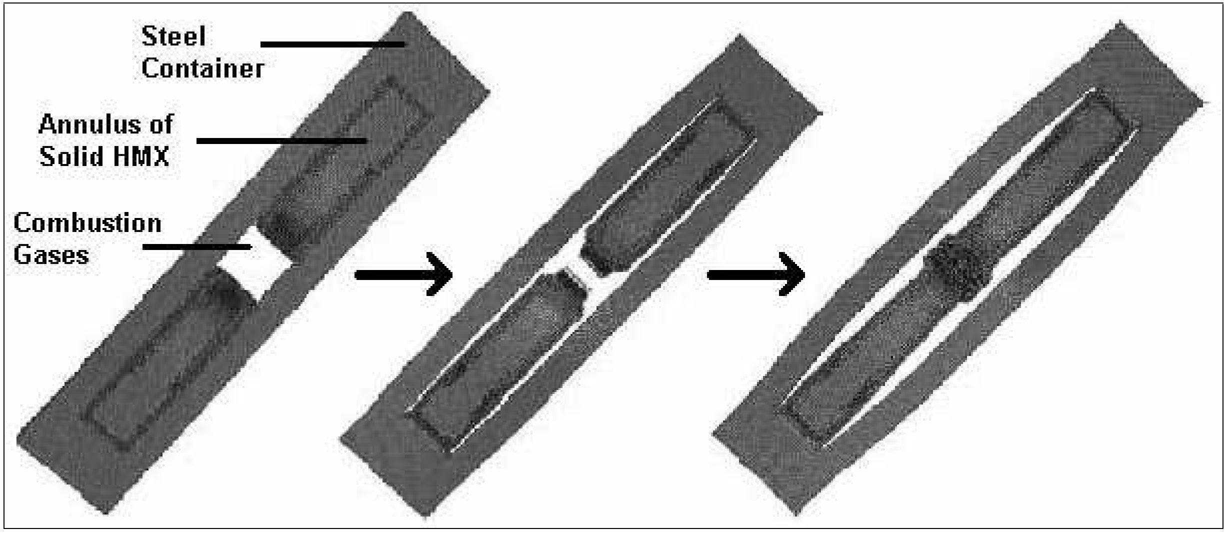

Figure 38 - Pressurization of Container

To reduce computational cost, the size of the container in the simulation is smaller than the size of the experimental validation container. The outer shell is a steel container. The interior is high explosive with temperature contours that show the thermal wave penetration. A two-dimensional cross section of the container shows the pressurization in three snapshots as it progresses in time.

6.2 A Post-Ignition Model with Gas Products at Equilibrium

The C-SAFE container simulation includes heat transfer, a global mechanism for HMX reaction rate, deformation of the container, and deformation of the high explosive. In addition, a one-dimensional ignition model is available to predict time to ignition

(Beckstead 1994). Work has also been performed on multi-dimensional effects of ignition (Baer 1994). No known work has been performed to model multi-dimensional effects after ignition for fast heating rates. This post-ignition study explores the multi-dimensional effect of flame spreading.

In this model, HMX properties are used to approximate those of PBX-9501. Figure 39 shows a simplified model of a gap that could exist between the container and the HMX. This model is used to qualitatively investigate the point at which the HMX will ignite.

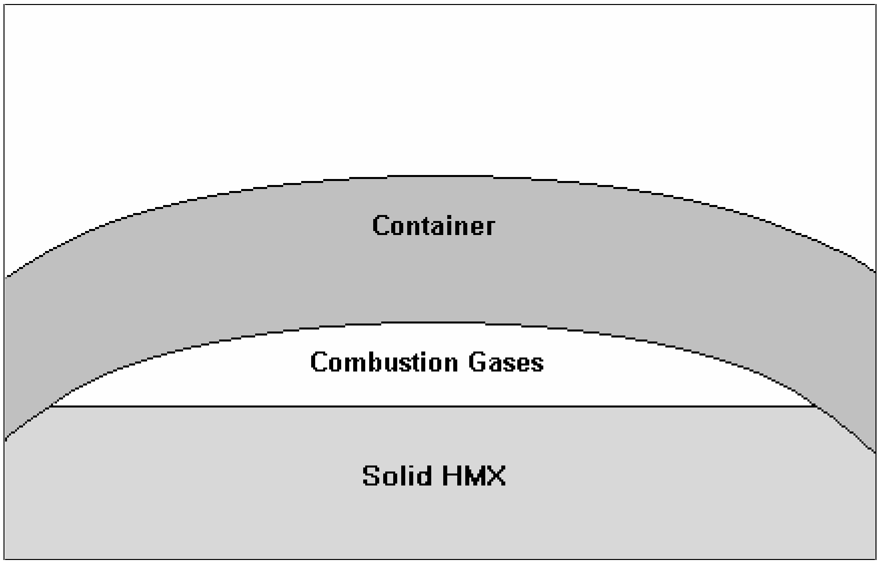

Figure 39 - Model of Container

In the proposed situation for the C-SAFE simulation, the container is one meter above a pool fire and receives an assumed heat flux (~10^4 W/m^2) at the outside wall (Beckstead 1999). This heat conducts through the steel container and into the HMX. The thermal contact resistance between the steel casing and solid is equivalent to a 1-3 mm air gap (Eddings, et. al. 2000). The proposed C-SAFE simulation predicts the heat up, reaction of the HMX, pressurization, and deformation of the container. The proposed simulation continues until the time of rupture of the container.

6.2.1 Heat Transfer Analysis

A simplified simulation of the container was performed to reveal the most likely initiation point of the HMX reaction. A cross-section of the container was modeled in Fluent™ to determine a realistic temperature profile. Figure 40 shows the overall cross-section of a 30 cm diameter cylinder after 2,000 seconds. An arbitrary gap, filled with simulated combustion gases is ~2 cm at the widest part. In this heat transfer simulation, the outside of the container is subjected to a constant temperature boundary condition of 550 K. The melting temperature of HMX is slightly greater than 550 K. The boundary condition temperature of 550 K was selected to ensure the validity of the solid HMX assumption.

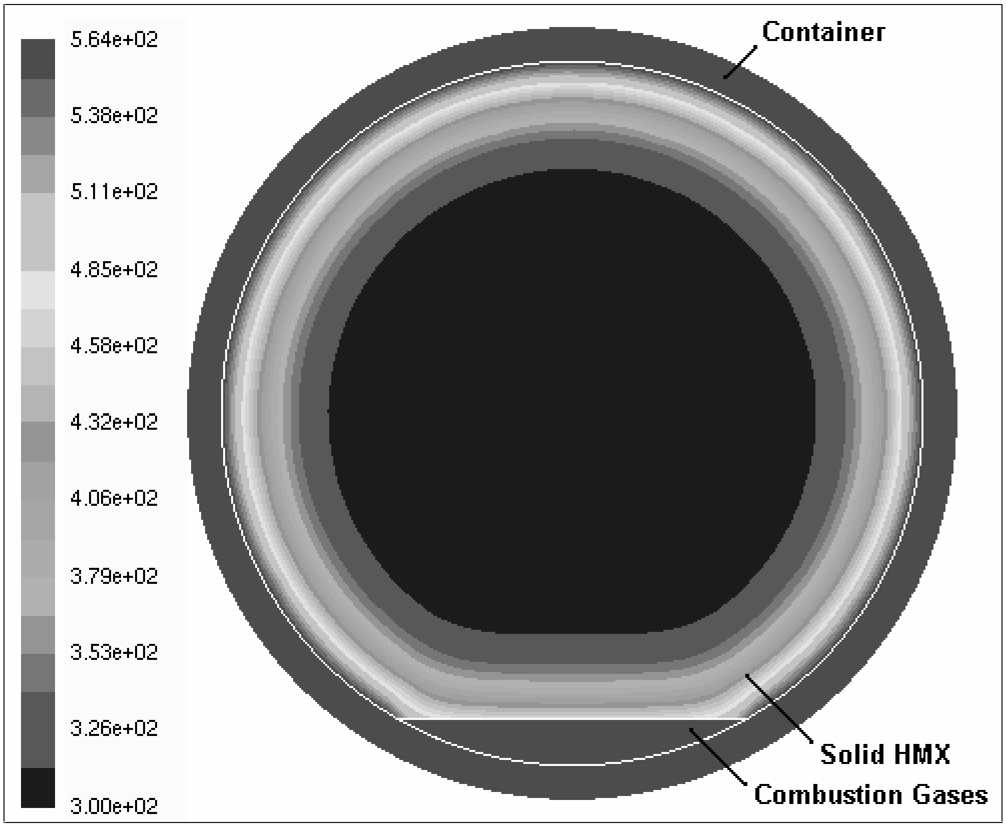

Figure 40 - Heat Transfer Simulation

The container is assumed to be made out of stainless steel (ANSI 316) with a thermal conductivity of 13.4 W/m-K. The heated solid HMX has a thermal conductivity of 0.4 W/m-K (Beckstead 1999, Bedrov, Smith, and Sewell 2000). The gap between the container and solid HMX has the same properties as air, and the heat transfer coefficient at the air-solid interface is assumed to be 25 W/m^2-K. This figure shows that the solid HMX is an excellent insulator. Because of this, reaction will likely occur where the solid HMX comes into contact with the container, and where the thermal contact resistance is the lowest. Figure 41 shows the same heat transfer simulation zoomed in at the solid-gas interface.

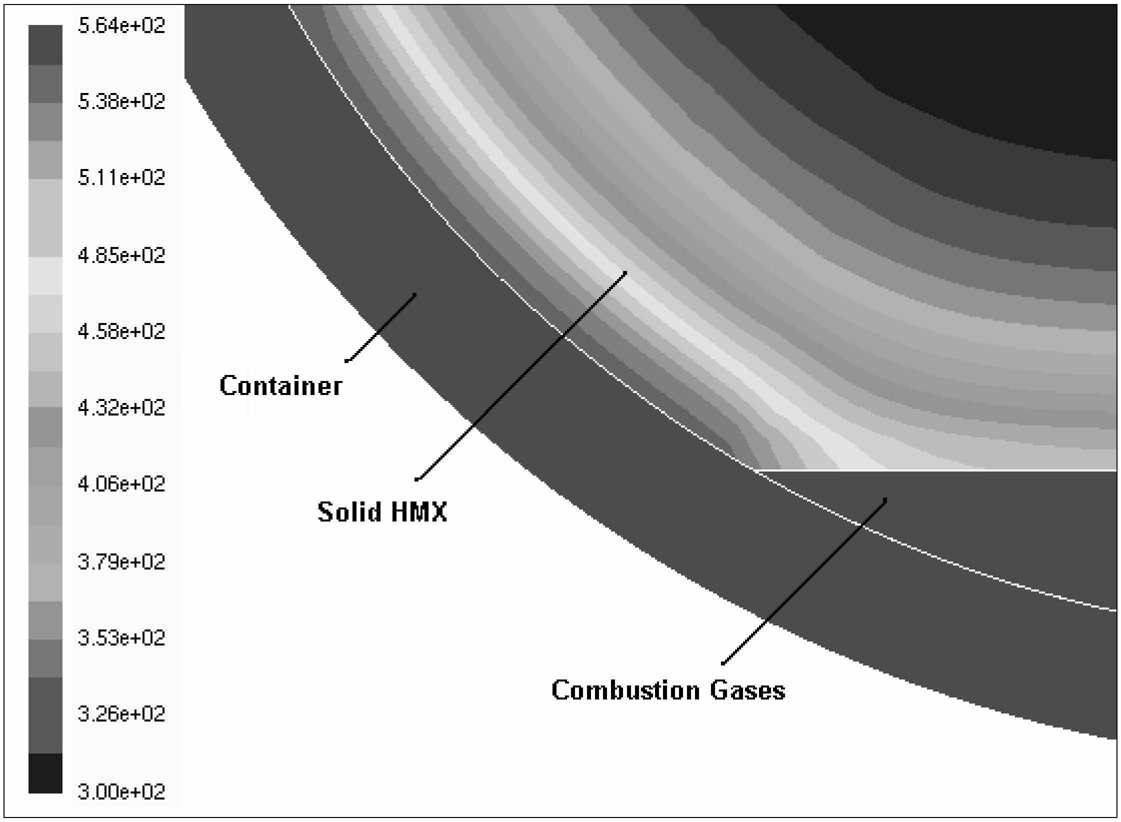

Figure 41 - Heat Transfer at the Solid-Gas Interface

Heat transfer by conduction from the container to the solid HMX is larger than the heat transfer from the gas to the solid HMX. Accordingly, the highest temperature at the solid-gas interface is at the contact points.

6.2.2 Open System Simulation

In an open system reaction scenario the reaction occurs at the separation point and proceeds around the outside of the solid HMX. Since the gap thickness is much less than the container diameter, the angular effects are assumed to be negligible (Eddings, et. al. 2000). The simulation is approximated as a straight sheet of HMX covered by stainless steel.

6.2.2.1 The Model

A simplified model of the HMX combustion in the container is shown in Figure 42.

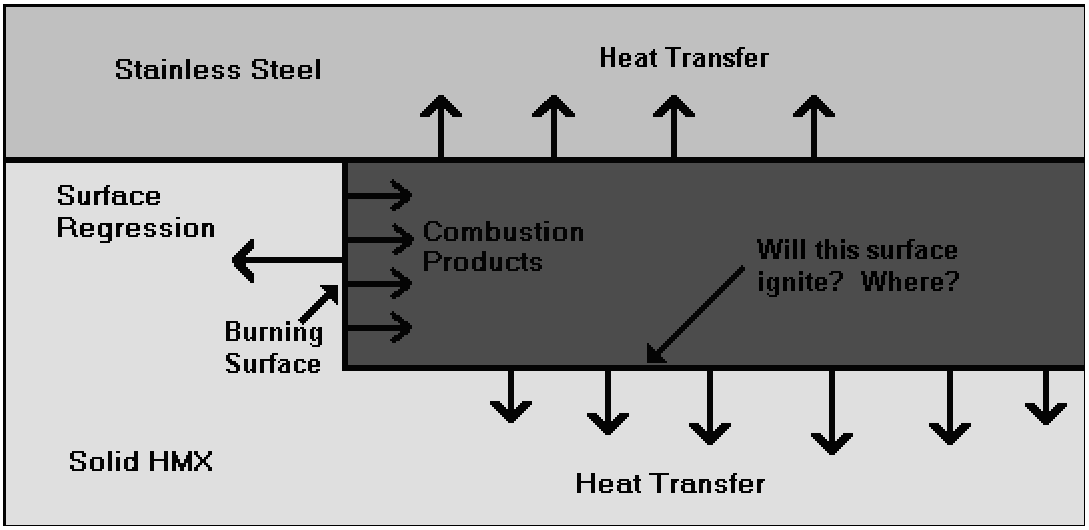
Stainless Steel
Heat Transfer
Surface Regression
Combustion Products
Will this surface ignite? Where?
Burning Surface
Solid HMX
Heat Transfer

Figure 42 - Open System Model

In this simulation, ignition is assumed to have occurred at the left, vertical plane. Heat feedback is propagating further burning into the preheated HMX near the steel/HMX interface. This creates a moving burning surface, with combustion gases that leave the burning surface at 3200 K. The combustion gas flows in a gap (assumed to be 5 mm wide) between the steel and unignited HMX, and transfers heat to both solids.

6.2.2.2 Ignition Model

If enough heat is transferred to the horizontal solid HMX it will ignite and begin to burn, releasing additional combustion gases. Figure 43 shows an ignition line generated from experimental heating tests for solid HMX (Beckstead 1999).

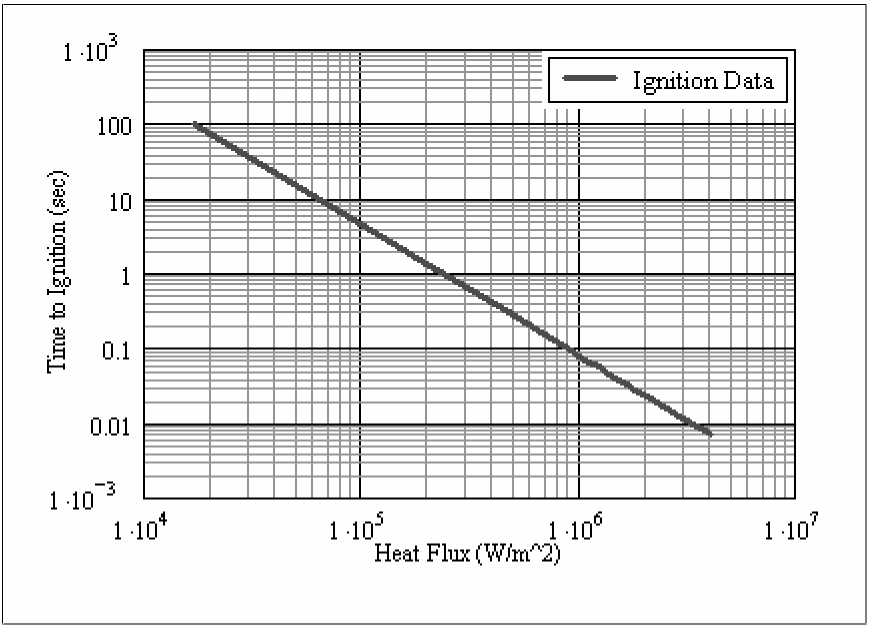

Figure 43 - Ignition Data from Heating Tests

Knowing the heat flux to a surface and using data from Figure 43, the time to ignition can be estimated. If the hot gases do not transfer enough heat to the unignited HMX surface for ignition, then a rigorous combustion simulation should only have one burning front. However, if the hot gases from one surface cause other HMX surfaces to ignite then two-dimensional flame spreading must be modeled.

Using a Lagrangian approach, the regressing burning surface is taken to be stationary. From a one-dimensional, steady-state combustion simulation developed at BYU (Davidson 1996), the burning rate of HMX preheated to 550K at 20 atm is calculated to be 1.22 gm/cm^2-sec. This is equivalent to a surface regression rate of 0.71 cm/sec, based on the HMX density of 1.9 gm/cm^3 (Beckstead 1999). With the burning surface in a stationary reference frame, the steel and solid HMX are assumed to move at the surface regression rate.

The gap between the steel and HMX is taken to be 5 mm, while a steel thickness of 150 mm (the thickness is arbitrarily large to allow adiabatic boundary conditions) and an HMX thickness of 100 mm are assumed. The gap thickness is much smaller than the solid thickness so that adiabatic boundary conditions can be employed around the outer solid edges. The regressing surface has an inflow boundary condition of 12.2 kg/sec-cm^2 and the gas exit an outflow boundary condition. Since the Reynolds number for the flowing gases is under 100, all flow is laminar. Consequently, a locally parabolic assumption at the gas outflow is valid.

6.2.2.3 Grid Independent Study

A simulation was performed in Fluent™ to determine the heat flux to the solid HMX surface. The grid layout is shown in Figure 44.

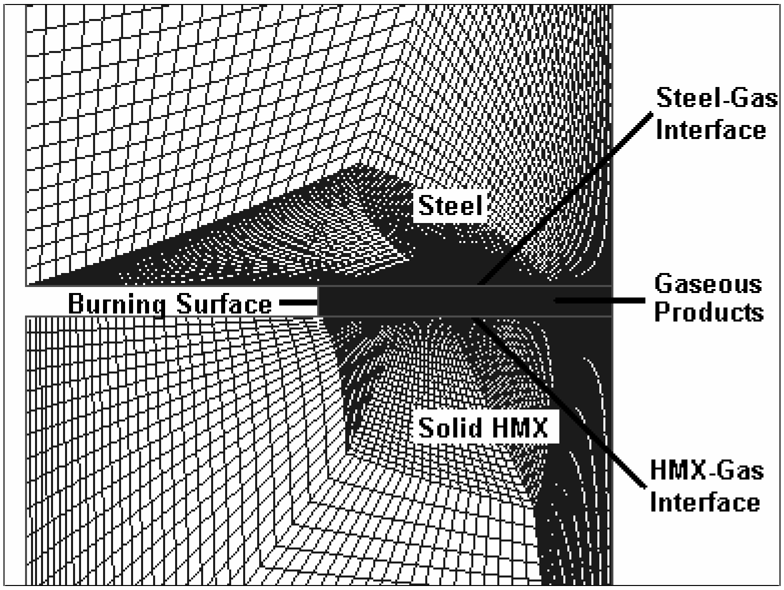

Figure 44 - Grid Layout

In order to reduce the total number of nodes used, the grid is clustered in the areas of high temperature gradients. Gambit™ was used to create the unstructured grid. An unstructured grid allows for a very high density of nodes to be clustered around the gas chamber and fewer nodes to be used at the extremes of the model. A grid independent study dictates the use of 200 nodes with grid clustering around the gas cavity where there are high temperature and velocity gradients.

Various discretization schemes were also studied. A discretization scheme of 2nd order for the pressure and QUICK (Quadratic Upstream Interpolation for Convection-Dominated Kinetics) for the energy and momentum equations was selected. QUICK and 2nd order were chosen because they are higher order and tend to be more accurate than lower order schemes such as 1st order, upwind. Also, SIMPLE (Semi-Implicit Method for Pressure-Linked Equations) was the method used to couple the pressure and velocity terms in the continuity and momentum equations.

6.2.2.4 Simulation Results

Figure 45 illustrates the temperature contours (in Kelvin), showing the area of high temperature gradients around the flowing channel.

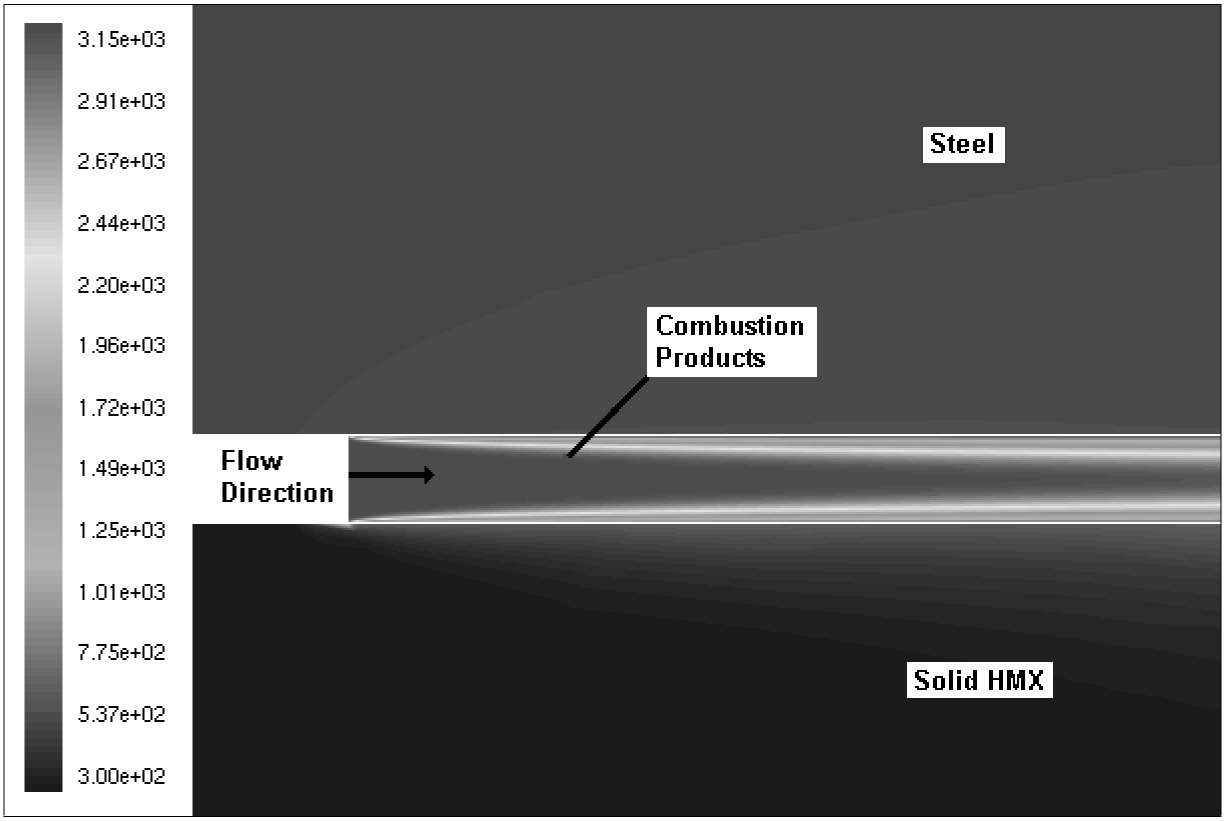

Figure 45 - Temperature Contours

The heat transfer from the combustion gases to the solid surfaces is greatest near the reacting surface. As the gases cool in the boundary layer, the heat flux to the solid surfaces decreases.

Time for ignition data is based on a constant heat flux. In the simulation, the heat flux has a stationary profile. However, with a Lagrangian approach, the surface is moving and the heat flux that an individual point sees is changing. To account for the movement of the surfaces, the heat flux is computed through the following expression:

$$q'' = \frac{\sum_{i=1}^{n} q_i^{''} \Delta t_i}{\Delta t} \tag{13}$$

where q''_i is the instantaneous heat flux at a node, Δt_i is the time the differential surface is subjected to the heat flux, and Δt is the time to travel from the burning surface to the final position. Figure 46 shows the average and instantaneous heat fluxes across the gas/HMX interface. The distance on the x-axis refers to the distance from the regressing surface.

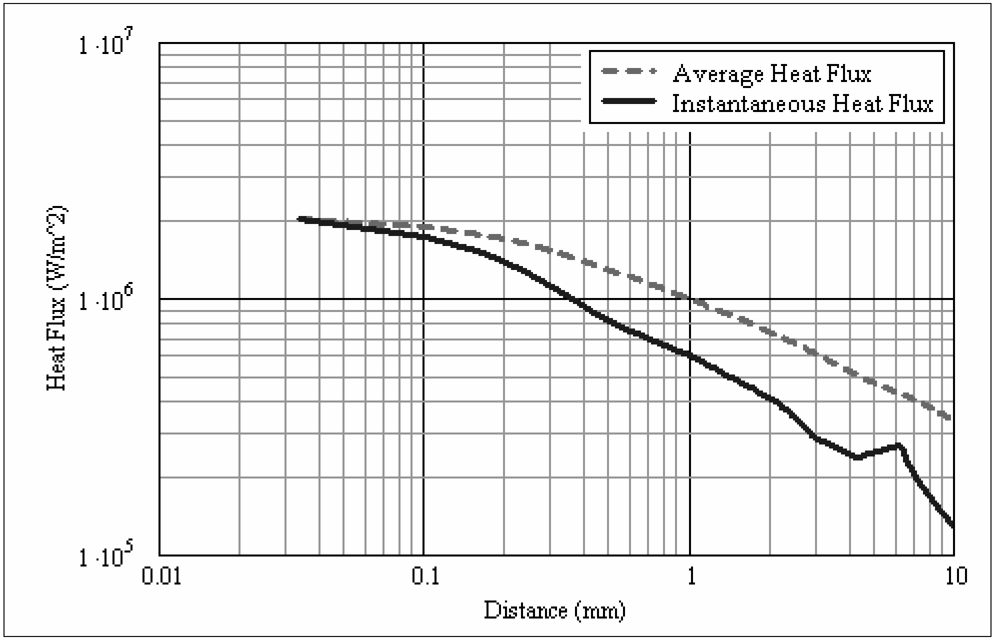

Figure 46 - Comparison of Heat Fluxes

Using the average heat flux, the distance to ignition is computed by locating the point (in space) at which the heat flux is sufficient to ignite the surface. Ignition data relates heat flux to time for ignition (see Figure 43). The time of the incident heat flux is related to the distance away from the regressing surface by the surface regression velocity ($\Delta x = v\ \Delta t$). Figure 47 shows the calculated results of average heat flux versus distance along the gas/HMX interface, compared to the empirical data correlation.

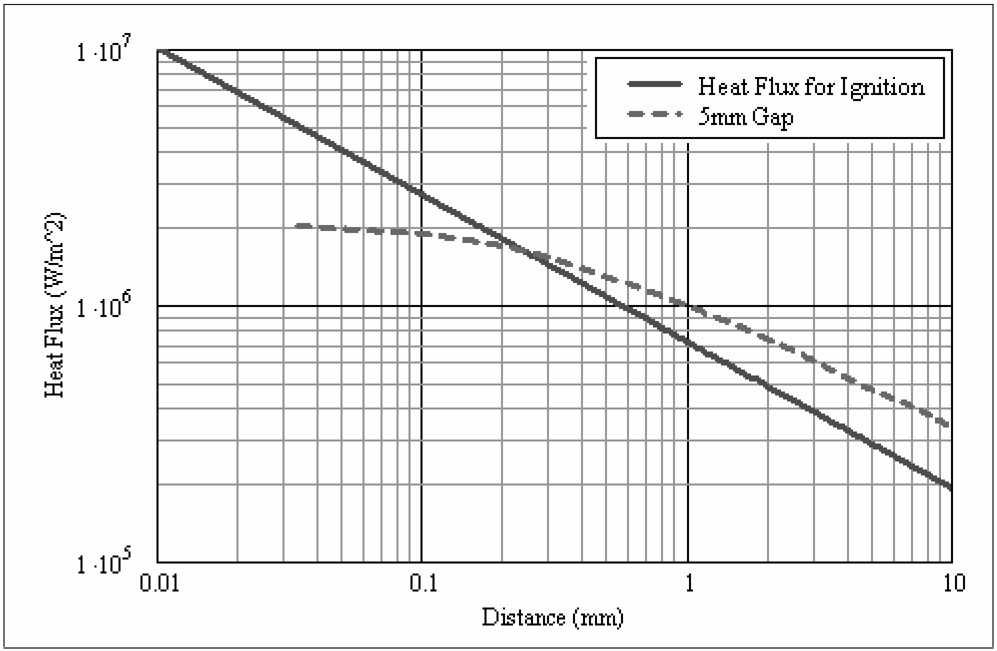

Figure 47 - Distance to Ignition for a 5 mm Gap

At 0.23 mm the average heat flux reaches a value sufficient for ignition. This indicates that with the open system geometry, when ignition occurs at one point, the resulting combustion gases will ignite other surfaces nearby.

6.2.2.5 Gap Thickness Parametric Study

A parametric study was performed to study the effect of gap thickness on flame spreading. A preheated band of HMX varies in thickness depending on the rate of heating to the outside of the container. At high heating rates (~10^5 W/m^2) the thermal wave only penetrates ~2-3 mm into the solid HMX before ignition. At low heating rates (~10^4 W/m^2) the thermal wave penetrates up to ~40 mm into the solid HMX before ignition (Beckstead 1999). After ignition the burning front preferentially burns through the preheated HMX because of the 40% faster burning rate over non-preheated HMX (0.72 cm/sec compared to 0.52 cm/sec). By burning the preheated HMX, a gap forms between the steel and unignited HMX. Simulations were performed with gap widths of 1 mm, 2 mm, 5 mm and 10 mm. Figure 48 shows the results of the simulations with the ignition heat flux line.

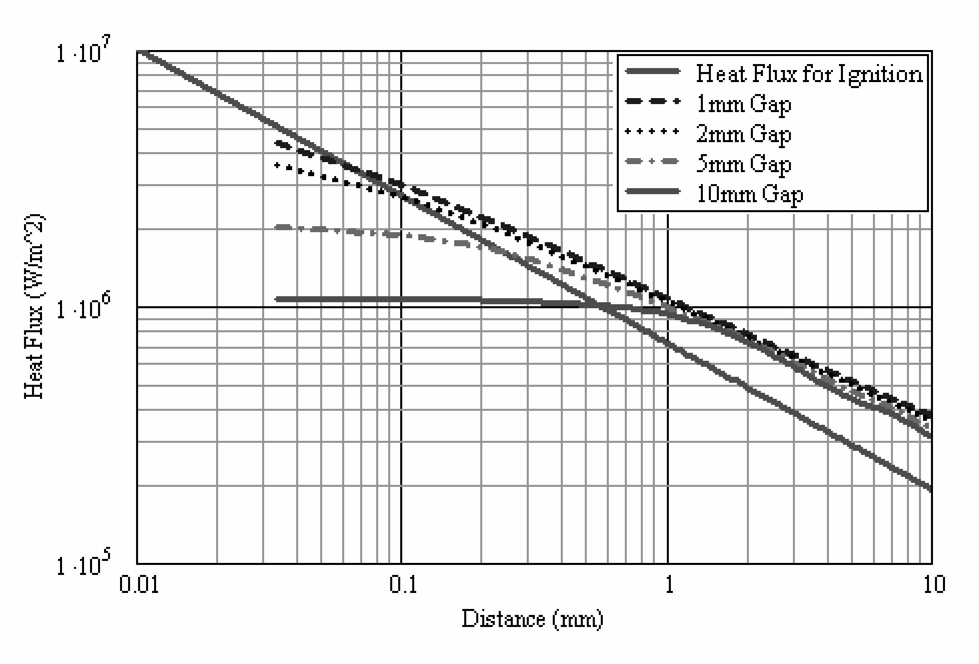

Figure 48 - Ignition Prediction for Various Gap Widths

The ignition distance for a gap of 10 mm is ~0.55 mm while a gap of 1 mm requires only ~0.07 mm to ignite. This study shows that as the gap width increases, ignition of the horizontal surface is delayed. The important point is that flame spreading is significant for all gap widths tested.

6.2.2.6 Conclusions for the Open System Simulation

The results of this study indicate that the single burning front assumption is not valid after ignition of the HMX. Once a single point ignites, the combustion gases ignite other surfaces nearby, regardless of the width of the gap. This spreading effect leads to accelerated combustion through flame propagation. In a rigorous simulation of the high explosive combustion, two-dimensional flame spreading must be modeled.

6.2.3 Closed System Simulation

For an open system flame spreading is significant. However, in a closed system the velocity of the gases is lower and therefore, flame spreading may not be significant. Another important factor is pressurization. When solid HMX begins to react in the closed system, the container pressurizes. As the container pressurizes, the reaction rate of HMX increases. The closed system exhibits positive feedback, and the reaction rate accelerates.

There is a void volume in the center of the HMX annulus that will accumulate combustion gases and slow down the pressurization of the container. In addition, the volume of the container can expand. This expansion is due to a ballooning effect of the container walls. Experimental results show that the volume of the container can increase by as much as 25% before rupture (Eddings, et. al. 2000). The combined void volume of the annulus and expansion of the container decreases the rate of pressurization and delays the rupture of the container.

6.2.3.1 The Model

The closed system model of the HMX combustion in the container is shown in Figure 49.

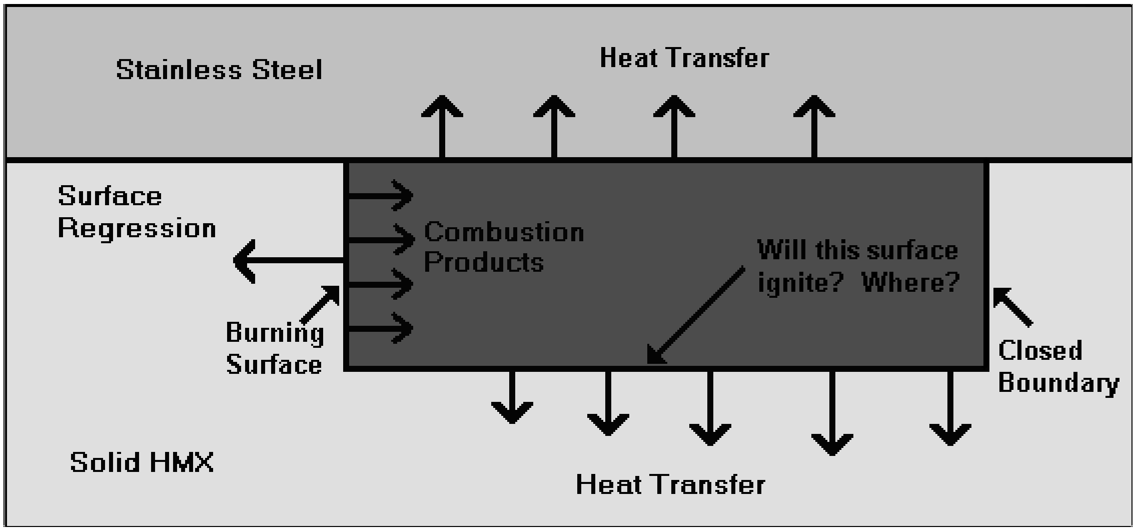
Stainless Steel
Heat Transfer
Surface
Regression
Combustion
Products
Will this surface
ignite? Where?
Burning
Surface
Closed
Boundary
Solid HMX
Heat Transfer

Figure 49 - Closed System Model

This simulation is similar to the open system simulation in that the left surface is assumed to regress at the steady state burning rate of 0.72 cm/sec with combustion gases leaving the burning surface at the equilibrium temperature of 3200 K. The combustion gases enter the pocket (assumed 5 mm x 10 mm) between the steel and unignited HMX, and transfer heat to both solids. The difference between this simulation and the open system simulation is that the right boundary is closed. With a closed system, pressurization occurs and time must be added as another variable in the calculation. The simulation was run for 0.01 seconds with time steps of 0.00005 seconds. Larger time steps lead to solver instability in Fluent™.

In an unsteady calculation, initial conditions must be specified. The initial temperature for the simulation is set at 550 K, the melting temperature of HMX. The initial pressure is 1 atm, and the combustion gases are modeled as an ideal gas with the same properties as air.

The surface regression enlarges the area of the pocket by less than 1% during the total simulation time of 0.01 seconds. This enlarging of the pocket is assumed to be negligible and, therefore, all vertical boundaries are taken to be stationary. The most significant enlargement of the pocket will occur as the pressure increases. High pressure in the gap will deform the steel or HMX solid and cause them to separate. This deformation is beyond the scope of the closed system simulation.

6.2.3.2 Ignition Model

The ignition model for the closed system simulation is the same as the open simulation ignition model (discussed in Section 6.2.2.2).

6.2.3.3 Simulation Results

As in the open system simulation, the closed system surface regression rate is assumed to be 1.22 gm/cm^2-sec. With that surface regression rate and the given geometry, the ideal gas pressure is calculated to increase linearly from 1 atm initially to 150 atm in 0.01 seconds. Because of unrestricted flow within the closed pocket, the flow should be laminar and there should not be recirculation of the gases. Figure 50 shows the velocity profile at 0.00005 seconds with the vectors corresponding to the velocity direction and magnitude (in m/s).

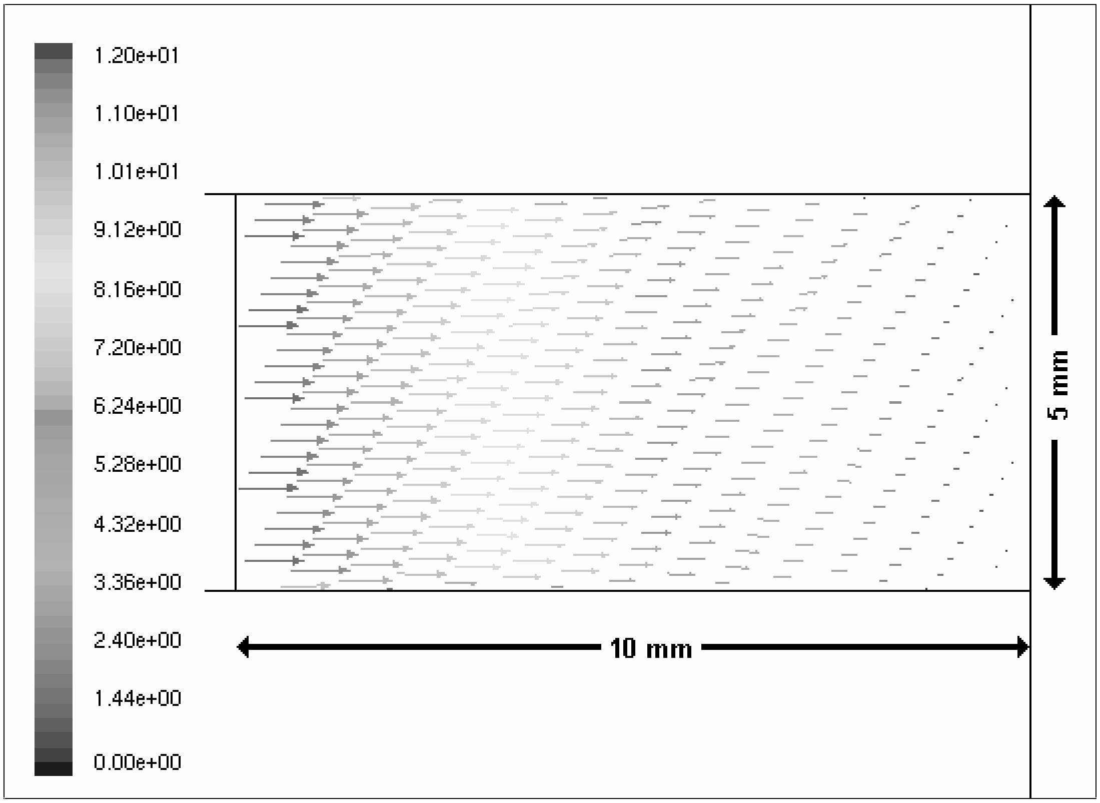

Figure 50 - Initial Velocity Profile

The combustion gases reach equilibrium ≈100 μm from the burning surface. Because the gases reach equilibrium quickly, thermal effects are more significant than chemical effects, such as caused by radicals, in igniting the HMX. Figure 51 shows the temperature contours (in Kelvin) after 0.01 sec of simulation time, showing the area of high thermal gradients within and around the pocket.

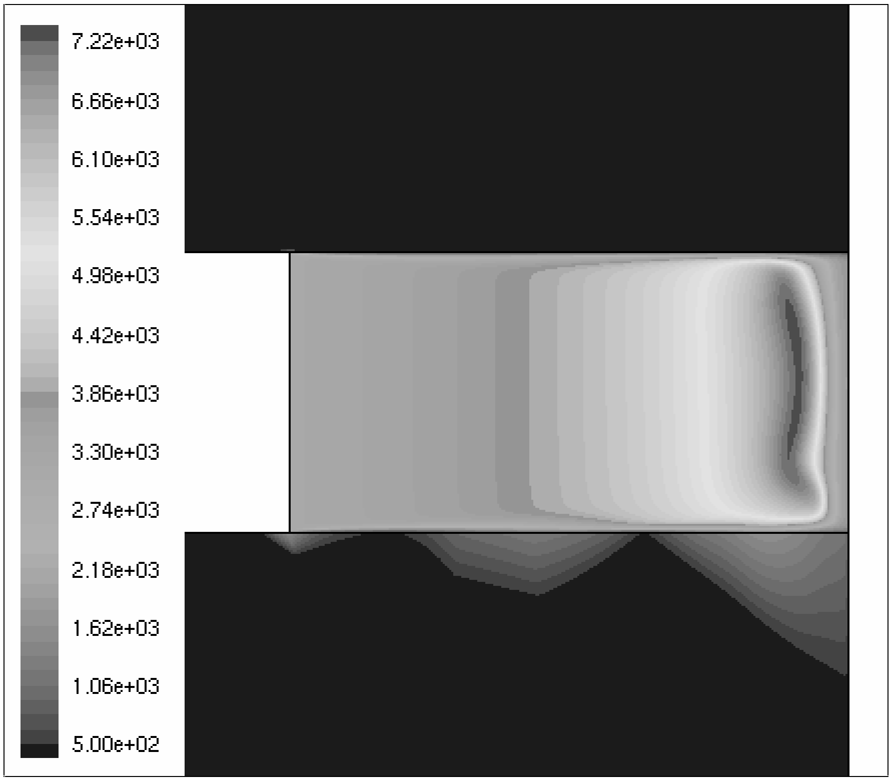

Figure 51 - Temperature Profile in the Closed System Simulation

The temperature rises above the equilibrium temperature of 3200 K because of pressurization. An adiabatic system with ideal gas undergoing pressurization increases in temperature according to the following equation.

$$\frac{T_2}{T_1} = \left(\frac{P_2}{P_1}\right)^{\frac{\gamma-1}{\gamma}} \tag{15}$$

Even though this simulation is not an adiabatic system, the same trend applies. The pressurization increases the temperature of the gases. The rise in temperature also increases the heat flux to the solid HMX and steel. In the simulation, a pocket of gas approaches 7500 K due to pressurization. As the temperature increases, many of the equilibrium products will dissociate into the elements and moderate the rise in temperature. A more rigorous simulation, such as an ILDM gas-phase calculation (provided the full kinetic mechanism accounts for dissociation), would account for species dissociation, and would result in a much lower temperature.

Another shortcoming of the closed system simulation is that phase changes are not modeled. In the simulation, the surface temperature of the solid HMX rises above 1500 K. The surface temperature of the liquid-gas interface in the steady-state one-dimensional model is 775 K. This implies that it is near the HMX boiling point and that vaporization of the HMX should occur in the closed system simulation. A more rigorous simulation would account for the vaporization and reaction of HMX in the gas phase.

The heat flux to the unignited HMX is calculated to predict flame spreading in the closed pocket. Figure 52 shows the results of this analysis.

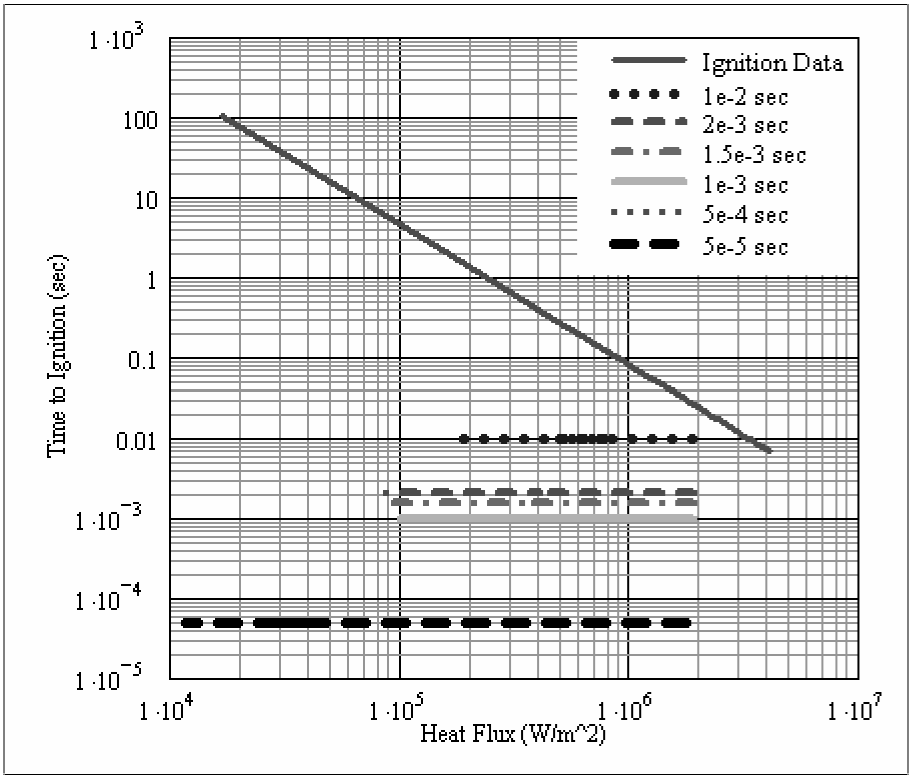

Figure 52 - Heat Flux Analysis for Flame Propagation

The heat flux along the horizontal surface of HMX does not reach a value sufficient for ignition within 0.01 seconds.

6.2.3.4 Conclusions for the Closed System Simulation

The flame will not spread within the pocket for this model because the heat flux to the solid HMX does not reach ignition values for the horizontal surface. Extrapolating the results suggests that ignition may occur around 0.02 seconds. By this time the pressure within the pocket is expected to increase to ~400 atm. The total time of the closed system simulation would be dictated by the yield stress of the steel container. After the pressure in the container is sufficient to overcome the yield stress, the fixed-boundary closed system simulation is no longer valid.

Chapter 7 Conclusions

One of the major obstacles to manifold implementation in CFD codes is the lack of automation for manifold generation and implementation. This report describes a method that automates the manifold process. The automated manifold generation is accomplished through the Chemkin paradigm of interchangeable reaction mechanisms. The manifold generation code reads a mechanism file, simulates a PSR reactor, calculates the composition and temperature of a mixture of reactants and PSR products, and computes the reaction trajectory of that mixture in a batch reactor. The batch reactor results are then used to generate the manifold. As new mechanisms are developed for HMX or as other solid propellants are modeled, a new manifold can be generated simply by switching out mechanism files.

This project also provides an additional example of using the ILDM method. Up to this point, the applications of the ILDM method have been with simple combustion reactants such as short-chained hydrocarbons, H_2, and O_2. This project is the first known attempt to use the manifold method for a complex reactant molecule such as HMX.

A 3-D (in enthalpy, pressure, and mass fraction of N_2) manifold was implemented in a 1-D (in space) steady-state simulation. There were large errors near the surface of the burning HMX ($< 60\ \mu m$) and good agreement with full kinetics beyond that.

A 4-D (in enthalpy, pressure, mass fraction of N_2, and mass fraction of NO) manifold increases the accuracy of the approximation. At 20 atm the 4-D manifold provides an accurate representation of detailed kinetics starting at the peak of the enthalpy profile (~19 μm). Within 19 μm of the burning surface, a near-surface model is required. The near-surface model is generated by extracting the first 19 μm of the steady-state, 1-D full kinetics solution.

If coarse gridding (>60 μm) were used in the C-SAFE simulation, the 3-D manifold would be sufficient. If coarse gridding is not sufficient, the 4-D manifold with a near-surface model should be used.

With the ILDM method, only a limited number of differential equations (equal to the dimension of the manifold) must be solved. This speeds up the convergence by eliminating much of the stiffness in the differential equations. In this project, computational cost was reduced by ~10 times for the ILDM method.

The multidimensional effects of HMX combustion were explored with a 2-D (in space) simulation using gases that approximate the properties of HMX combustion gases at equilibrium. In the open-system simulation, flame spreading is shown to be significant. In the closed-system simulation, flame spreading is delayed by the restriction to flowing gases.

Chapter 8 Future Work

The project described in this report is the beginning of the process to generate, implement, and evaluate an ILDM for HMX in the University of Utah's 3-D CFD code, ARCHES. The same techniques that were used in this research project to implement the manifold method into the one-dimensional (in space) combustion code will be used to implement the manifold method into ARCHES. Future work will need to be performed by another researcher to accomplish this goal.

Modeling the reaction of HMX in the gas space of a container will give insight to heat feedback, local quenching, and flow of gases in order to predict time to detonation or deflagration. The simplified open and closed system simulations performed in this project offer insights into some of the physical processes, such as heat transfer. However, a more accurate representation of the open and closed systems should include species involved in chemical reactions as well as deformation of the HMX and steel due to pressurization. The kinetics calculation can be accomplished by implementing the ILDM for HMX. Deformation of the container and its contents is currently being investigated by other C-SAFE researchers.

Chapter 9 References

Baer, M. R., Gross R. J., Gartling D. K., and Hobbs M. L., "Multidimensional Thermal-Chemical Cookoff Modeling", **1994 JANNAF Propulsion Systems Hazards Meeting**, 1994.

Beckstead, M. W., "An Ignition Model for Modern Double Base Propellants", **31st JANNAF Combustion Meeting**, 1994, CPIA No. 620, Vol. II, pp. 163-180.

Beckstead, M. W. and Hendershot R. J., "Calculated Conditions for Fast Cook-Off", **36th JANNAF Combustion Meeting**, 1999, CPIA No. 691, Vol I, pp. 123-132.

Bedrov, D., Smith, G. D., and Sewell, T. D., "Thermal Conductivity of Liquid Octahydro-1,3,5,7-tetranitro-1,3,5,7-tetrazocine (HMX) from Molecular Dynamics Simulations", **Chemical Physics Letters**, 2000, 324, pp. 64-68.

Blasenbrey, T., Schmidt, D., and Maas, U., "Automatically simplified Chemical Kinetics and Molecular Transport and its Application in Premixed and Non-Premixed Laminar Flame calculations", **Twenty-Seventh Symposium (International) on Combustion**, 1998, The Combustion Institute, Pittsburgh, pp. 505-511.

Bongers, H. **Reduced Reaction Mechanisms, an Introduction**. URL: http://www.combustion.tue.nl/~hbongers/, 2002.

Burden, R. L. and Faires, J. D. **Numerical Analysis**. Pacific Grove, CA: Brooks/Cole Publishing Company, 1997.

C-SAFE Program. **C-SAFE, Center for the Simulation of Accidental Fires and Explosions**. URL: http://www.csafe.utah.edu, 2001.

Davidson, J. E. and Beckstead M. W., "A Three-Phase Model of HMX Combustion", **26th Symposium (Int'l) on Combustion**, 1996, The Combustion Institute, pp. 1989-1996.

Eddings, E. G., Sarofim, A., Ciro, W., and Beckstead, M. W., "Fast Cook-Off Tests of an HMX-based Propellant in Pool Fires", **19th JANNAF Propulsion Systems Hazards Meeting**, 2000, CPIA No. 704, Vol I, pp. 63-72.

Glarborg, P., Kee, R. J., Grcar, J. F., and Miller, J. A., "PSR: A Fortran Program for Modeling Well-Stirred Reactors", **Sandia Report**, 1992, SAND86-8209, UC-4.

Kee, R. J., Rupley, F. M.., and Miller, J. A., "A Fortran Chemical Kinetics Package for the Analysis of Gas Phase Chemical Kinetics", **Sandia Report**, 1989, SAND89-8009B, UC-706.

Lam, S. H. and Goussis, D. A., "Understanding Complex Chemical Kinetics with Computational Singular Perturbation", **Twenty-Second Symposium (International) on Combustion**, 1988, The Combustion Institute, Pittsburgh, pp. 931-941.

Maas, U. and Pope, S. B., "Implementation of Simplified Chemical Kinetics Based on Intrinsic Low-Dimensional Manifolds", **Twenty-Fourth Symposium (International) on Combustion**, 1992a, The Combustion Institute, Pittsburgh, pp. 103-112.

Maas, U. and Pope, S. B., "Simplifying Chemical Kinetics: Intrinsic Low-Dimensional Manifolds in Composition Space", **Combustion and Flame**, 1992b, 88, pp. 239-264.

Maas, U. and Pope, S. B., "Laminar Flame Calculations Using Simplified Chemical Kinetics Based on Intrinsic Low-Dimensional Manifolds", **Twenty-Fifth Symposium (International) on Combustion**, 1994, The Combustion Institute, Pittsburgh, pp. 1349-1356.

Niemann, H., Schmidt, D., and Maas, U., "An Efficient Storage Scheme for Reduced Chemical Kinetics Based on Orthogonal Polynomials", **Journal of Engineering Mathematics**, 1997, 31, pp. 131-142.

Norris, A. T. and Pope, S. B., "Modeling of Extinction in Turbulent Diffusion Flames by the Velocity-Dissipation-Composition PDF Method", **Combustion and Flame**, 1995, 100, pp. 211-220.

Pope, S. B., "Computationally Efficient Implementation of Combustion Chemistry Using *In Situ* Adaptive Tabulation", **Combustion Theory Modeling**, 1997, 1, pp. 41-63.

Tomlin, A. S., Turanyi, T., and Pilling, M. J., "Mathematical Tools for the Construction, Investigation and Reduction of Combustion Mechanisms", Chap. 4 in Comprehensive Chemical Kinetics edited by Compton, R. G. and Hancock, G., **Low-Temperature Combustion and Autoignition**, 1997, 35, pp. 293-437.

Xiao, K., Schmidt, D., and Maas, U., "PDF Simulation of Turbulent Non-Premixed CH_4/H_2-Air Flames Using Automatically Reduced Chemical Kinetics", **Twenty-Seventh Symposium (International) on Combustion**, 1998, The Combustion Institute, Pittsburgh, pp. 1073-1080.

Yang, B. and Pope, S. B., "An Investigation of the Accuracy of Manifold Methods and Splitting Schemes in the Computational Implementation of Combustion Chemistry", **Combustion and Flame**, 1998a, 112, pp. 16-32.

Yang, B. and Pope, S. B., "Treating Chemistry in Combustion with Detailed Mechanisms—*In Situ* Adaptive Tabulation in Principal Directions—Premixed Combustion", **Combustion and Flame**, 1998b, 112, pp. 85-112.

Appendix A

Results from the 1-D, steady-state simulation using a 3-D manifold, a 4-D manifold, and full kinetics.

List of Graphs in Appendix A	
Properties	**Intermediate Species (cont.)**
TEMPERATURE	CNO
ENTHALPY	NCO
RATE N2	NCN
Major Products	C2N2
H2O	CN
CO2	N2O
CO	HCN
N2	HONO
Intermediate Species	HNO
NO	NNH
H2COHNNO2	NH3
HNC	NH2
HMXRO	NH
HMXR	NO2
HMX	N
H2CNNO2	HCO
H2CNNO	CH2O
H2CNO	H2O2
H2CNH	HO2
H2CN	OH
HNO3	H
NO3	O
HCNO	O2
HOCN	H2
HNCO	

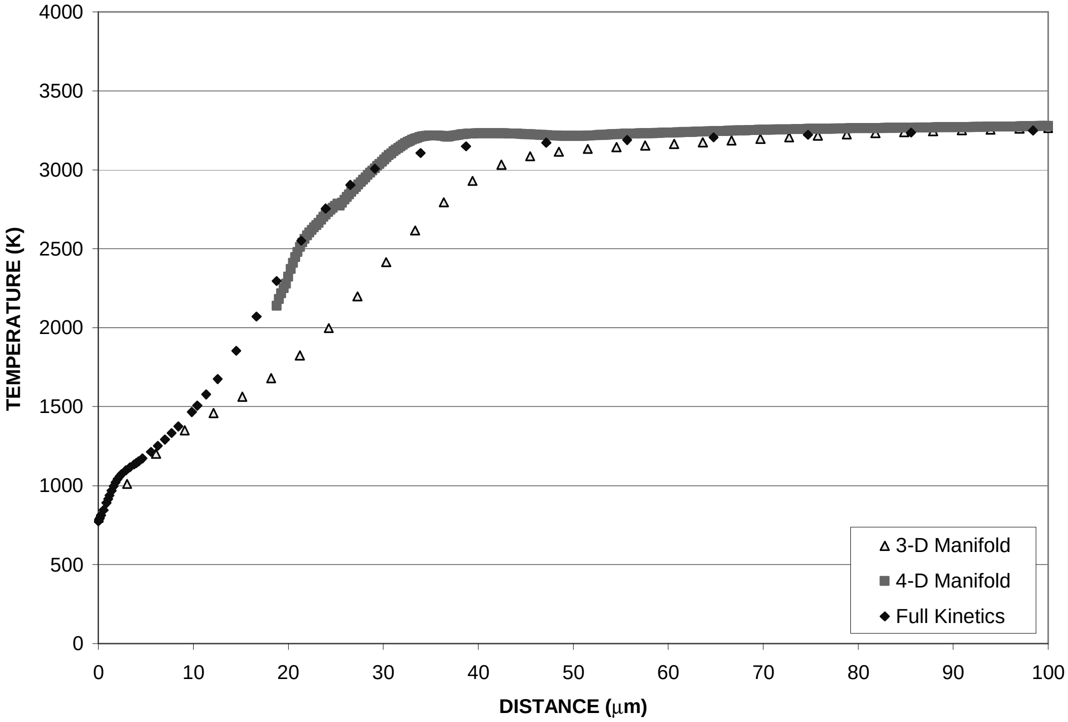

TEMPERATURE (K)
4000
3500
3000
2500
2000
1500
1000
500
0
0
10
20
30
40
50
60
70
80
90
100
DISTANCE (μm)
△ 3-D Manifold
■ 4-D Manifold
◆ Full Kinetics

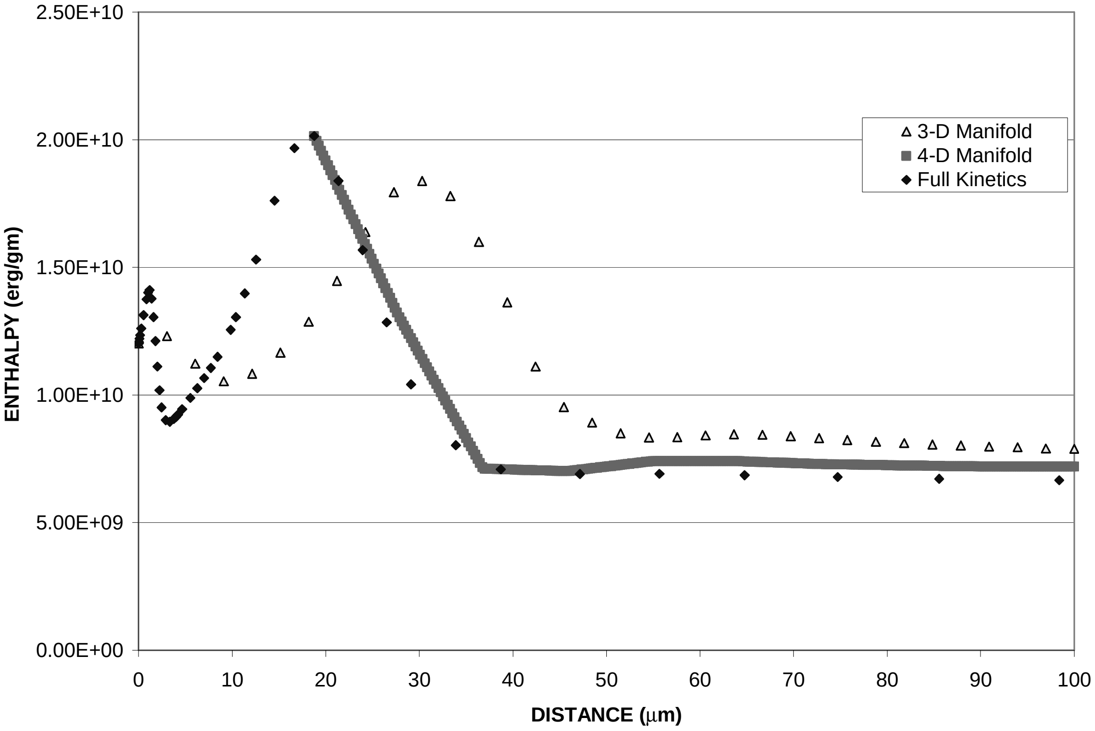

ENTHALPY (erg/gm)
2.50E+10
2.00E+10
1.50E+10
1.00E+10
5.00E+09
0.00E+00
0
10
20
30
40
50
60
70
80
90
100
DISTANCE (μm)
△ 3-D Manifold
■ 4-D Manifold
◆ Full Kinetics

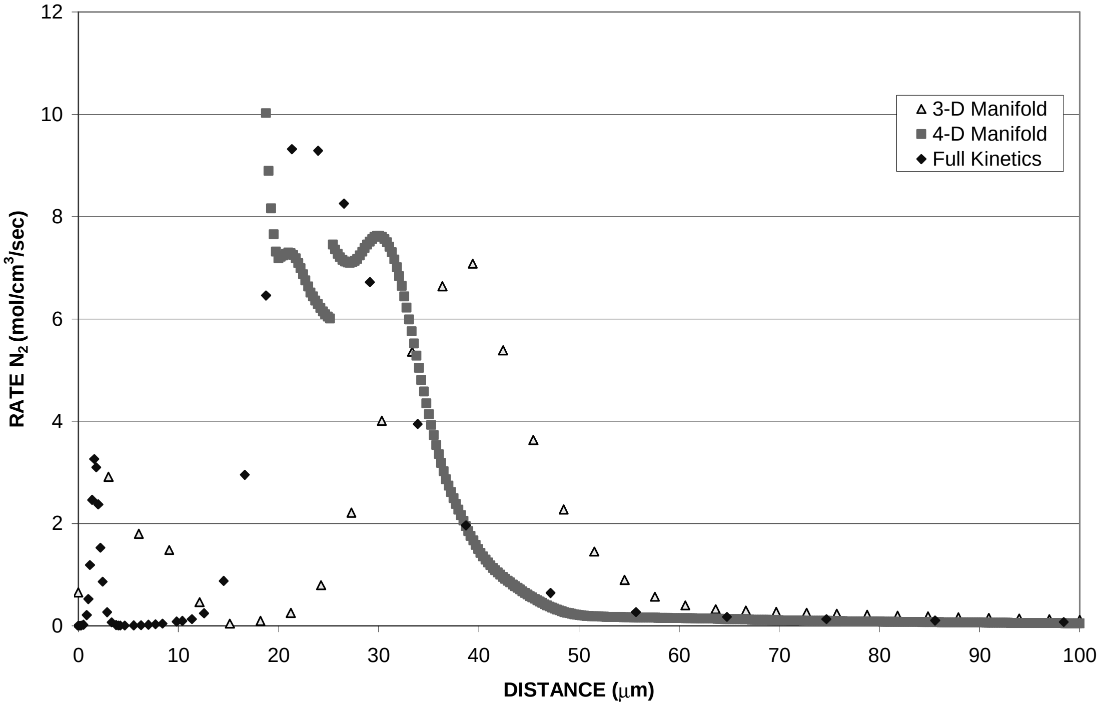
12
10
8
6
4
2
0
RATE N_2 (mol/cm^3/sec)
0
10
20
30
40
50
60
70
80
90
100
DISTANCE (μm)
△ 3-D Manifold
■ 4-D Manifold
◆ Full Kinetics

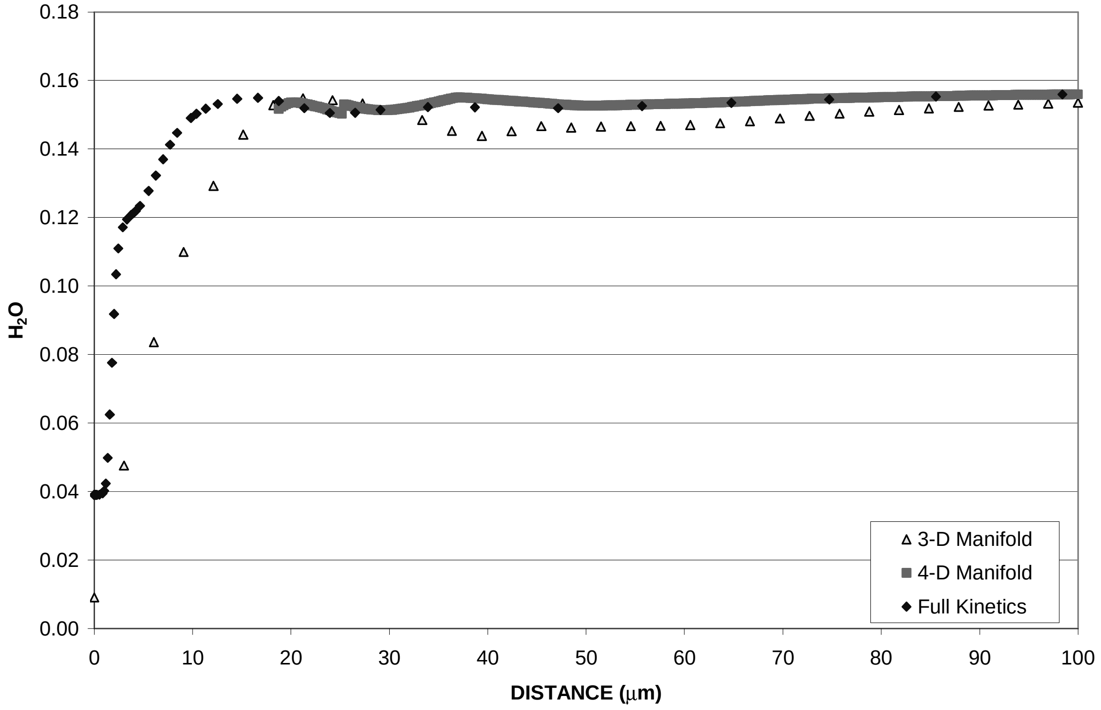
0.18
0.16
0.14
0.12
0.10
0.08
0.06
0.04
0.02
0.00
H_2O
0
10
20
30
40
50
60
70
80
90
100
DISTANCE (μm)
△ 3-D Manifold
■ 4-D Manifold
◆ Full Kinetics

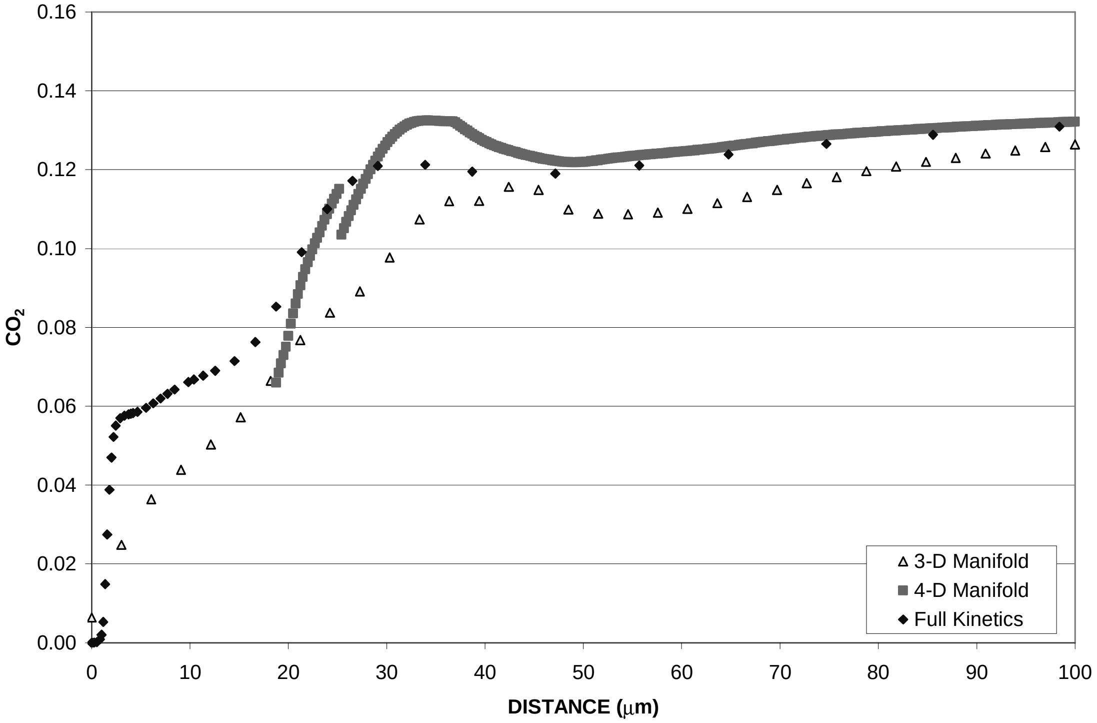
0.16
0.14
0.12
0.10
0.08
0.06
0.04
0.02
0.00
CO_2
0
10
20
30
40
50
60
70
80
90
100
DISTANCE (μm)
3-D Manifold
4-D Manifold
Full Kinetics

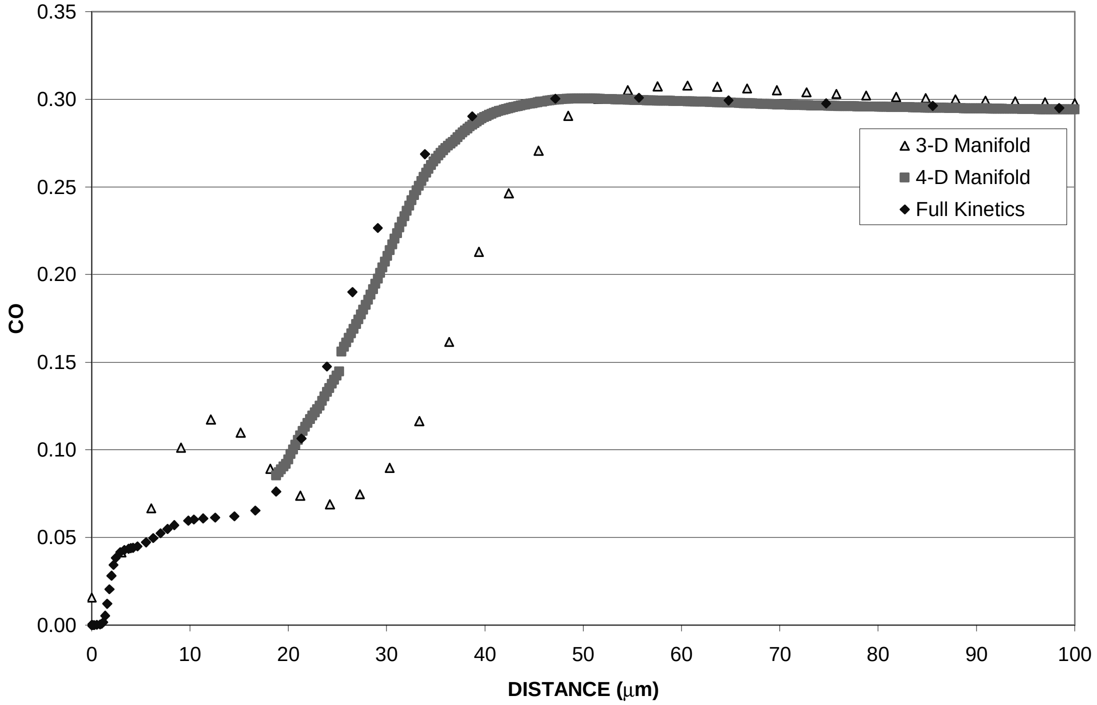
0.35
0.30
0.25
0.20
0.15
0.10
0.05
0.00
CO
0
10
20
30
40
50
60
70
80
90
100
DISTANCE (μm)
3-D Manifold
4-D Manifold
Full Kinetics

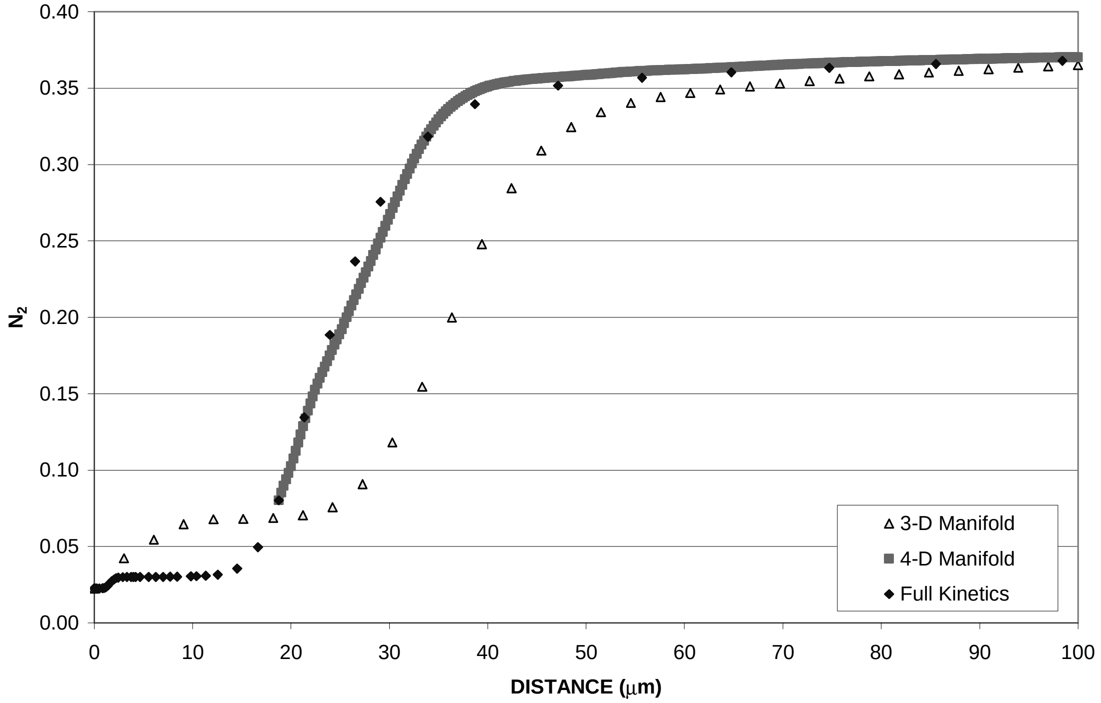
0.40
0.35
0.30
0.25
0.20
0.15
0.10
0.05
0.00
N_2
0
10
20
30
40
50
60
70
80
90
100
DISTANCE (μm)
△ 3-D Manifold
■ 4-D Manifold
◆ Full Kinetics

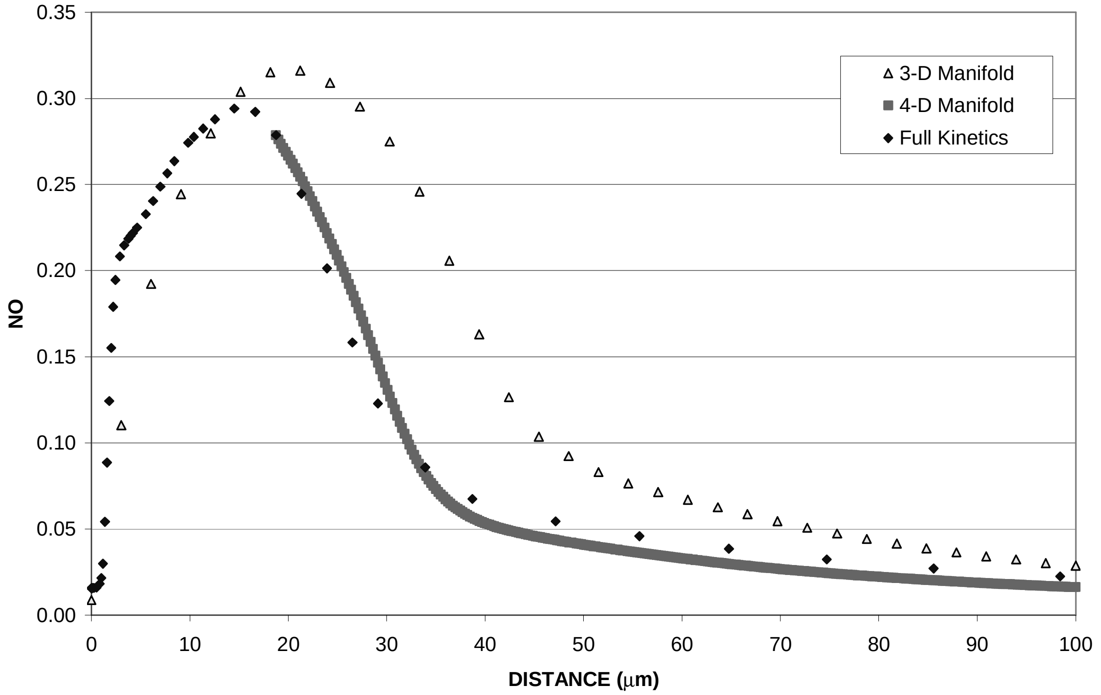
0.35
0.30
0.25
0.20
0.15
0.10
0.05
0.00
NO
0
10
20
30
40
50
60
70
80
90
100
DISTANCE (μm)
△ 3-D Manifold
■ 4-D Manifold
◆ Full Kinetics

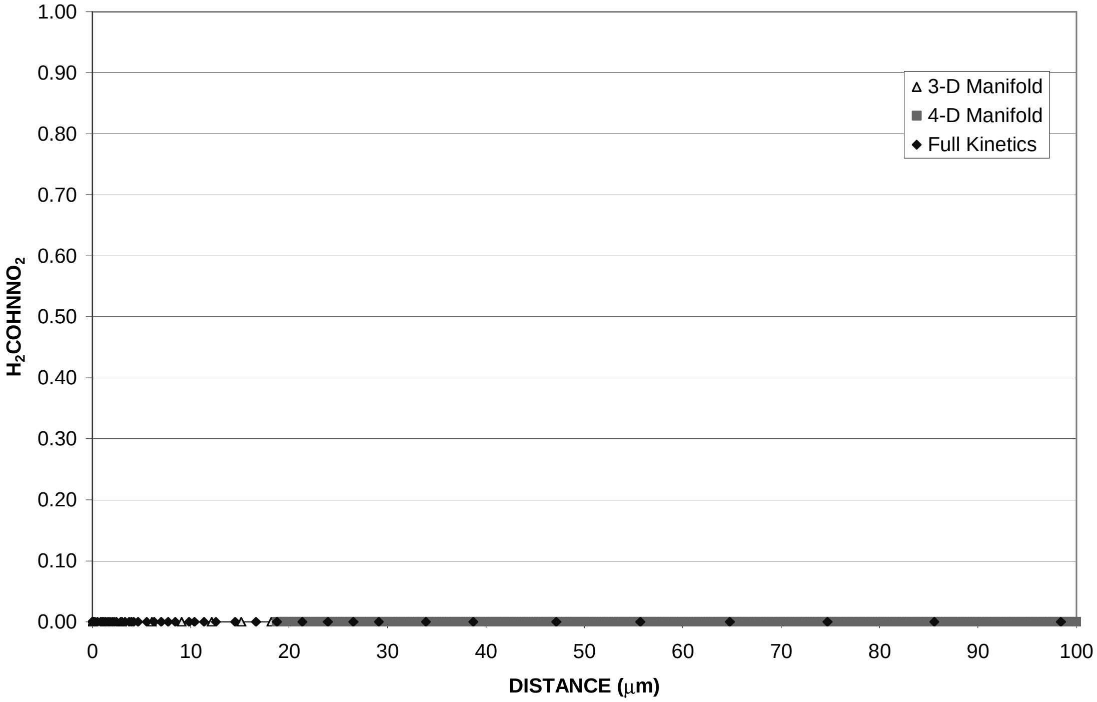
1.00
0.90
0.80
0.70
0.60
0.50
0.40
0.30
0.20
0.10
0.00
$H_2COHNNO_2$
0
10
20
30
40
50
60
70
80
90
100
DISTANCE (μm)
△ 3-D Manifold
■ 4-D Manifold
◆ Full Kinetics

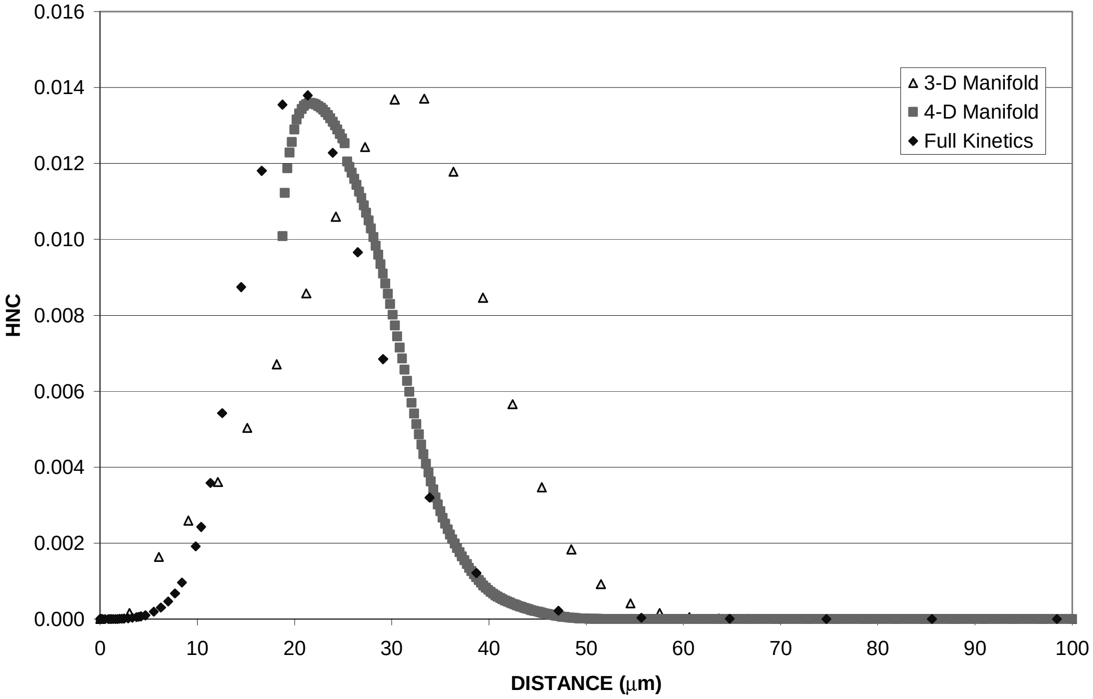
0.016
0.014
0.012
0.010
0.008
0.006
0.004
0.002
0.000
HNC
0
10
20
30
40
50
60
70
80
90
100
DISTANCE (μm)
△ 3-D Manifold
■ 4-D Manifold
◆ Full Kinetics

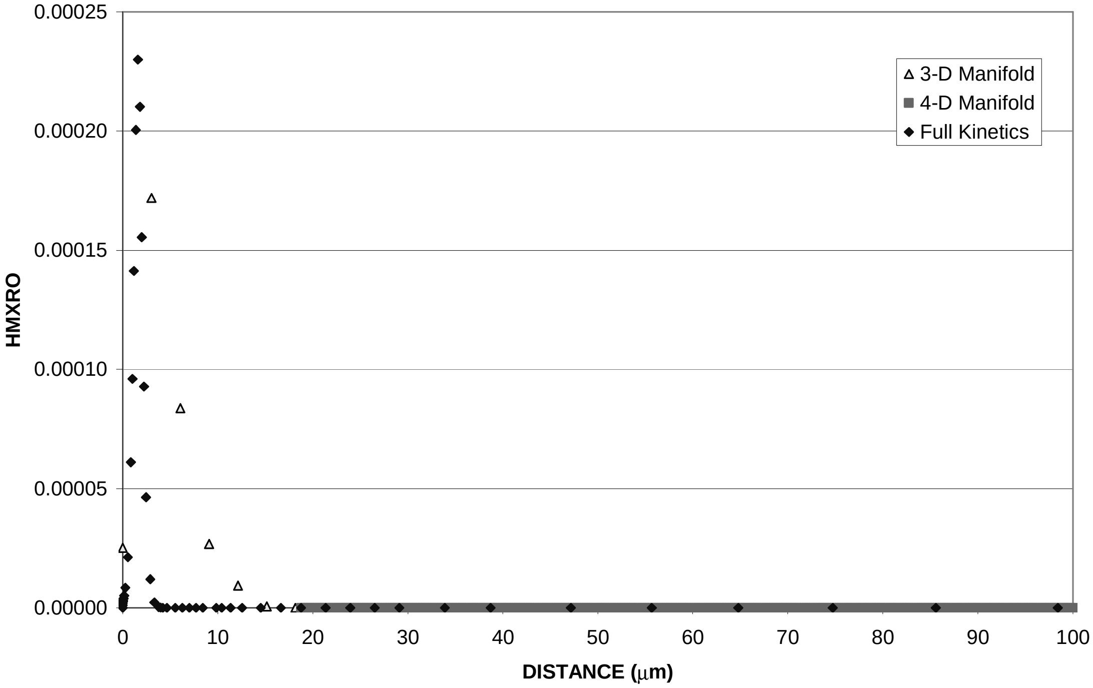
0.00025
0.00020
0.00015
0.00010
0.00005
0.00000
HMXRO
0
10
20
30
40
50
60
70
80
90
100
DISTANCE (μm)
3-D Manifold
4-D Manifold
Full Kinetics

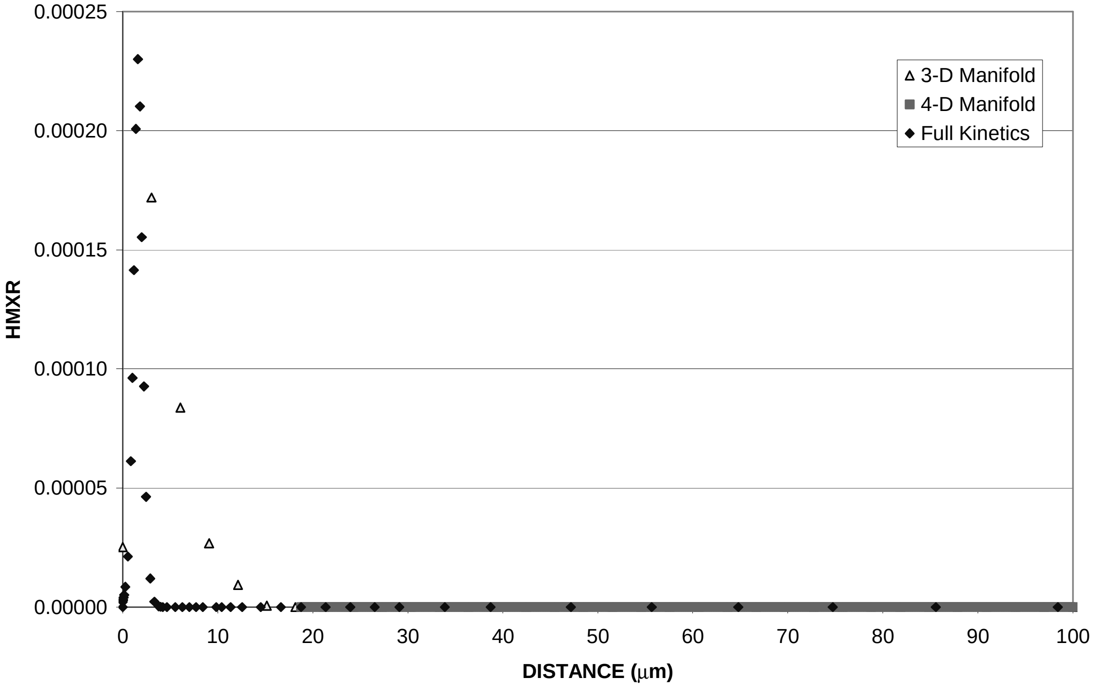
0.00025
0.00020
0.00015
0.00010
0.00005
0.00000
HMXR
0
10
20
30
40
50
60
70
80
90
100
DISTANCE (μm)
3-D Manifold
4-D Manifold
Full Kinetics

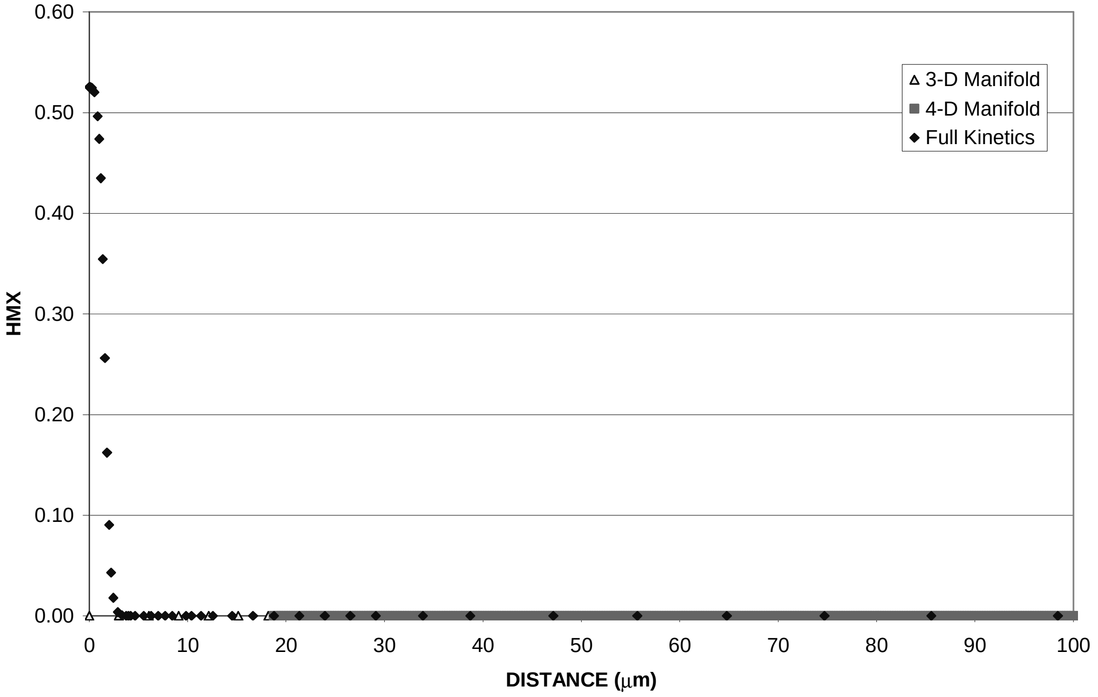
0.60
0.50
0.40
0.30
0.20
0.10
0.00
HMX
0
10
20
30
40
50
60
70
80
90
100
DISTANCE (μm)
△ 3-D Manifold
■ 4-D Manifold
◆ Full Kinetics

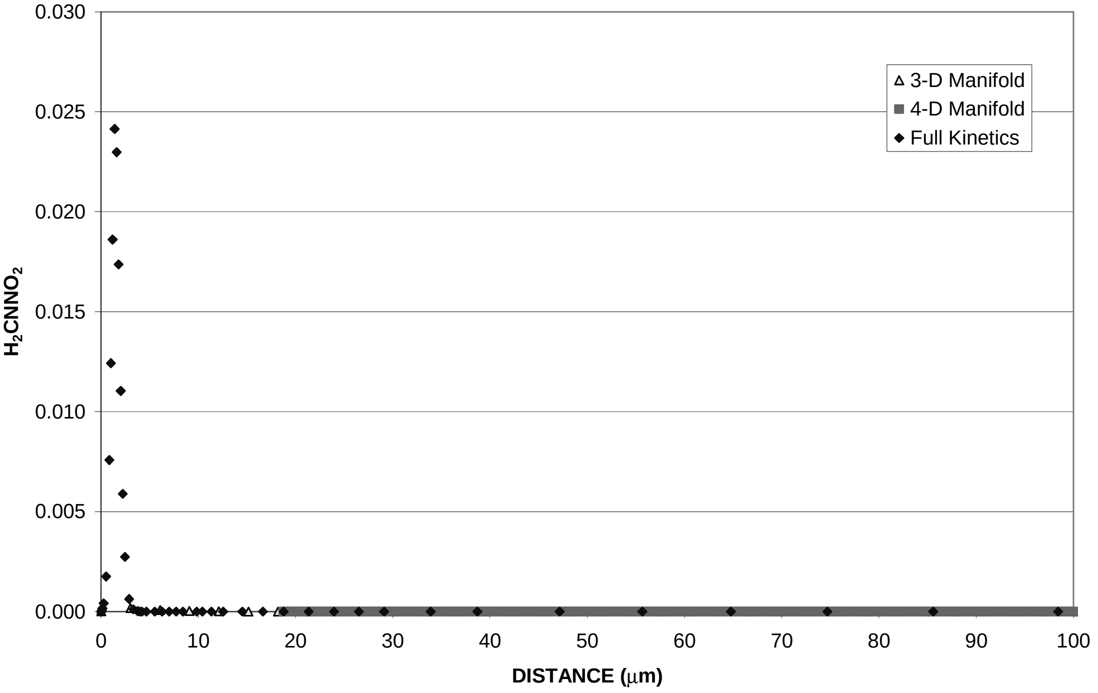
0.030
0.025
0.020
0.015
0.010
0.005
0.000
H_2CNNO_2
0
10
20
30
40
50
60
70
80
90
100
DISTANCE (μm)
△ 3-D Manifold
■ 4-D Manifold
◆ Full Kinetics

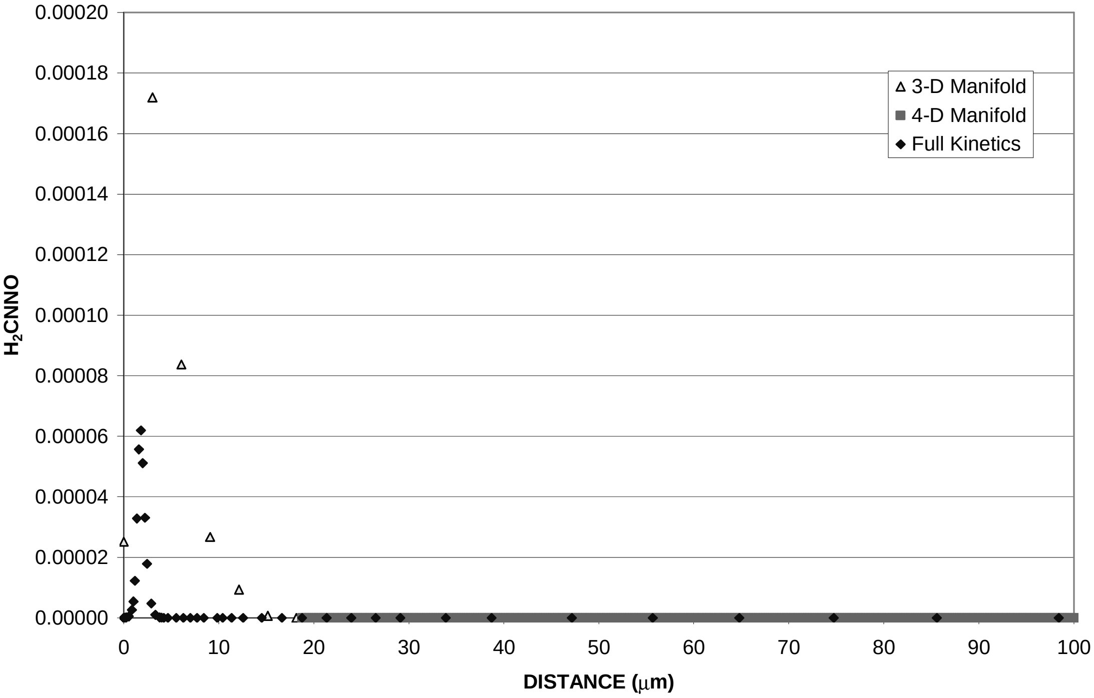
0.00020
0.00018
0.00016
0.00014
0.00012
0.00010
0.00008
0.00006
0.00004
0.00002
0.00000
H_2CNNO
0
10
20
30
40
50
60
70
80
90
100
DISTANCE (μm)
△ 3-D Manifold
■ 4-D Manifold
◆ Full Kinetics

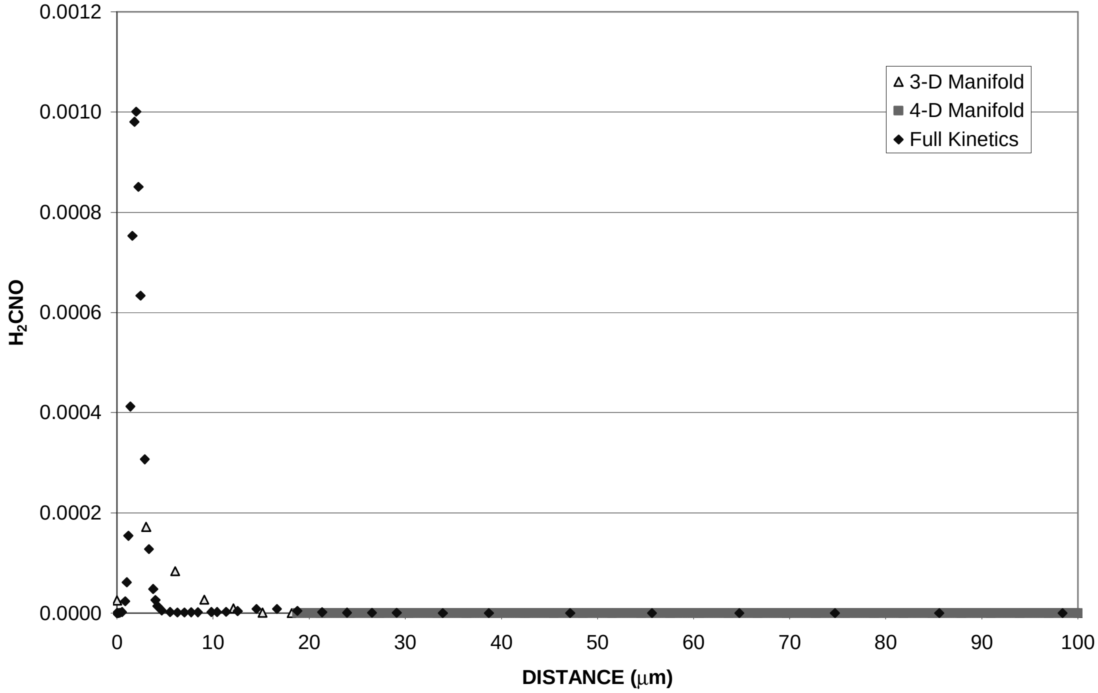
0.0012
0.0010
0.0008
0.0006
0.0004
0.0002
0.0000
H_2CNO
0
10
20
30
40
50
60
70
80
90
100
DISTANCE (μm)
△ 3-D Manifold
■ 4-D Manifold
◆ Full Kinetics

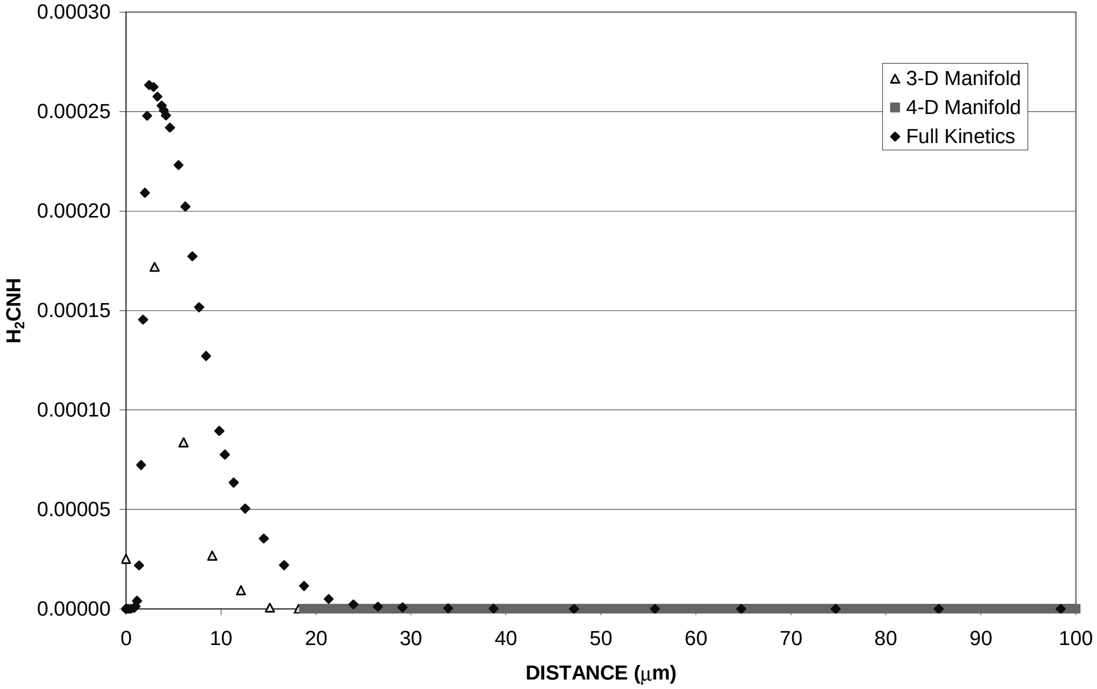

0.00030
0.00025
0.00020
0.00015
0.00010
0.00005
0.00000
H_2CNH
0
10
20
30
40
50
60
70
80
90
100
DISTANCE (μm)
3-D Manifold
4-D Manifold
Full Kinetics

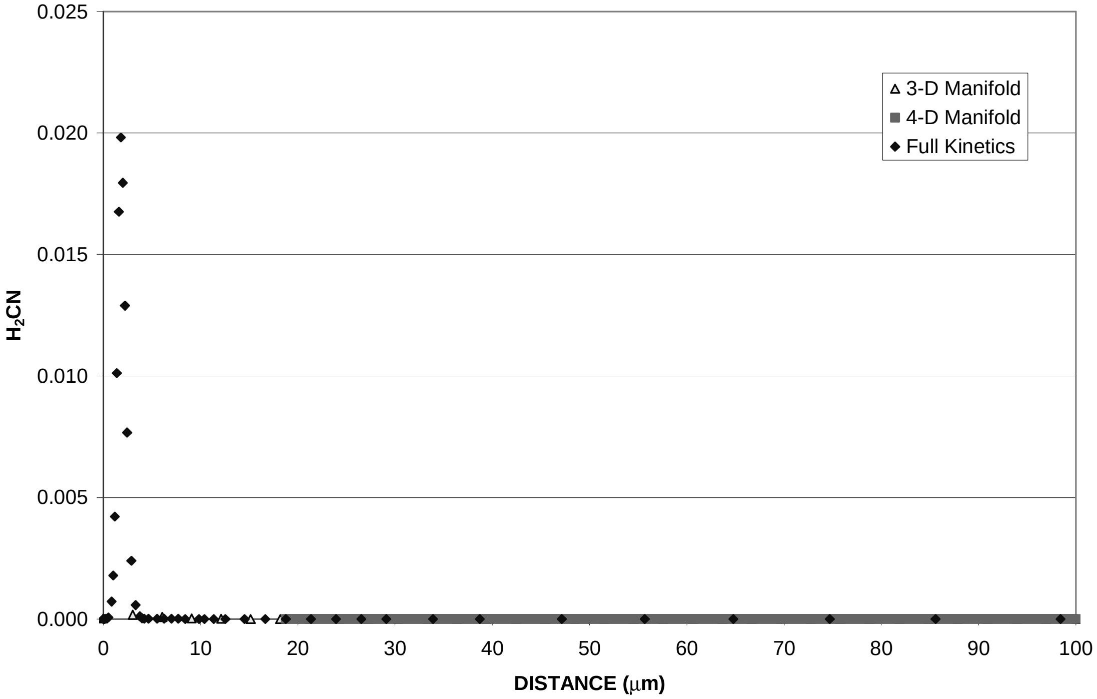

0.025
0.020
0.015
0.010
0.005
0.000
H_2CN
0
10
20
30
40
50
60
70
80
90
100
DISTANCE (μm)
3-D Manifold
4-D Manifold
Full Kinetics

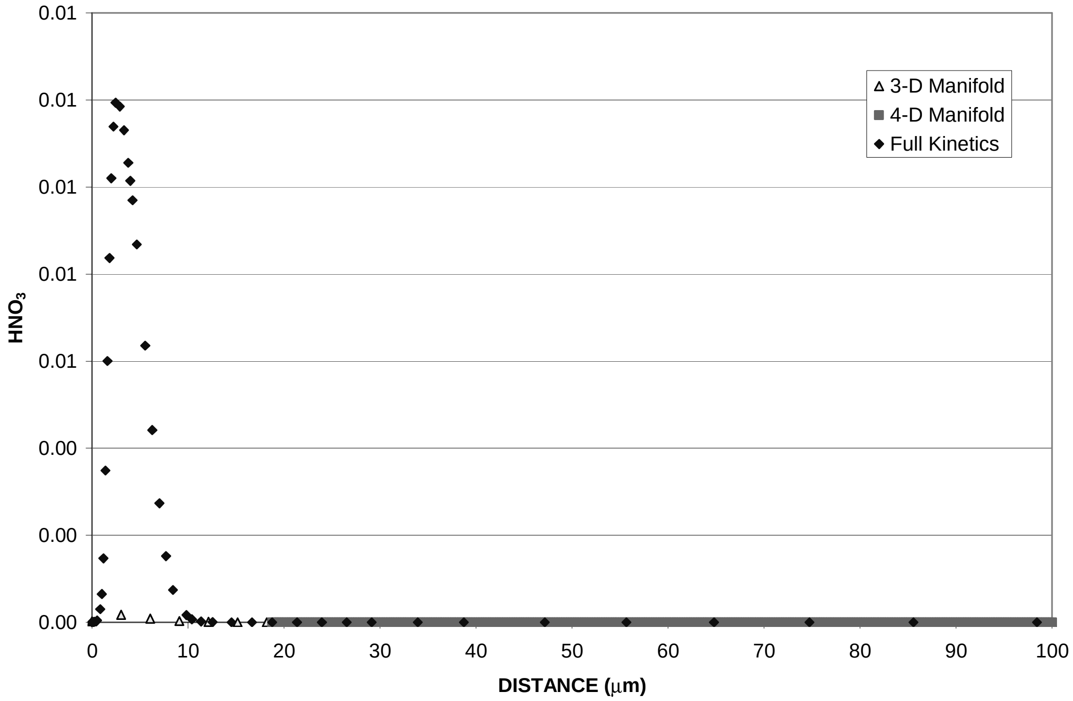
0.01
0.01
0.01
0.01
0.01
0.00
0.00
0.00
HNO$_3$
△ 3-D Manifold
■ 4-D Manifold
◆ Full Kinetics
0
10
20
30
40
50
60
70
80
90
100
DISTANCE (μm)

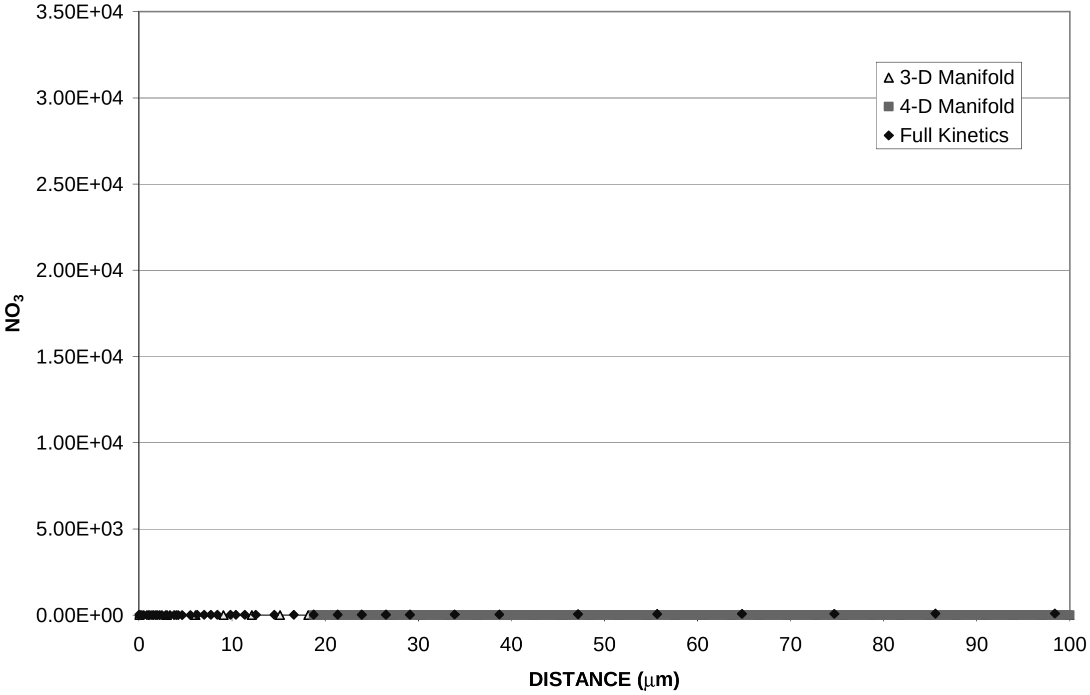
3.50E+04
3.00E+04
2.50E+04
2.00E+04
1.50E+04
1.00E+04
5.00E+03
0.00E+00
NO$_3$
△ 3-D Manifold
■ 4-D Manifold
◆ Full Kinetics
0
10
20
30
40
50
60
70
80
90
100
DISTANCE (μm)

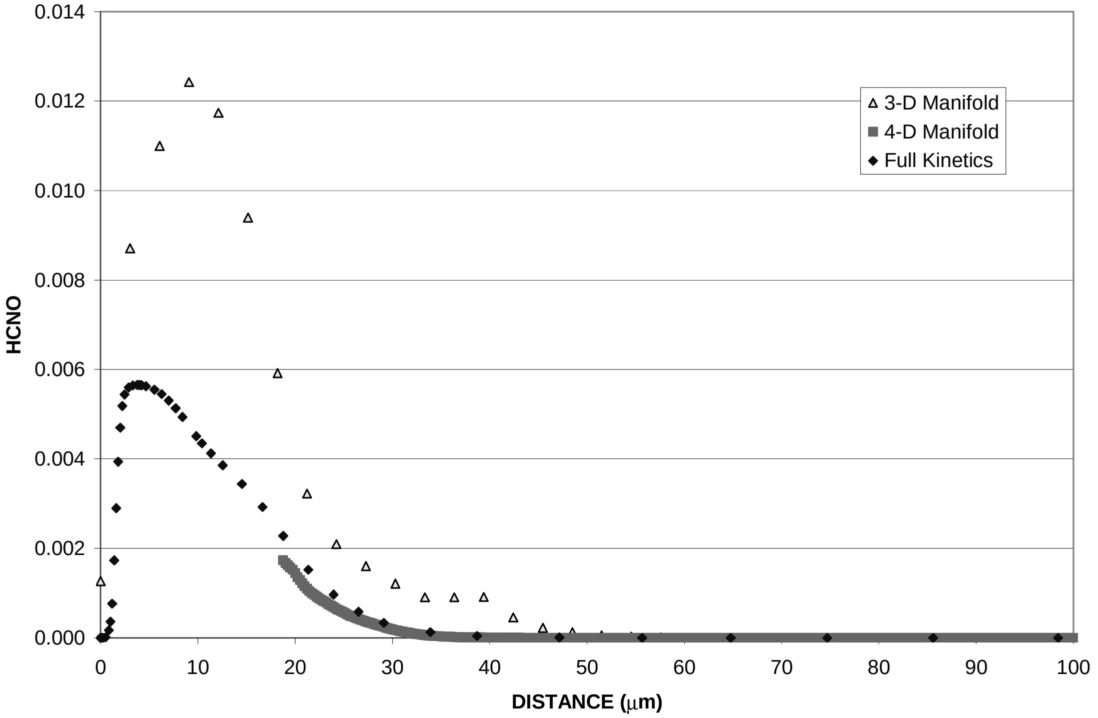
0.014
0.012
0.010
0.008
0.006
0.004
0.002
0.000
HCNO
△ 3-D Manifold
■ 4-D Manifold
◆ Full Kinetics
0
10
20
30
40
50
60
70
80
90
100
DISTANCE (μm)

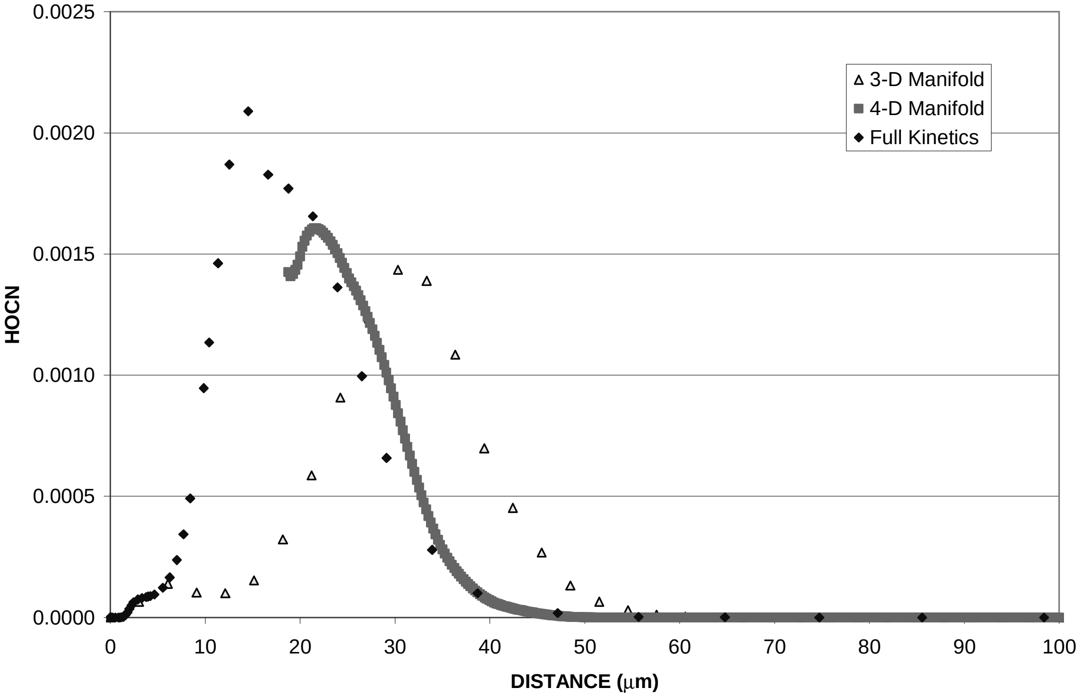
0.0025
0.0020
0.0015
0.0010
0.0005
0.0000
HOCN
△ 3-D Manifold
■ 4-D Manifold
◆ Full Kinetics
0
10
20
30
40
50
60
70
80
90
100
DISTANCE (μm)

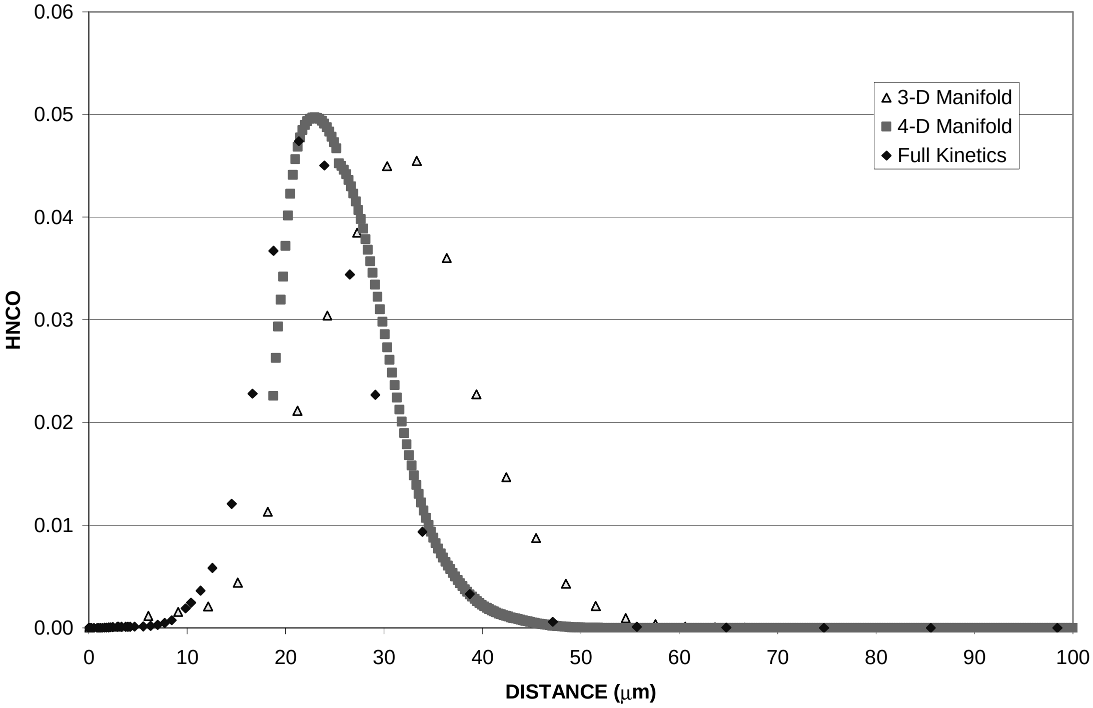

0.06
0.05
0.04
0.03
0.02
0.01
0.00
HNCO
0
10
20
30
40
50
60
70
80
90
100
DISTANCE (μm)
△ 3-D Manifold
■ 4-D Manifold
◆ Full Kinetics

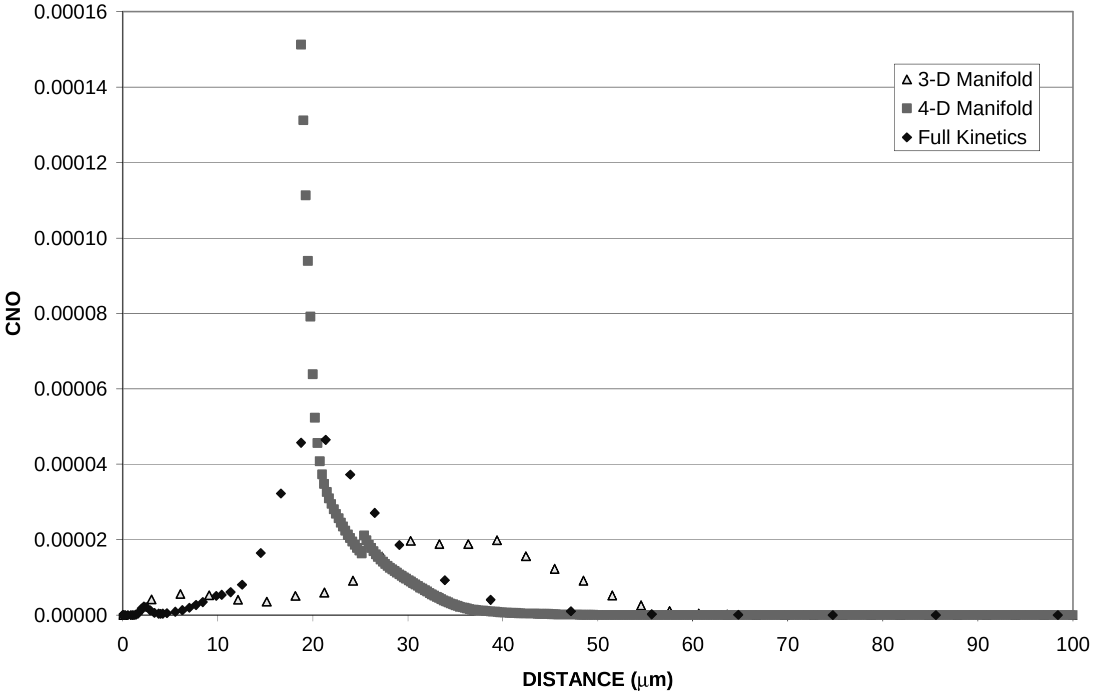

0.00016
0.00014
0.00012
0.00010
0.00008
0.00006
0.00004
0.00002
0.00000
CNO
0
10
20
30
40
50
60
70
80
90
100
DISTANCE (μm)
△ 3-D Manifold
■ 4-D Manifold
◆ Full Kinetics

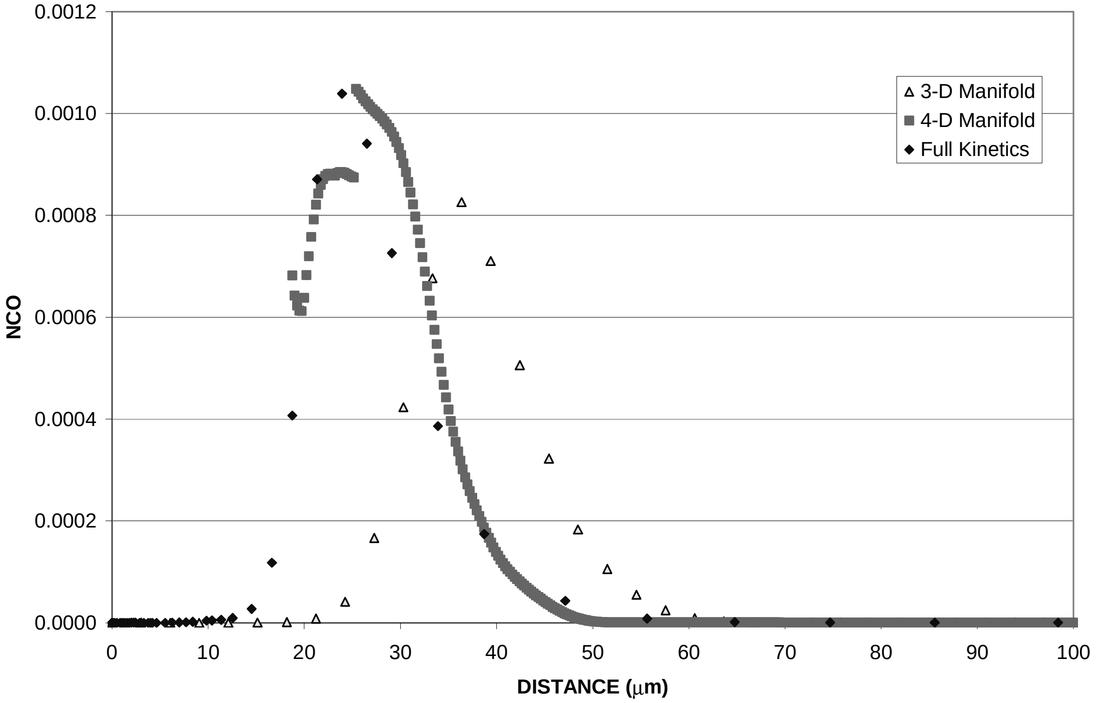

0.0012
0.0010
0.0008
0.0006
0.0004
0.0002
0.0000
NCO
0
10
20
30
40
50
60
70
80
90
100
DISTANCE (μm)
△ 3-D Manifold
■ 4-D Manifold
◆ Full Kinetics

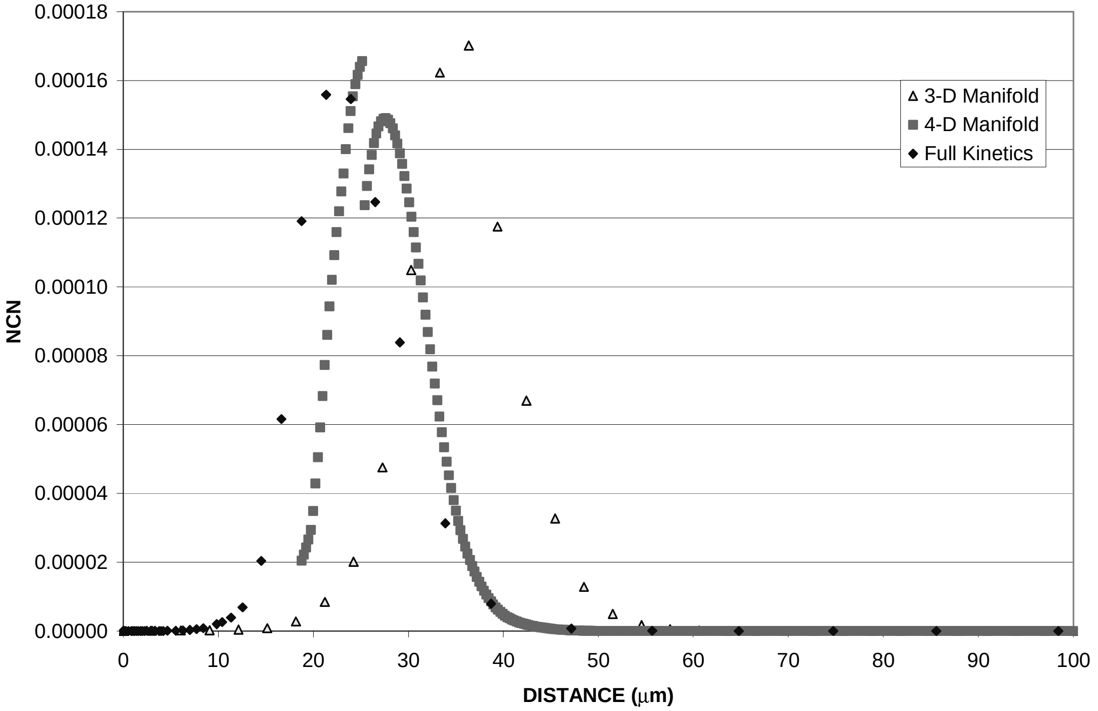

0.00018
0.00016
0.00014
0.00012
0.00010
0.00008
0.00006
0.00004
0.00002
0.00000
NCN
0
10
20
30
40
50
60
70
80
90
100
DISTANCE (μm)
△ 3-D Manifold
■ 4-D Manifold
◆ Full Kinetics

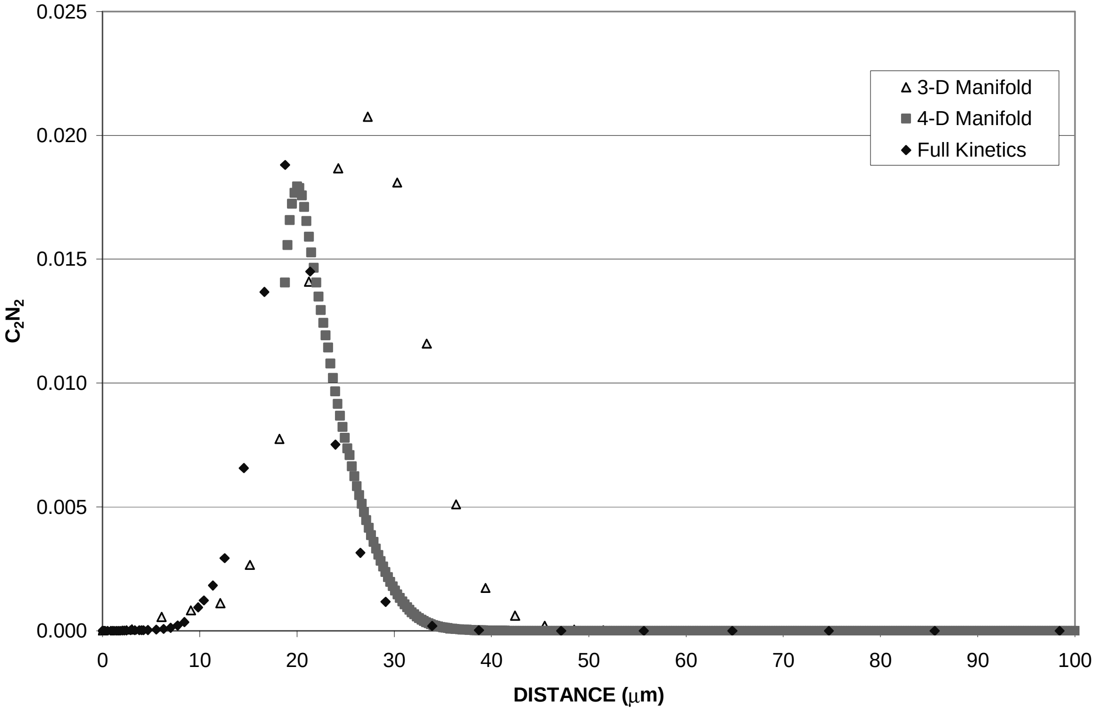
0.025
0.020
0.015
0.010
0.005
0.000
C_2N_2
0
10
20
30
40
50
60
70
80
90
100
DISTANCE (μm)
△ 3-D Manifold
■ 4-D Manifold
◆ Full Kinetics

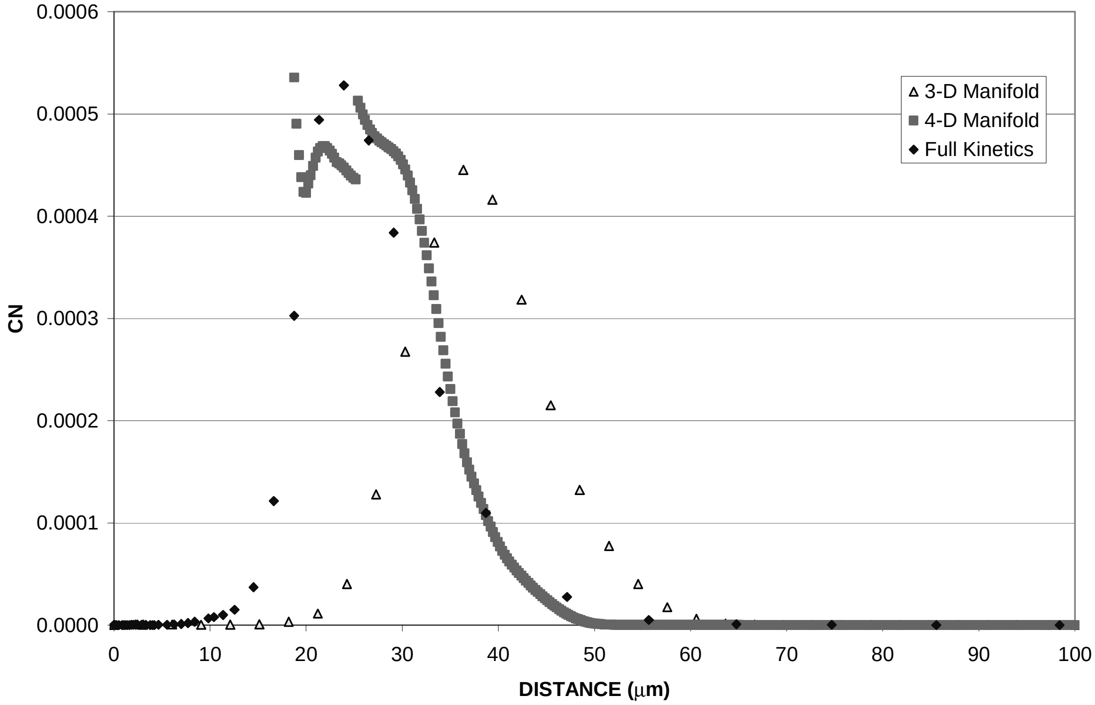
0.0006
0.0005
0.0004
0.0003
0.0002
0.0001
0.0000
CN
0
10
20
30
40
50
60
70
80
90
100
DISTANCE (μm)
△ 3-D Manifold
■ 4-D Manifold
◆ Full Kinetics

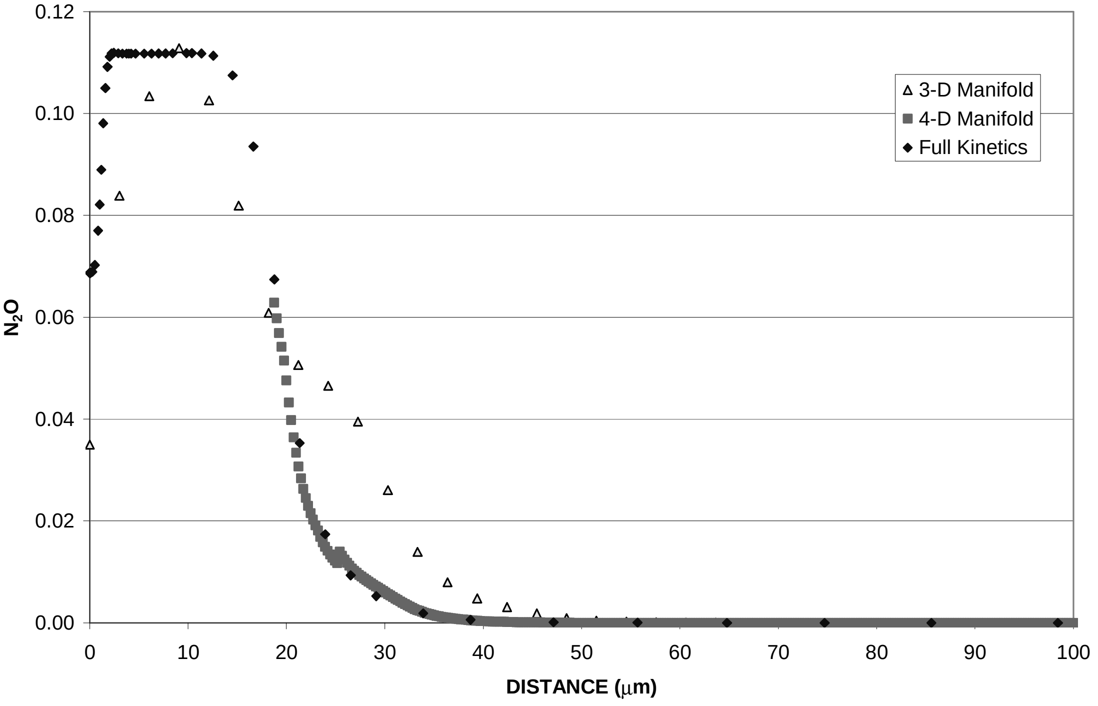
0.12
0.10
0.08
0.06
0.04
0.02
0.00
N_2O
0
10
20
30
40
50
60
70
80
90
100
DISTANCE (μm)
△ 3-D Manifold
■ 4-D Manifold
◆ Full Kinetics

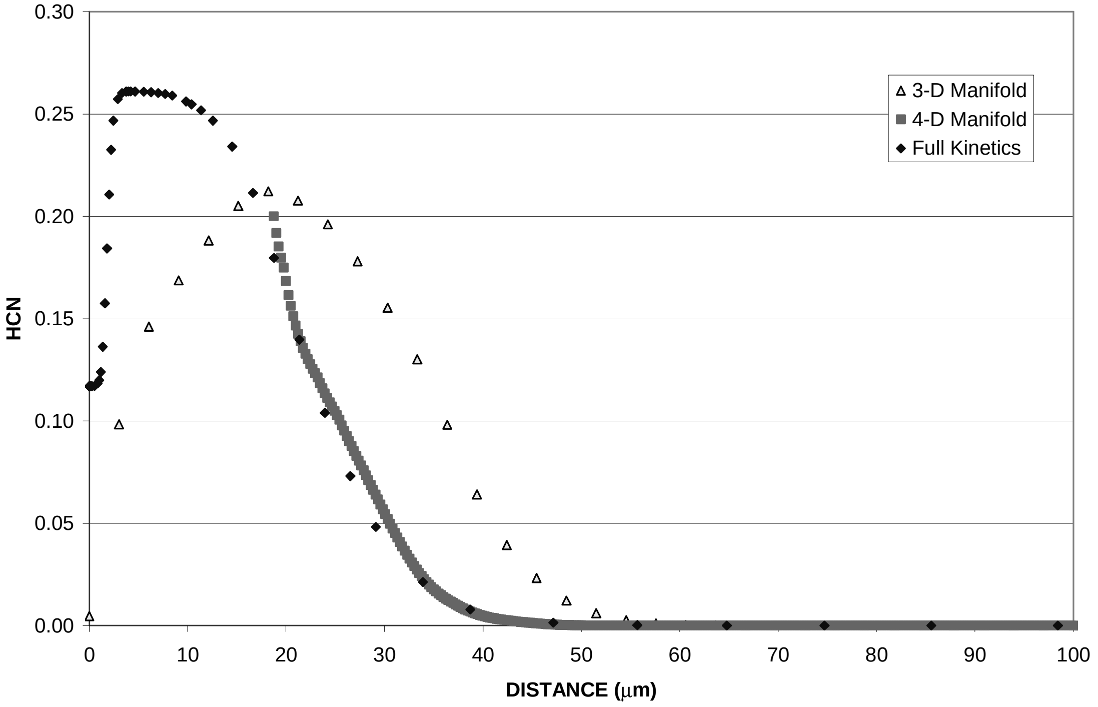
0.30
0.25
0.20
0.15
0.10
0.05
0.00
HCN
0
10
20
30
40
50
60
70
80
90
100
DISTANCE (μm)
△ 3-D Manifold
■ 4-D Manifold
◆ Full Kinetics

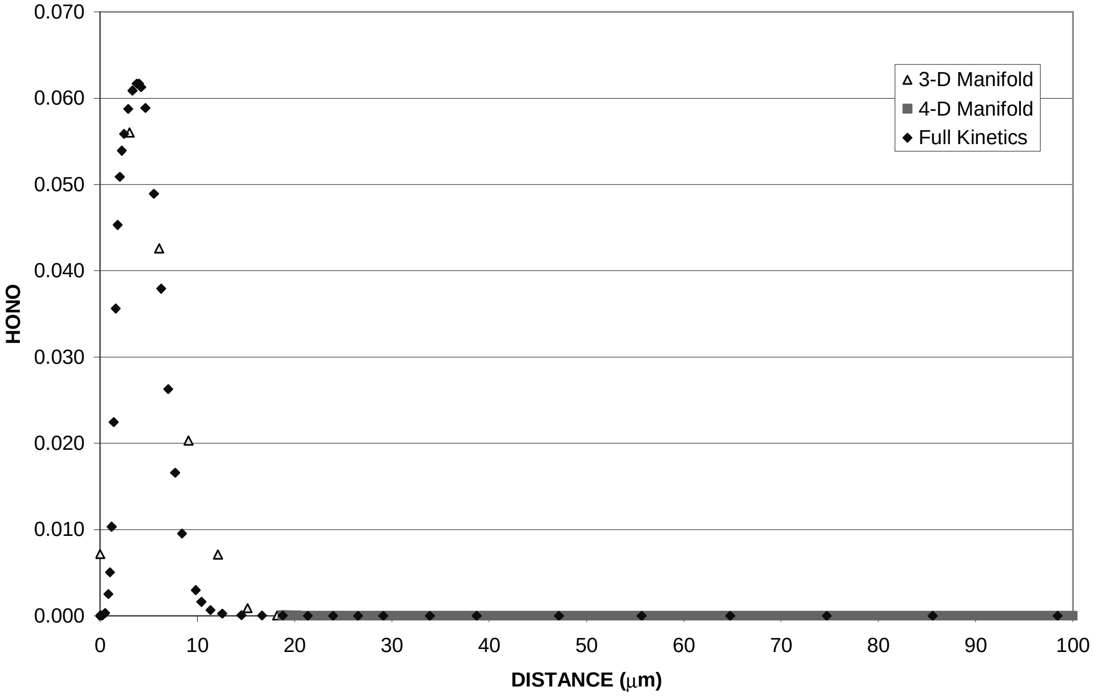
0.070
0.060
0.050
0.040
0.030
0.020
0.010
0.000
HONO
0
10
20
30
40
50
60
70
80
90
100
DISTANCE (μm)
3-D Manifold
4-D Manifold
Full Kinetics

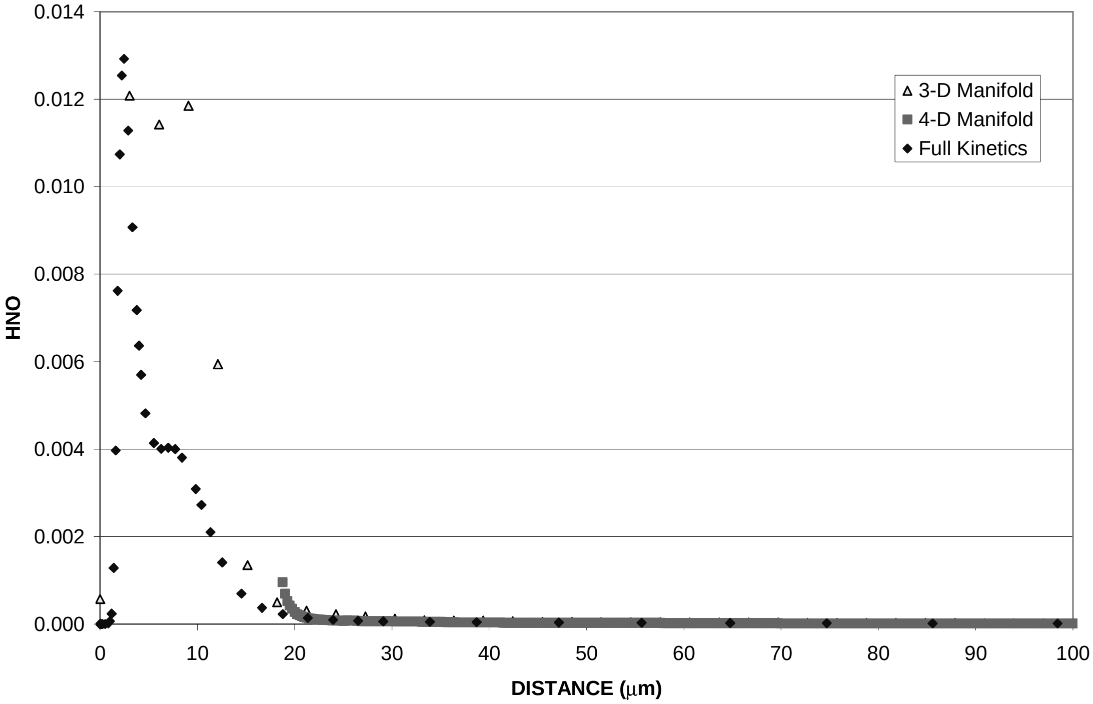
0.014
0.012
0.010
0.008
0.006
0.004
0.002
0.000
HNO
0
10
20
30
40
50
60
70
80
90
100
DISTANCE (μm)
3-D Manifold
4-D Manifold
Full Kinetics

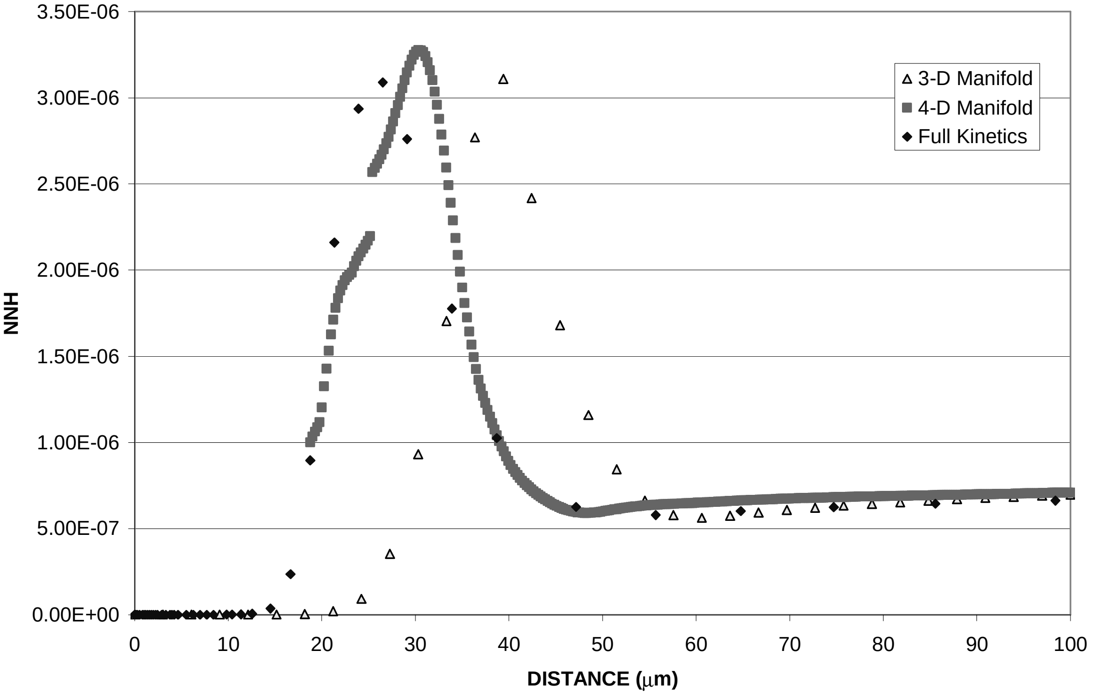
3.50E-06
3.00E-06
2.50E-06
2.00E-06
1.50E-06
1.00E-06
5.00E-07
0.00E+00
NNH
0
10
20
30
40
50
60
70
80
90
100
DISTANCE (μm)
3-D Manifold
4-D Manifold
Full Kinetics

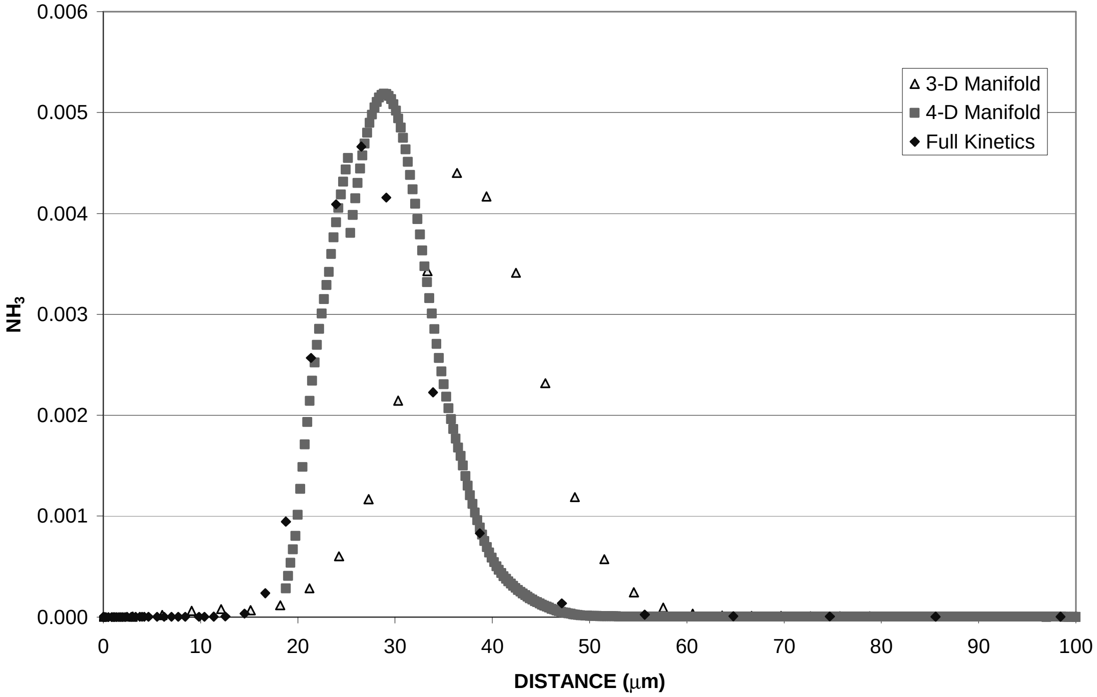
0.006
0.005
0.004
0.003
0.002
0.001
0.000
NH_3
0
10
20
30
40
50
60
70
80
90
100
DISTANCE (μm)
3-D Manifold
4-D Manifold
Full Kinetics

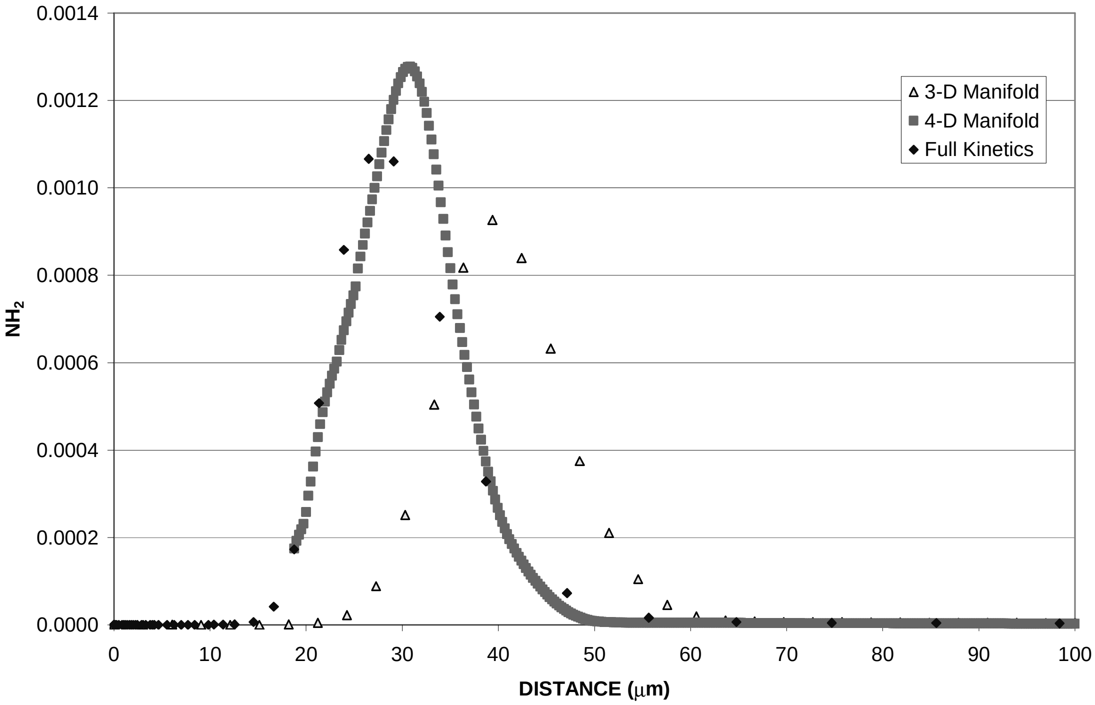
0.0014
0.0012
0.0010
0.0008
0.0006
0.0004
0.0002
0.0000
NH$_2$
0
10
20
30
40
50
60
70
80
90
100
DISTANCE (μm)
△ 3-D Manifold
■ 4-D Manifold
◆ Full Kinetics

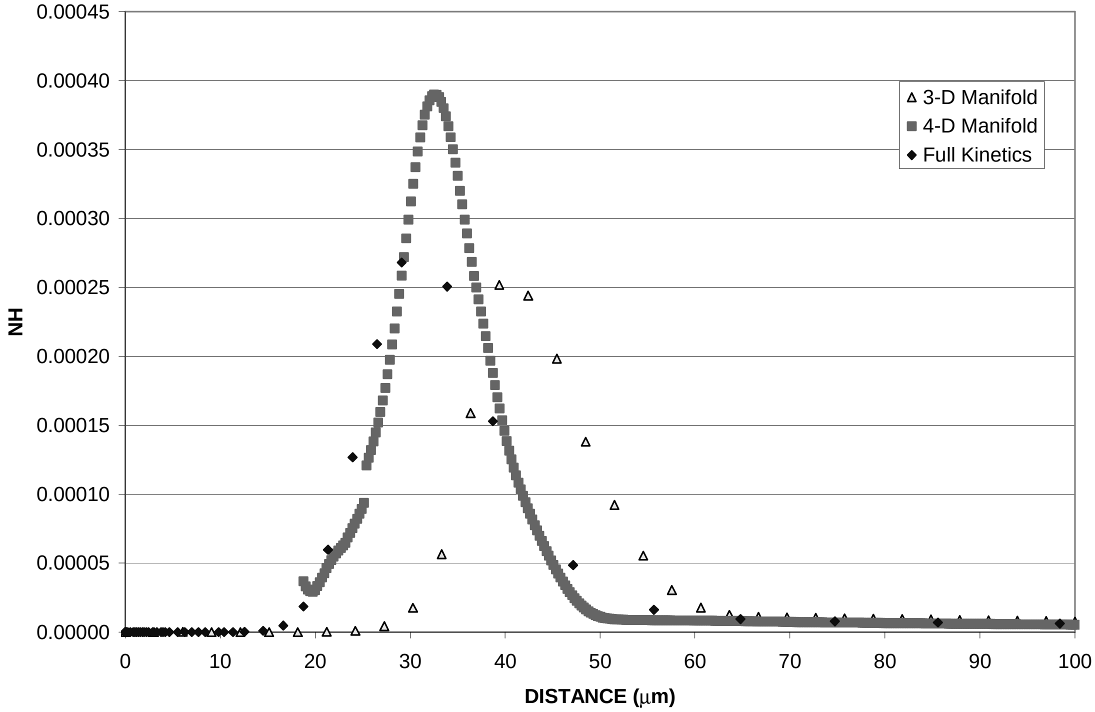
0.00045
0.00040
0.00035
0.00030
0.00025
0.00020
0.00015
0.00010
0.00005
0.00000
NH
0
10
20
30
40
50
60
70
80
90
100
DISTANCE (μm)
△ 3-D Manifold
■ 4-D Manifold
◆ Full Kinetics

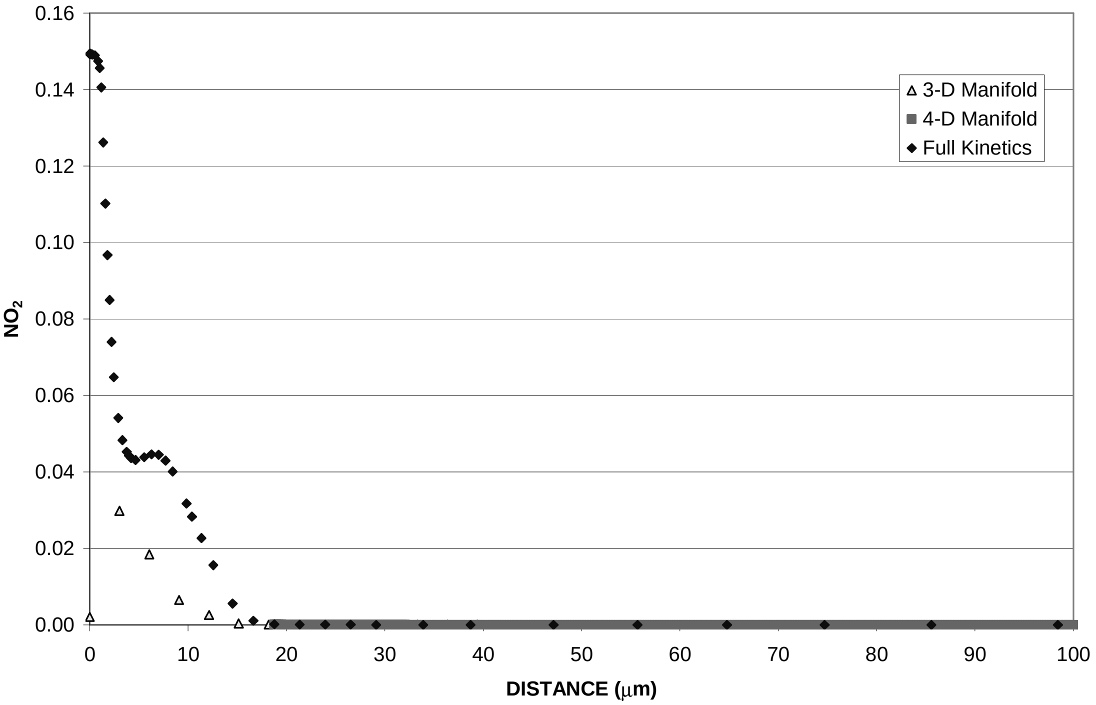

0.16
0.14
0.12
0.10
0.08
0.06
0.04
0.02
0.00
NO_2
0
10
20
30
40
50
60
70
80
90
100
DISTANCE (μm)
3-D Manifold
4-D Manifold
Full Kinetics

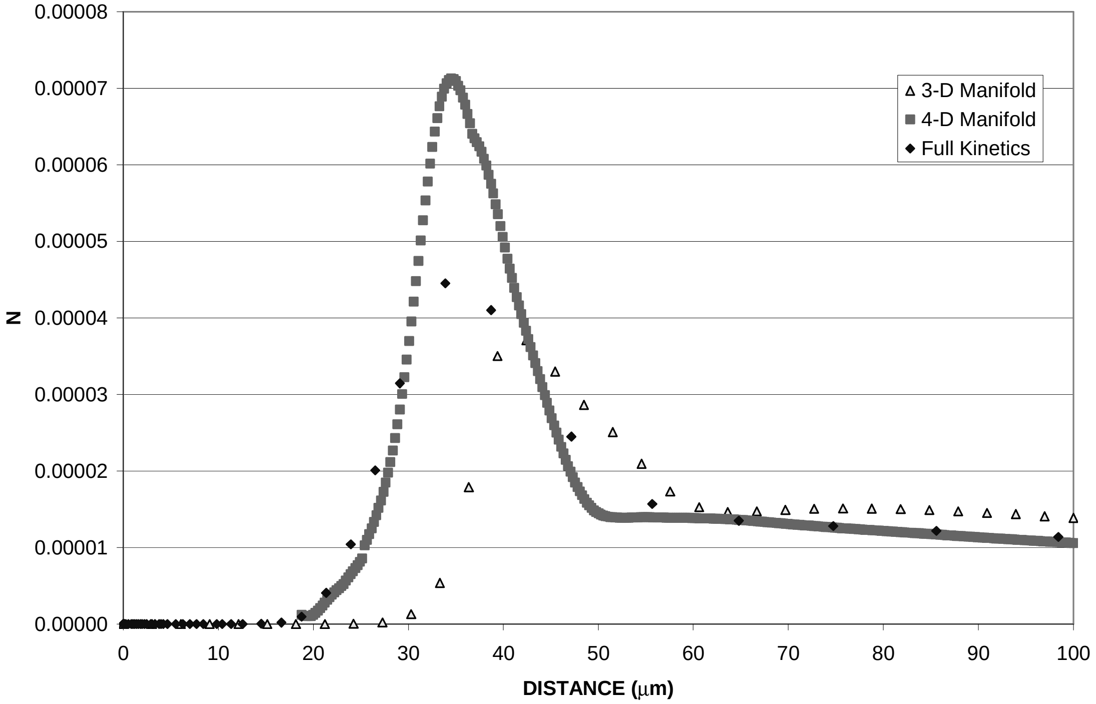

0.00008
0.00007
0.00006
0.00005
0.00004
0.00003
0.00002
0.00001
0.00000
N
0
10
20
30
40
50
60
70
80
90
100
DISTANCE (μm)
3-D Manifold
4-D Manifold
Full Kinetics

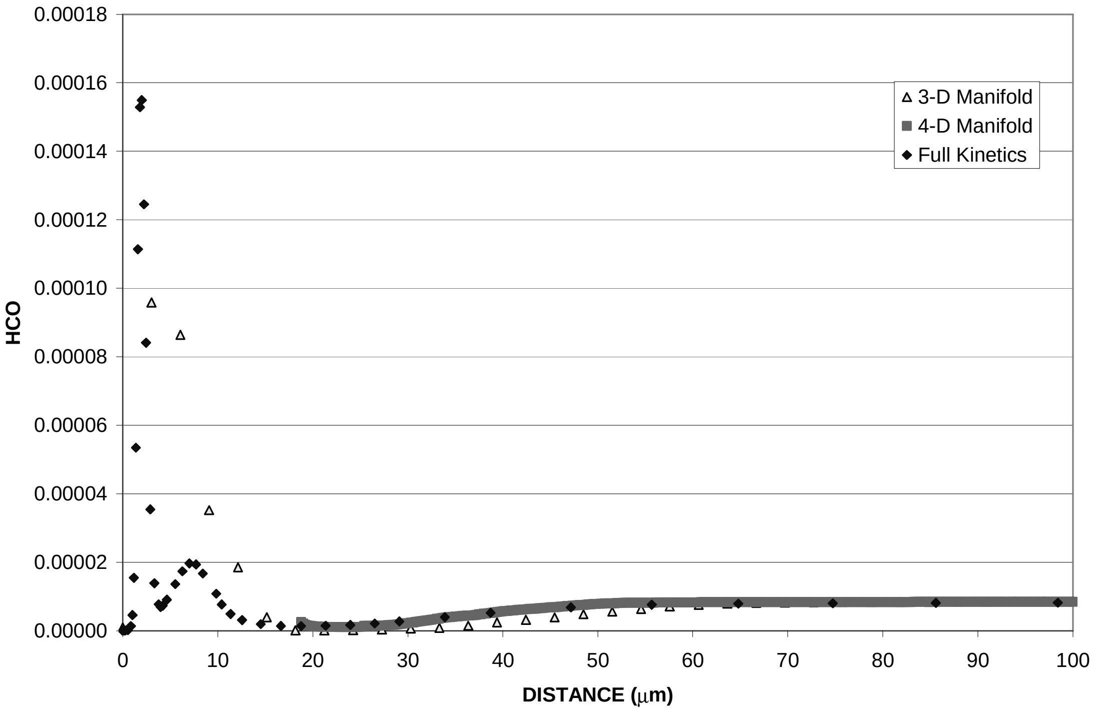
0.00018
0.00016
0.00014
0.00012
0.00010
0.00008
0.00006
0.00004
0.00002
0.00000
HCO
0
10
20
30
40
50
60
70
80
90
100
DISTANCE (μm)
△ 3-D Manifold
■ 4-D Manifold
◆ Full Kinetics

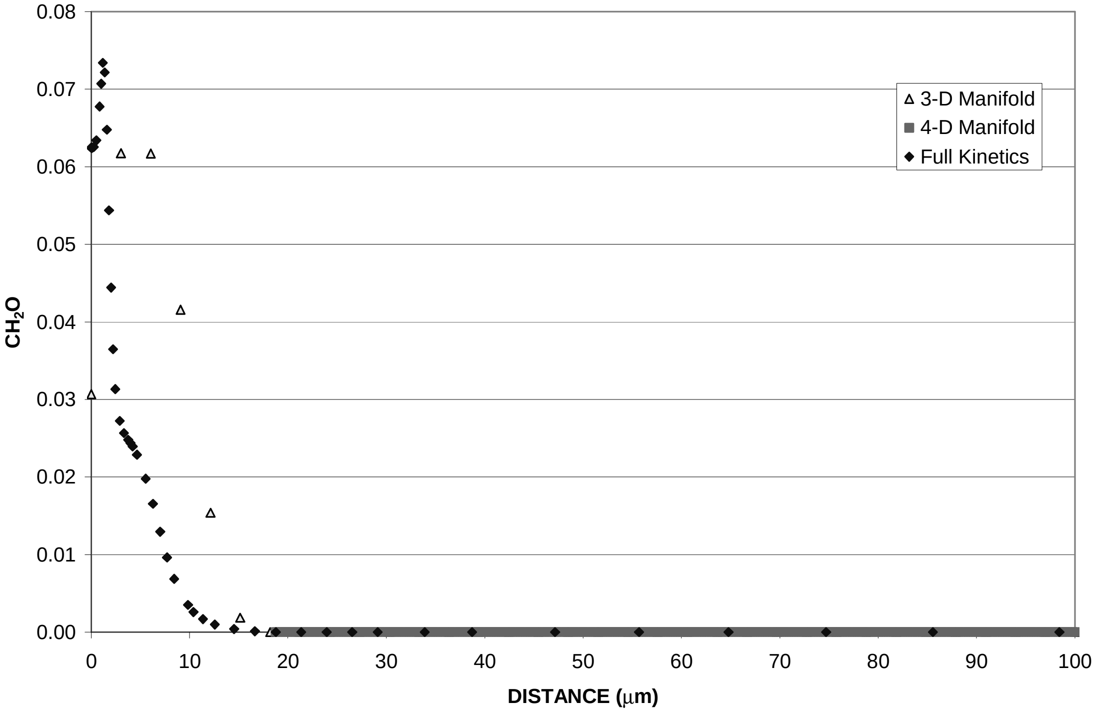
0.08
0.07
0.06
0.05
0.04
0.03
0.02
0.01
0.00
CH_2O
0
10
20
30
40
50
60
70
80
90
100
DISTANCE (μm)
△ 3-D Manifold
■ 4-D Manifold
◆ Full Kinetics

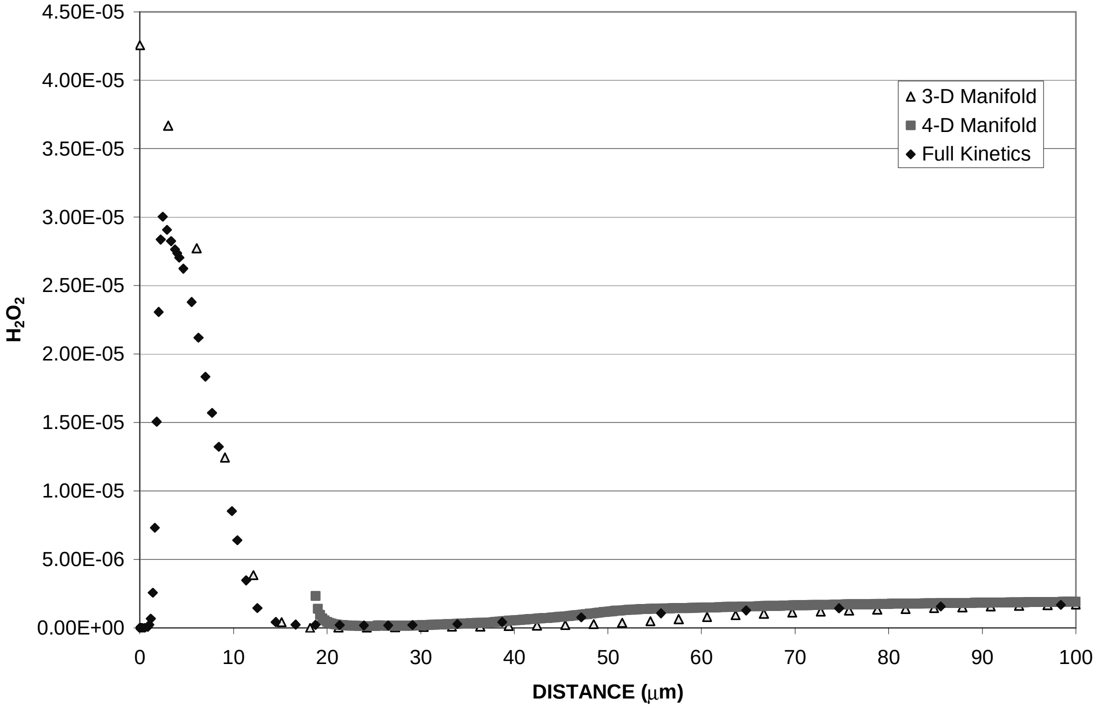
4.50E-05
4.00E-05
3.50E-05
3.00E-05
2.50E-05
2.00E-05
1.50E-05
1.00E-05
5.00E-06
0.00E+00
H_2O_2
0
10
20
30
40
50
60
70
80
90
100
DISTANCE (μm)
△ 3-D Manifold
■ 4-D Manifold
◆ Full Kinetics

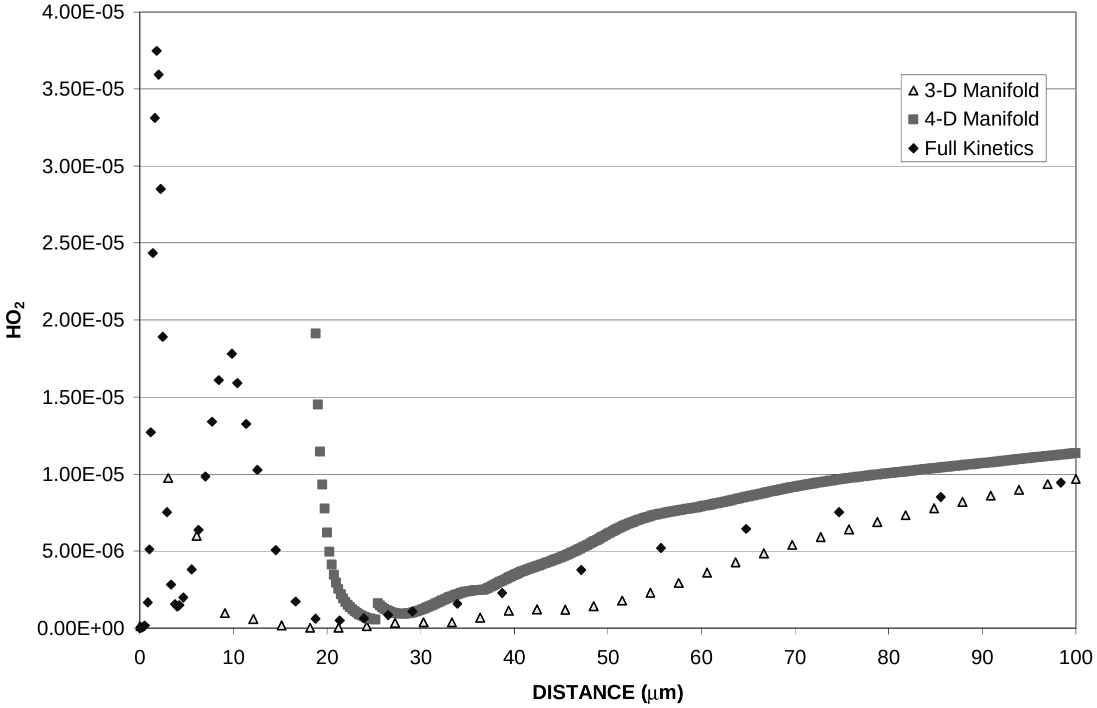
4.00E-05
3.50E-05
3.00E-05
2.50E-05
2.00E-05
1.50E-05
1.00E-05
5.00E-06
0.00E+00
HO_2
0
10
20
30
40
50
60
70
80
90
100
DISTANCE (μm)
△ 3-D Manifold
■ 4-D Manifold
◆ Full Kinetics

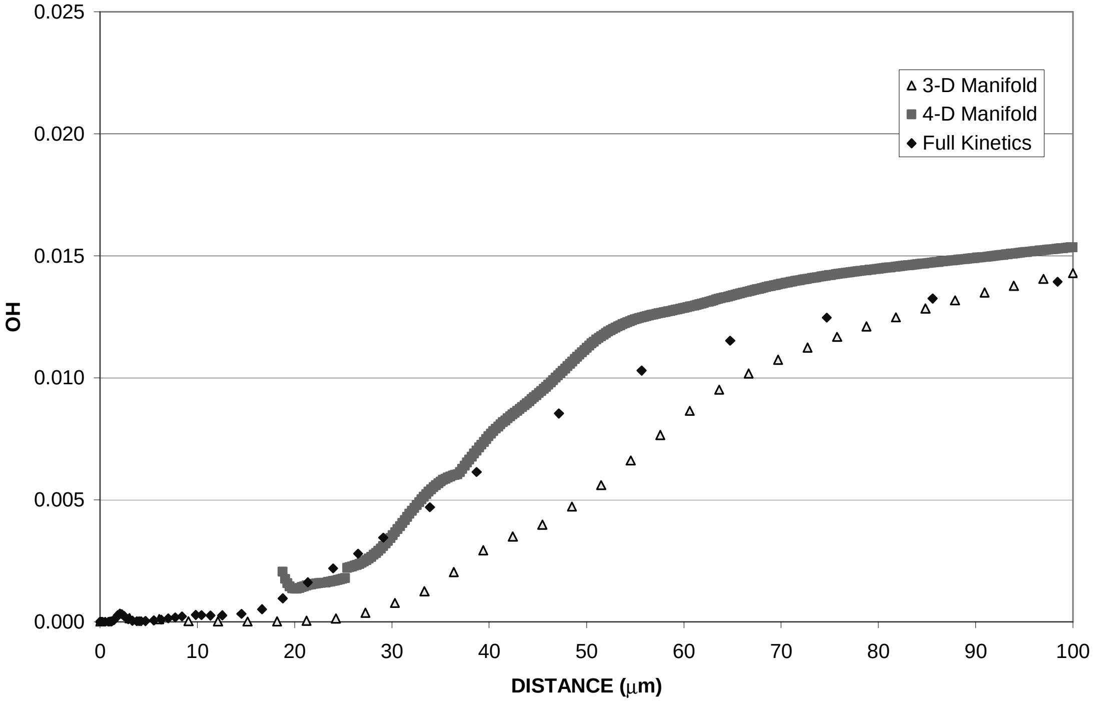
0.025
0.020
0.015
0.010
0.005
0.000
OH
0
10
20
30
40
50
60
70
80
90
100
DISTANCE (μm)
△ 3-D Manifold
■ 4-D Manifold
◆ Full Kinetics

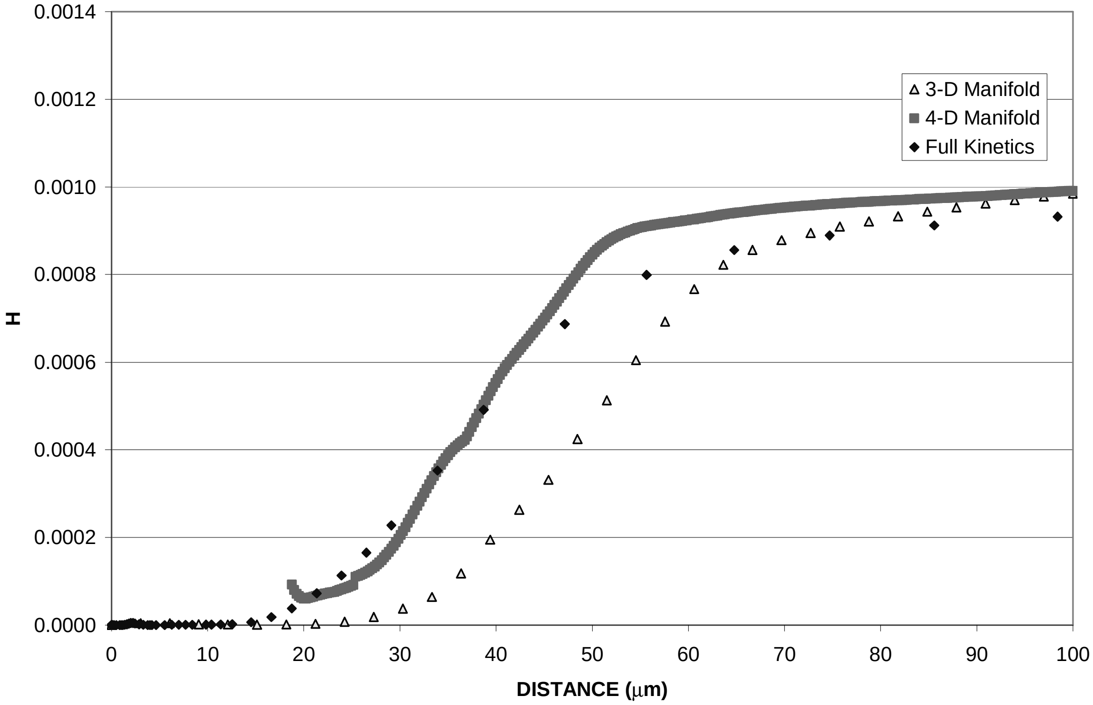
0.0014
0.0012
0.0010
0.0008
0.0006
0.0004
0.0002
0.0000
H
0
10
20
30
40
50
60
70
80
90
100
DISTANCE (μm)
△ 3-D Manifold
■ 4-D Manifold
◆ Full Kinetics

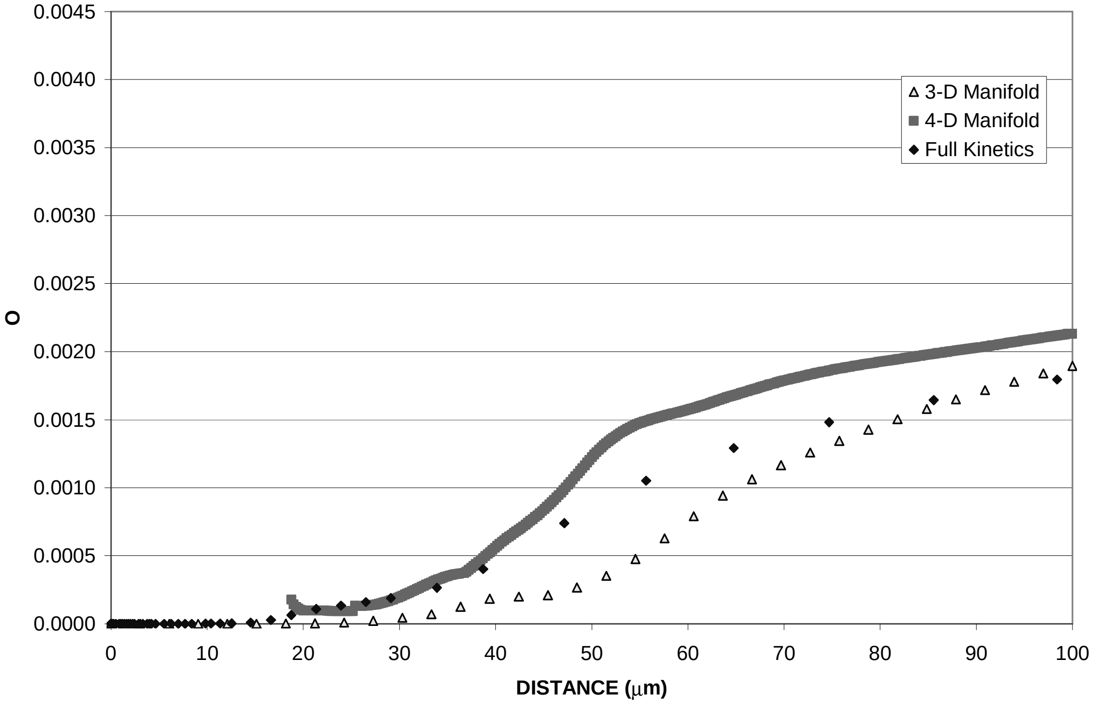
0.0045
0.0040
0.0035
0.0030
0.0025
0.0020
0.0015
0.0010
0.0005
0.0000
O
0
10
20
30
40
50
60
70
80
90
100
DISTANCE (μm)
△ 3-D Manifold
■ 4-D Manifold
◆ Full Kinetics

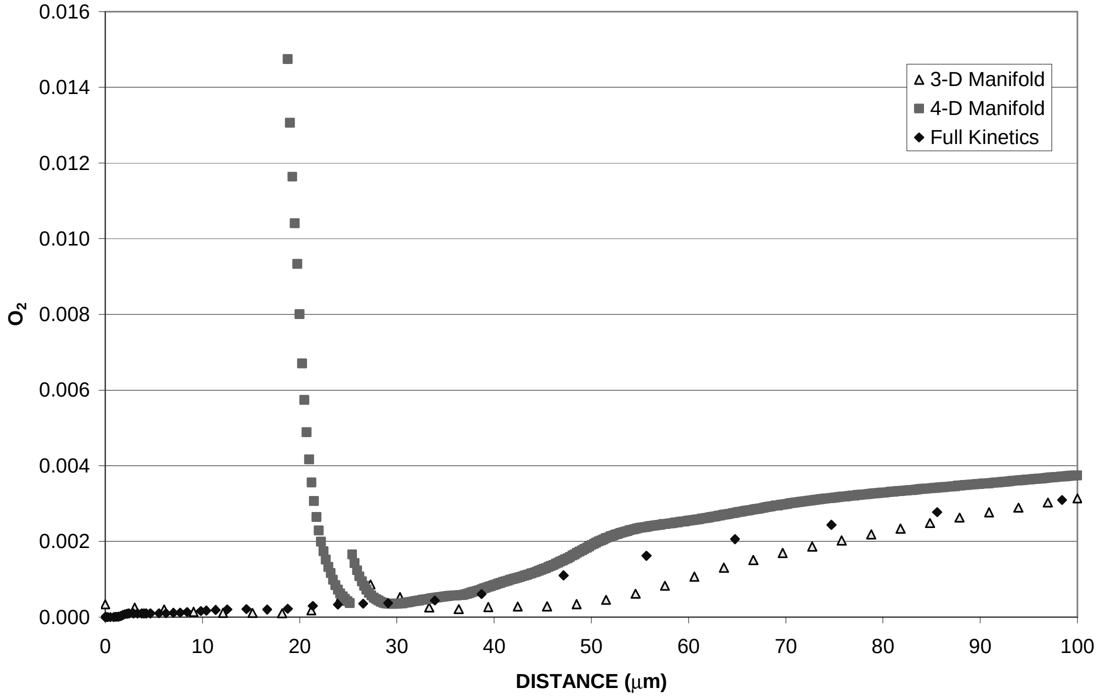
0.016
0.014
0.012
0.010
0.008
0.006
0.004
0.002
0.000
O_2
0
10
20
30
40
50
60
70
80
90
100
DISTANCE (μm)
△ 3-D Manifold
■ 4-D Manifold
◆ Full Kinetics

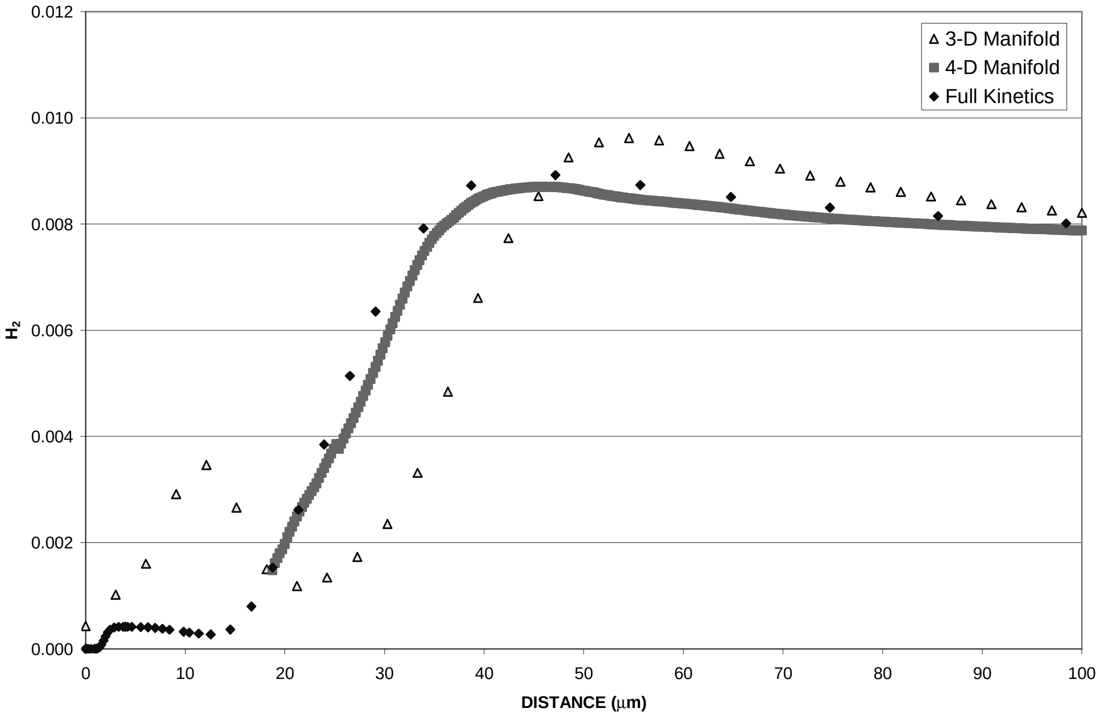
0.012
0.010
0.008
0.006
0.004
0.002
0.000
H2
0
10
20
30
40
50
60
70
80
90
100
DISTANCE (μm)
△ 3-D Manifold
■ 4-D Manifold
◆ Full Kinetics